EXCITON CORRELATIONS WITHIN AN ELECTRON GAS

THÈSE N^{O} 3726 (2007)

PRÉSENTÉE LE 26 JANVIER 2007

À LA FACULTÉ DES SCIENCES DE BASE

Laboratoire d'optoélectronique quantique

PROGRAMME DOCTORAL EN PHOTONIQUE

ÉCOLE POLYTECHNIQUE FÉDÉRALE DE LAUSANNE

POUR L'OBTENTION DU GRADE DE DOCTEUR ÈS SCIENCES

PAR

Jean BERNEY

ingénieur physicien diplômé EPF

de nationalité suisse et originaire de L'Abbaye (VD)

acceptée sur proposition du jury:

Prof. O. Martin, président du jury

Prof. B. Deveaud-Plédran, Dr M. Portella-Oberli, directeurs de thèse

Prof. G. Bastard, rapporteur

Prof. A. Imamoglu, rapporteur

Prof. J.-E. Moser, rapporteur

ÉCOLE POLYTECHNIQUE
FÉDÉRALE DE LAUSANNE

Suisse

2007

Acknowledgements

This thesis marks the end of almost four years of research, a period during which I often had to rely on a number of people whom I would like to thank here.

Of particular importance for me were the support and confidence of my two thesis supervisors, Prof. Benoît Deveaud and Dr. Marcia Portella-Oberli. I want to thank Prof. Benoît Deveaud not only for making this project possible, but also for offering me so much freedom in my work. Through his effervescent enthusiasm and erudition he was a constant source of inspiration and motivation. I am grateful to Dr. Marcia Portella-Oberli for her thoroughly supervising my work and showing me how to extract the *substantifique moëlle* out of every single experimental result. I praise her affability and generosity.

I would also like to thank the thesis defense committee for the time and effort devoted to reading and evaluating this thesis: Prof. Gérald Bastard, LPMC, Ecole Normale Supérieure, Paris, Prof. Atac Imamoglu, Institute of Quantum Electronics, ETHZ, Zürich, Prof. Jacques Edouard Moser, EPFL, Lausanne. Further I acknowledge financial support from FNRS within quantum photonics NCCR.

In my office, I appreciated the constructive discussions with Maxime Richard and Samuel Sonderegger. My thanks also go to Marc-André Dupertuis, Vicenzo Savona, Christiano Ciuti, Monique Combescot and Roland Zimmermann for enlightening discussions. A big thank you is also reserved for Jaceck Szczytko and Lars Kappei for introducing me to experimental physics and for their very fruitful collaboration. This work would not have been possible without the solid technical expertise of Jean-Daniel Ganiére, the top of the line samples of Franois Morier-Genoud and the mechanical skills of Roger Rochat. I thank Lucas Schifferle for the work he performed in my laboratory during his Master thesis, as well as Stefan Kunderman for sharing his electronics skill.

The whole institute was responsible for creating a fantastic atmosphere, making this a very enjoyable experience. Therefore I do not want to leave out Blandine Alloing, Augustin Baas, Laurent Balet, Christian Blumer, Ounsi

El Daif, Andrea Dunbar, Andrea Feltrin, Rolando Ferini, Reto Joray, Reda Kaitouni Idrissi, Konstantinos Lagoudakis, David Leuenberger, Alexander Markus, Michele Merano, Pablo Moreno, Tim Ottenburg, Taofiq Paraiso, Philipp Ridha, Michele Saba, Lorena Sabin, Ferran Salleras Vila, Carl Zinoni as well as the many students present during that time. Finally I am very grateful to my family, especially to my parents, and my friends who encouraged me during my PhD. I would like to spatially thank Julie who supported me during such an endeavor.

Abstract

I report on the effect of a moderate excess electron population on nonlinearities in modulation-doped CdTe quantum wells. I show that the electron population does not qualitatively affect the nature of correlations between excitons. In this respect, I bring strong evidence of the existence of unbound and bound (stable) two-exciton states in the presence of electrons and charged excitons (trions). In time-resolved pump and probe experiment, they lead to the observation of electromagnetically induced transparency and optical Stark shift of the exciton resonance. Rabi flopping of excitons within a sea of electrons is also clearly evidenced through ac Stark splitting and gain without inversion. The quantum coherence is more robust to electron induced dephasing than what would have been expected.

I demonstrate third and higher-order exciton correlations in the presence of electrons, which manifest, for increasing exciton densities, through the blue-shift of counter-polarized exciton resonance, the red-shift of the biexciton resonance and the exciton to biexciton crossover. I also evidence correlated behavior of excitons and trions under excitation which manifests itself by crossed trion-exciton effects. I observe a wealth of phenomena encompassing bleaching, crossed bleaching, induced-absorption and energy shifts of the resonances. Significant differences are found between the nonlinear optical effects induced by an exciton and a trion population.

Electron scattering with electron and exciton is shown to strongly broaden the high energy tail of exciton and trion resonance lineshapes. Variation of electron density result in a clear modification of both resonance lineshapes.

The dynamics of the formation of trions is also studied. I propose a two-channel mechanism for their formation; they are formed through bi- and tri-molecular processes. This implies that both negatively and positively charged excitons coexist in a quantum well, even in the absence of excess carriers. The model is applied to a time-resolved photoluminescence experiment performed on a very high quality InGaAs quantum well sample, in which the photoluminescence contributions at the energy of the trion, exciton and at the band edge can be clearly separated and traced over a broad range of

times and densities. The unresolved discrepancy between the theoretical and experimental radiative decay time of the exciton in a doped semiconductor is explained.

Keywords: semiconductor, modulation-doped quantum well, exciton, charged exciton, trion, many-body effects, nonlinearities, optical coherence, electromagnetical induced transparency, optical Stark shift, gain without inversion, Stark splitting, Mollow triplet, dynamics, formation, electron scattering.

Résumé

Ce travail de thèse contient une étude expérimentale des propriétés non linéaires d'un puits quantique de CdTe à modulation de dopage. J'y montre que les électrons présents dans un puits ne modifient pas qualitativement la nature des corrélations entre excitons. Aussi, j'identifie clairement l'existence d'états à deux excitons liés (stables) et non liés en présence d'électrons et d'excitons. Des expériences de pompe et sonde me permettent de tirer parti de ces états à deux excitons et d'observer des phénomènes tels que la transparence électromagnétique induite ou l'effet Stark optique de la résonance excitonique. J'observe indirectement des oscillations de Rabi dans une mer d'électrons à travers le triplet de Mollow. Quand bien même les électrons induisent un fort déphasage des excitons, la cohérence quantique s'avère très résistante.

Je mets en évidence l'existence de corrélations de Coulomb au troisième et même au cinquième ordre en présence d'électrons. Lors d'une augmentation de la densité d'excitons, ces corrélations se manifestent à travers la renormalisation des résonances excitonique et biexitonique ainsi que d'un transfert de force d'oscillateur de l'exciton au biexciton. Je mets également en évidence des effets de corrélation entre excitons et trions. J'observe nombre d'effets non-linéaires allant du blanchissage au blanchissage croisé des résonances, en passant par leur absorption induite ou leur renormalisation. D'importantes différences entre les effets non-linéaires induits par des excitons ou des trions sont montrés.

Les collisions entre électrons et excitons et entre électrons et trions élargissent la queue à haute énergie des excitons et des trions et contribuent à les rendre fortement asymétriques. Par conséquent, des variations de populations électroniques peuvent être responsables de fortes variations du spectre d'absorption.

La dynamique de formation du trion est également étudiée. Je propose un mécanisme de formation à deux canaux. Soit le trion est formé au cours d'un processus bi-moléculaire où un exciton et un porteur libre s'assemblent, soit le processus est tri-moléculaire et le trion est directement formé à partir de porteurs libres. J'en déduis qu'inévitablement, des populations d'excitons chargés négativement et positivement cohabitent dans un puits quantique

même en l'absence d'excès de porteurs. Mon model est corroboré par une expérience de photoluminescence résolue en temps réalisée sur un puits quantique d'InGaAs de qualité inégalée. Dans cet échantillon, les contributions des trions et du plasma de porteurs libres à la luminescence des excitons peuvent être parfaitement séparées et mesurées sur un large intervalle de temps et de densités. J'explique alors pourquoi le temps de vie des excitons augmente en présence d'électrons.

Mots-clés: semiconducteur, puits quantique, modulation de dopage, cohérence optique, excitons, excitons chargés, trions, effets à N-corps, nonlinearités optiques, transparence électromagnétique induite, Stark shift optique, gain sans inversion, triplet de Mollow, dynamique, formation.

Contents

1 Introduction

The emergence of artificially tailored semiconductor nanostructures in the 70's and the new physical phenomena arising from the confinement of the carriers down to their de Broglie wavelength has provided a fantastic laboratory for the study of Coulomb correlations. Notably, Coulomb bound electron-hole pairs —excitons (X)— and their series of sharp resonances in the low-excitation spectra quickly turned out to be the most important source of optical nonlinearities in wide-gap materials and a direct probe of the many-body interaction occurring in semiconductors. For instance, in quantum wells, Fermi exclusion principle manifests through the renormalization of the exciton binding energy with increasing density (Haug and Schmitt-Rink, 1985; Chemla and Miller, 1985; Schmitt-Rink *et al.*, 1989) and higher-order exciton interactions yield two-exciton bound states —biexcitons (XX). Despite the strong Coulomb correlation that contribute to increasing the dephasing rate, the possibility to control excitons both optically and coherently (Heberle *et al.*, 1995) lead to the observation of the ac Stark coupling under excitation of a strong non-resonant optical pulse (Frohlich *et al.*, 1985; Von Lehmen *et al.*, 1986; Mysyrowicz *et al.*, 1986), Rabi flopping (Cundiff *et al.*, 1994; Deveaud *et al.*, 2001) and more recently electromagnetically induced transparency (EIT) (Ferrio and Steel, 1998; Phillips and Wang, 2002).

A major step was achieved in the development of semiconductor nanostructures with the arrival of modulation-doped heterostructures (Dingle *et al.*, 1978). During growth of such structures, the dopants are restricted to the barrier material so that they do not affect the mobility of the electronic gas formed in the quantum well. They ionize with the free carriers migrating to the lower-energy quantum wells and can form a high density electronic gas. Apart from having yielded some of the transistors with the smallest noise and the highest operating frequency of the market, this technique has allowed to study many-body phenomena that could not have been evidenced at lower electronic densities, notably the band-gap renormalization (Kleinman and Miller, 1985) and the Fermi edge singularity (Ruckenstein *et al.*, 1986). The observation of charged exciton – trions — by Kheng *et al.* (1993) has given rise to new

investigation. After the first controversy related to proper identification of the charged excitons, several important questions related to their properties were addressed. For example detailed studies were performed on the selection rules (Lovisa *et al.*, 1997; Kheng, 1995), dynamics (Finkelstein *et al.*, 1995; Vanelle *et al.*, 2000; Yonn *et al.*, 1996; Tribollet *et al.*, 2003), localization of charged exciton in quantum well (Brinkmann *et al.*, 1999; Wagner *et al.*, 1999; Yonn *et al.*, 1996), interaction between neutral and charged exciton states (Gilliot *et al.*, 1999; Brunhes *et al.*, 1999), laser action (Puls *et al.*, 2002), radiative time (Finkelstein *et al.*, 1998; Ciulin *et al.*, 2000a), localization, coherence and diffusion (Portella-Oberli *et al.*, 2002).

Still, little is known on the effect of the presence of an additional electron gas on nonlinearities in semiconductors, neither in the coherent regime, nor in the uncoherent one. It is however a topic of major interest for applications such as transport of light by a charged exciton (Sanvitto *et al.*, 2001) and for the quantum-information science (Nielsen and Chuang, 2000). Recent schemes for the implementation of quantum information processing devices in semiconductor nanostructures aim at marrying advantages of both spintronics and optoelectronics, using electrons as quantum memory and excitons for optical gating (Pazy *et al.*, 2003; Nazir *et al.*, 2004). Such an approach takes advantage of the slow electron spin decoherence (Tribollet *et al.*, 2003) and of the strong correlations between excitons (Pazy *et al.*, 2003; Feng *et al.*, 2004) as well as of the possibility to control them optically and coherently (Stievater *et al.*, 2001; Kamada *et al.*, 2001). Therefore, the optical and coherent generation and control of exciton correlations within a sea of electrons is a major milestone on the roadmap to quantum information devices.

This thesis work is an investigation of the dynamics of the nonlinearities in modulation-doped quantum wells. We first demonstrate through cw linear optical measurements (Chapter 3) that electrons scatter with excitons and trions, affecting profoundly the shape of their resonance; the high energy tail of both trion and exciton resonance is broadened and the exciton oscillator strength is reduced.

In pump and probe experiments (Chapter 4) in which we can selectively excite an exciton or a trion population, we demonstrate that, on one hand, due to exciton-electron collisions, a photogenerated exciton gas heats the electron gas. On the other hand, the trion creation process remove electrons from the quantum well and strongly reduce the scattering. Both excitons and trions resonance are therefore affected by electrons. We also evidence correlated behavior of excitons and trions under excitation which manifests itself by

crossed trion-exciton effects. We observe a wealth of phenomena encompassing bleaching, crossed bleaching, induced-absorption and energy shifts of the resonances. Significant differences are found between the nonlinear optical effects induced by an exciton and a trion population. We also evidence high-order exciton correlations, up to the fifth-order, in the presence of electrons.

We identify biexcitons and demonstrate their stability through coherent optical Stark measurements (Chapter 4). In the coherent regime, we prove that both ac Stark splitting with gain and electromagnetically induced transparency are observable within an electron gas, despite electron induced dephasing.

Finally, we show that the dynamics of exciton, trion and electron-hole plasma can be ruled by a simple rate equation model, in which we account for bimolecular formation of excitons from an electron-hole plasma, bimolecular formation of trions from excitons and free carriers and trimolecular formation from free carriers (Chapter 6).

2 Samples and Experimental Methods

In the present work, we selected two semiconductor quantum wells for their outstanding quality. We devised a strategy to populate those wells with electrons and control their population. The near-band gap optical spectra were consequently modified and exhibited notably a trion resonance below the exciton line. The first sample, a CdTe modulation-doped quantum well, featured well separated exciton and trion resonances. It was consequently used to investigate the optical properties of quantum wells within an electron gas (Chapter 3, 4 and 5). The second sample, a GaAs half microcavity, produced photoluminescence spectra with a signal over noise ratio so spectacular that the exciton, trion and electron-hole plasma signal could be measured at the same time. We used it to study the dynamics of trion formation from an electron-hole plasma.

This chapter describes consecutively samples and experiments performed on each sample.

2.1 Optical properties of the CdTe modulation-doped quantum well

2.1.1 Sample

Our most studied sample is a high quality, one-side modulation doped CdTe/$Cd_{0.27}Mg_{0.73}Te$ heterostructure (Wojtowicz *et al.*, 1998), containing a single CdTe quantum well of 8 nm (Fig. 2.1). A remote donor layer of iodine is embedded in the cap layer, 10 nm apart from the quantum well. Its thickness varies throughout the sample in four steps (19 Å, 29 Å, 49 Å and 80 Å). The steps are 11 mm long and labeled from A to D respectively. The electrons from the donors can either fall in the quantum well or be trapped by surface states, both process competing. Although more electrons get trapped by the surface states, an important electron concentration is obtained in the well. It varies

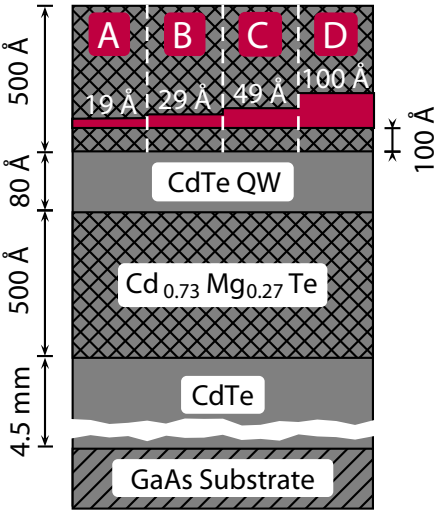

Figure 2.1: CdTe Sample.

step-likely from 3×10^{10} (step A) to 1.2×10^{11} cm^{-2} (step D). For a given step, additional control of the electron density can be achieved by illuminating the sample with light more energetic than the energy gap of the barrier, i.e. larger than 2.03 eV. In this case, electron-hole pairs are created in the barrier. Holes are attracted by electrons trapped in the surface states, while electrons are repelled towards the quantum well. By increasing the light intensity, the electron gas density can be increased. For step C, for instance, the practical electron concentrations range from 4.3×10^{10} cm^{-2} to 1.2×10^{11} cm^{-2}. Since dopants are embedded in the barrier, they do not interfere with the optical properties of the quantum well and a very high mobility is achieved.

At low temperature (< 35 K), two strong resonances separated by 3 meV arise below the band gap in the luminescence and reflectivity spectra. They are attributed to heavy hole excitons and negatively charged excitons. At 5 K (Fig. 2.2) they appear at 1625.7 meV and 1622.4 meV respectively. We will see in Chapter 3 that the reflectivity spectra are absorption-like and can be directly

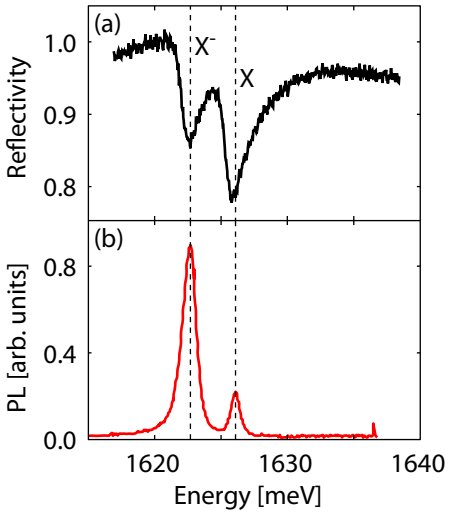

Figure 2.2: (a) Reflectivity and (b) photoluminescence spectra of the modulation-doped CdTe quantum well at 5 K on part C.

interpreted.

2.1.2 CW linear reflectivity experiments

We performed reflectivity measurements of the sample at 5 K. A white light source was spectrally filtered so that any high energy component (> 1.7 eV) likely to modify the density of the electron gas in the quantum well was suppressed. The light was collimated and focused on the sample. The reflection was then spectrally resolved by an imaging monochromator and recorded by a CCD camera. We kept the incident light intensity low and made sure we were working in a linear regime.

The light coming from a blue GaN light emitting diode (LED) was focused on the sample and completely covered the white light spot. By monitoring the intensity of the blue LED we could change the density of electrons in the well. The diffusion time of electrons from the barrier to the quantum well is macroscopic; it usually took from 5 s to 15 s for the system to reach an

equilibrium whenever the LED power was tuned. Reflectivity spectra were recorded for various electron densities. Results are presented and discussed in Chapter 3.

2.1.3 Pump and probe experiments

Pump and probe experimental setup. As both exciton and trion resonances are well separated, it is possible to excite solely one of them and create selectively excitons or trions. We performed spectrally and temporally resolved pump and probe experiments in reflectivity at 5 K (Fig. 2.3). The 100 fs spectrally broad output pulses of a Ti:Saphire laser were split into two: a small portion circulated through a delay line and probed both exciton and trion resonances, while the major portion passed through a pulse shaper to generate spectrally narrow tunable pulses of 0.3 meV (for 4 ps). This spectral resolution was adjusted so as to selectively pump a single resonance. Fig. 2.4(a) illustrates the case where the pump is tuned to the exciton resonance. Both pump and probe

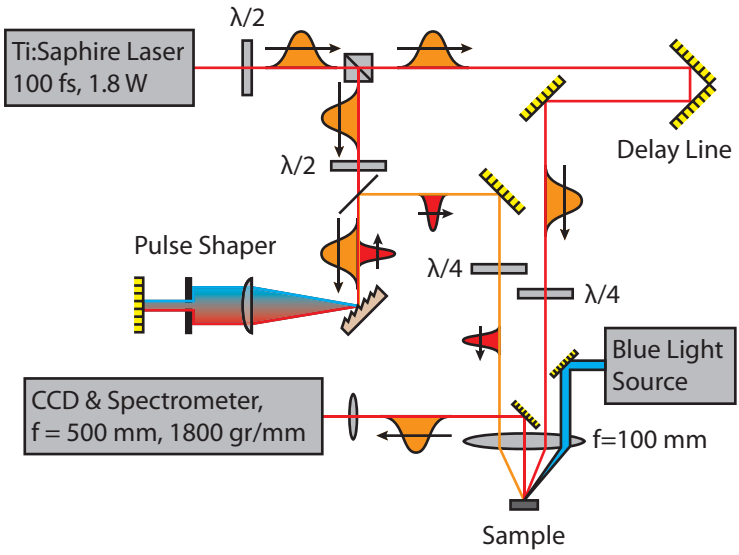

Figure 2.3: Pump and probe experimental setup.

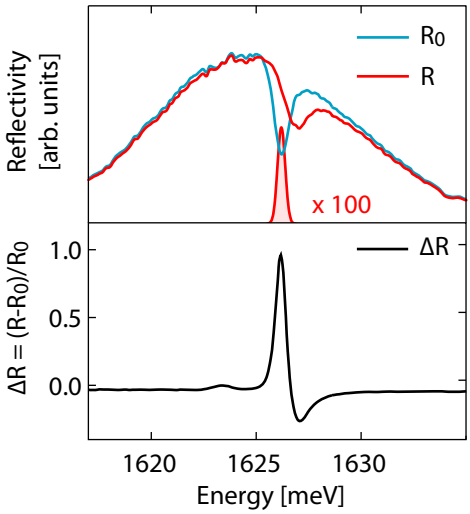

Figure 2.4: (a) Probe reflectivity spectra obtained without pump excitation (R_0) and with pump excitation (R). The pump (red filled spectrum) is tuned at the exciton resonance. These spectra were measured at 5 K on step B. Pump and probe were crossed-polarized with zero delay. (b) Differential spectrum $\Delta R = (R - R_0)/R_0$.

spectra are represented. The pump/probe intensity ratio was kept larger than 50 for all experiments so that probe reflectivity spectra remained linear in the probe field. The polarization of both pump and probe pulses could be chosen independently, allowing to investigate any possible relative polarization configurations, readily linear crossed-polarized, circularly co-polarized and circularly counter-polarized.

We recorded the reflectivity and differential reflectivity spectra[1] for various delay times between pump and probe pulses and various pump intensities (Fig. 2.3b). Results are presented in Chapter 4 (incoherent regime) and 5 (coherent regime).

[1] If R_0 is the reflectivity spectrum of the probe without the pump and R with the pump, the differential reflectivity is defined as $\Delta R = (R - R_0)/R_0$

Selection of a homogenous excitation region. The pump spot on the sample had a gaussian excitation profile inducing inhomogenous spatial non-linearities. Pump and probe spots had the same diameter ($\sim$ 50 μm) and were overlapping. After reflection, each spatial point of the probe carried on information corresponding to a different non-linear regime. We focused the probe on the entrance slit of a monochromator with a 500 mm lens (250 μm spot size). By narrowing the slit down to (25 μm) we were able to select only a vertical profile of the probe. The monochromator resolved spectrally each point of the profile on the slit and sent it to a 256 $\times$ 1024 pixels CCD camera. Each line of pixel on the CCD had a height of 25 μm and was corresponding to a homogenous region of excitation. We could advantageously probe different pump intensity regime in a single experiment by recording a full CCD image.

Electron density control. Unfortunately, no control of the electron density could be achieved by illuminating the sample with blue light in pump and probe experiments. The reason is not clearly identified, but it seams that the pump affects the electron control mechanism. The electron densities obtained with pump excitation were identical to the one obtained without blue light illumination no matter how strong we did illuminate the sample.

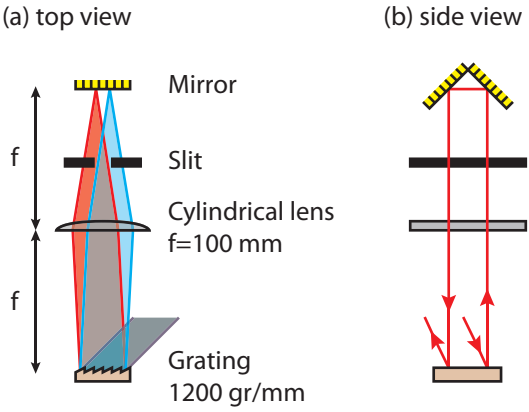

Figure 2.5: Pulse Shaper. (a) Top view. (b) Side view.

Pulse shaper. The principle of the pulse shaper is the following. A grating is placed in the focal plane of a cylindrical lens (Fig. 2.5). An incident laser is diffracted by the grating and goes trough the lens. Vertically, the laser beam is not modified. Horizontally, it is Fourier transformed by the lens. We image the laser spectrum in the Fourier plane of the grating. If we lower the image thanks to a periscope as shown in Fig. 2.5(b) and send it back through the lens-grating system, the outgoing laser beam is collimated back and perfectly identical to the incoming beam.

Now, if we placed a vertical slit in the Fourier plane and selected only a small part of the laser spectrum, the outgoing laser beam temporal profile would correspond to the Fourier transform of a square function, i.e. a sampling (sinc) function. The wavefront would not be gaussian but have small pre- and post-pulses. A quasi-Gaussian wavefront, can easily be obtained by placing the slit off the Fourier plane. The temporal artefact is blurred out and the outgoing laser practically become Gaussian, both spectrally and temporally. By adjusting the width of the slit, we can modify the spectral width of the laser and consequently the temporal width. The outgoing pulse is nearly Fourier transformed.

2.2 Optical properties of the GaAs quantum well

2.2.1 Sample

We have selected a particular sample, with a single $In_xGa_{1-x}As$ 80 Å quantum well ($x = 5\%$), because of its unequalled quality. This quantum well is embedded in the middle of a λ GaAs layer (λ corresponds to the wavelength of the quantum well excitonic resonance), which was grown over a 10 period distributed Bragg reflector. This distributed Bragg reflector allows to measure directly the absorption of the sample in the reflection configuration. It also increases the optical coupling of the quantum well, but does not disturb the shape of the observed photoluminescence spectrum, because the resonance mode has a spectral width of about 40 nm. Such a distributed Bragg reflector changes the radiative properties of free carriers (several percent according to Yokoyama (1992)), but does not affect their relaxation properties which will be studied in Chapter 6. The sample was grown by molecular beam epitaxy. Due to inevitable lateral flux inhomogeneities in the growth process, the thickness of all layers in the sample vary by several percent over the lateral dimensions of

the sample. We performed reflectivity spectroscopy to determine the spectral position of the cavity.

The sample is not modulation-doped, contrary to our CdTe quantum well. Without external excitation, its optical properties do not feature any charged exciton. Nevertheless, impurities were non-intentionally introduced in the GaAs barriers during the growth process, most probably carbon and silicon. With proper excitation energy $\hbar\omega$, we can control the electron density accumulated in the well, as shown in Fig. 2.6, where we compare the luminescence of the sample collected for $\hbar\omega$ = 1.5072 eV and $\hbar\omega$=1.5174 eV. Since the trion luminescence is affected by the concentration of charged carriers in the well, the relative trion/exciton intensity changes with the excitation energy (Fig. 2.6b). Electrons appear when the excitation energy exceeds the energy between ionized acceptors. The electrons excited to the conduction band may then be trapped into the quantum well. With increasing excitation energy one can transfer electrons from the valence band to ionized donors, thereby increasing the density of holes which then eliminate electrons (Fig. 2.6c). At $\hbar\omega$ = 1.5174 eV, we estimate the excess electron concentration from impurity concentration: $n_e = 10^{10}$ cm^{-2}.

The excess carriers trapped in the quantum well have a tunneling time back to the charge centers in the barriers several orders of magnitude longer than the 82 MHz repetition rate of the laser that will be used in our experiments to excite the sample. Therefore, even for a very weak photon density, the population of available acceptor states in the barrier is quickly fully depleted and, even under pulsed excitation, the saturation value of the carrier population in the well is reached.

The high quality of the sample was evidenced through optical measurements. We do not observe any Stokes shift between the absorption and photoluminescence of plasma, 1*s* and 2*s* excitons (Szczytko *et al.*, 2004b, 2005).

2.2.2 Time-resolved photoluminescence experiments

The measurements described in Chapter 6 have been carried out on a standard time-resolved photoluminescence setup where special care has been taken to ensure high imaging quality. This is crucial in optical measurements where the density plays an important role for the observed effects. In this respect and very similarly to what has been done in the pump and probe experiment (2.1.3), the setup and alignment has been optimized to collect light only from regions with homogenous excited pair density, i.e. from the central part of

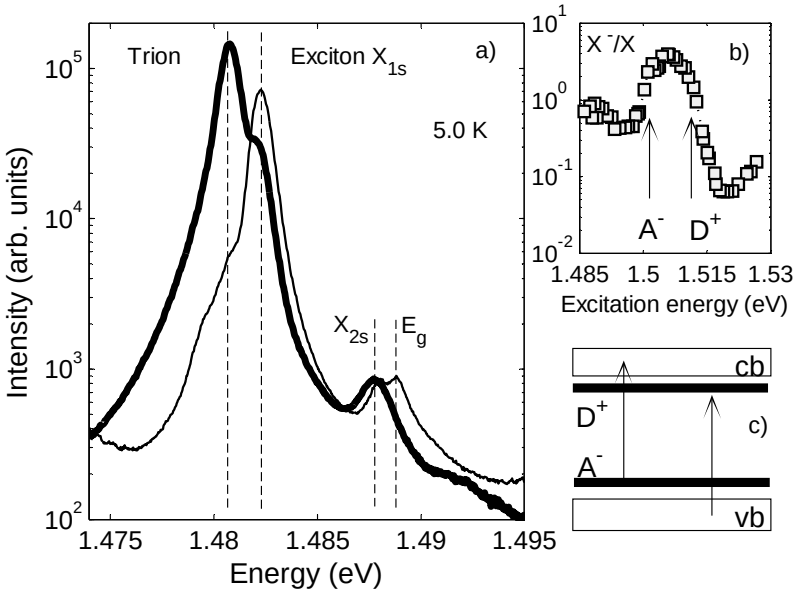

Figure 2.6: a) CW-luminescence collected for two different excitation energies: $\hbar\omega$ = 1.5072 eV (thick line) and $\hbar\omega$ = 1.5174 eV (thin line). The structures at 1.4807 eV, 1.4823 (1.4882 eV) and E_g = 1.4888 eV correspond respectively to the trion, heavy-hole exciton 1*s* (2*s*) and plasma transitions (all denoted by vertical dashed lines). b) The intensity ratio of the trion to exciton transitions as a function of the excitation energy. c) Schematic diagram of the electronic transitions from the ionized acceptors A^- to the conduction band *cb* and from the vallence band *vb* to the ionized donors D^+.

the excitation spot. The spatial filtering of the central spot region was done by means of imaging the sample surface on a pinhole (50 μm). The transmitted light was analyzed spectrally and temporally using a monochromator (1 meV resolution) and subsequent streak camera (3 ps resolution) in photocounting mode. The temporal resolution of the whole setup is limited to about 2030 ps, because of the spectral resolution of 0.1 meV.

The light excitation source was a Ti:Saphire laser (100 fs). In order to study the dynamics of the luminescence in different density domains, we performed our experiments with a variety of absorbed photon densities ($10^8 - 10^{10}$ cm^{-2}) at 5.0 K. The excitation energy were 1517.4 meV and 1507.2 meV, so that we could either work with zero or 10^{10} cm^{-2} excess electron concentration. Then, we recorded the time evolution of the exciton, trion and plasma luminescence intensities. We used spectra obtained under cw-excitation[2] to resolve the exciton and trion overlapping transitions. The experimental results are reported in Chapter 6.

[2]We subtract the pure exciton spectrum (1.5174 eV excitation) from the mingled spectrum (1.5072 eV excitation) and obtain the pure trion spectrum (Fig 2.6).

3 Linear Optical Properties of Modulation Doped Quantum Wells

'…down, down, until they disappeared into the very stone foundations of the building or into the earth, poured the harsh x rays, the trembling vectors of electric and magnetic fields, unimaginable to the human mind, or else the more comprehensible quanta that like shells out of guns pounded and riddled every thing in they path.'

(Aleksandr Isaevich Solzhenitsyn)

Past experimental studies have clearly pictured the linear optical properties of quantum wells in the presence of a moderate background electron density. They showed that the exciton resonance is strongly affected by the electron population. First of all electrons screen the excitons and reduce their oscillator strength (Chemla and Miller, 1985). Then, they fill up the conduction band and contribute to shift the exciton resonance towards higher energies (Huard *et al.*, 2000; Kossacki *et al.*, 1999; Yusa *et al.*, 2000). Finally they collide with excitons and broaden their absorption line (Huard *et al.*, 2000). Experimental comparison between exciton-electron and exciton-exciton scattering mechanism in bulk GaAs (Schultheis *et al.*, 1986), and in GaAs quantum wells (Honold *et al.*, 1989; Capozzi *et al.*, 1993), showed that the exciton-electron scattering efficiency is one order of magnitude larger than exciton-exciton process. Both scattering process are enhanced for the two-dimensional excitons as compared to bulk excitons.

Linear optical spectrum also feature a charged exciton resonance below the exciton resonance (Kheng *et al.*, 1993). Theoretical calculations of the binding energy of charged excitons were performed using variational (Stebe

and Stauffer, 1989; Thilagam, 1997; Stebe *et al.*, 1997) and full solution of the three-particle Schrödinger equation (Riva *et al.*, 2000; Esser *et al.*, 2000b). They showed that only the singlet state is bound in the absence of magnetic field. Considering the lineshape of the trion resonance, it was argued that the momentum of the electron initially present in a semiconductor and used in the absorption process of a trion yields a low-energy tail on the trion resonance (Suris *et al.*, 2001; Esser *et al.*, 2001). A simple derivation of the trion-electron scattering was also performed in GaAs quantum wells (Ramon *et al.*, 2003), but the overlap or the exciton and trion resonance did not allow to clear identify if such a simple model leads to correct predictions.

In this chapter, we investigate the effect of a two-dimensional electron gas on the optical properties of CdTe quantum wells. Due to the large separation between excitons and electrons, we are able to evidence the existence of a high-energy tail for both exciton and trion resonance. An electron-exciton and electron-trion scattering model, taking into account both elastic and inelastic scattering processes, show quantitative agreement with our results. These findings go in the direction of modern theory of excitons within an electron gas, that argue that a trion is intrinsically a many-body object, made of a hole, interacting with all electrons in the system (Combescot *et al.*, 2005).

This chapter is structured the following way. In Sec 3.1 we explain the principles of the transfer matrix formalism used to calculate the reflectivity of our sample. In Sec. 3.2, we review how the optical properties of the quantum well can be included in the calculation. In Sec. 3.3 we give an expression of the linear susceptibility for a quantum well that contains excitons and trions. Our experimental results are presented in Sec. 3.4, where we show that a calculation without electron scattering cannot possibly describe our system. Sec. 3.5 summarizes the exciton-electron and trion-electron calculation results that we performed. Finally, Sec. 3.6 demonstrates that linear optical spectra of modulation-doped quantum wells are quantitatively described by a matrix transfer calculation including both exciton- and trion-electron scattering.

3.1 Wave propagation in a stratified dielectric medium and transfer matrix formalism

The layered structure of our sample needs to be taken into account in order to consistently simulate the optical properties of the quantum well. Here we review

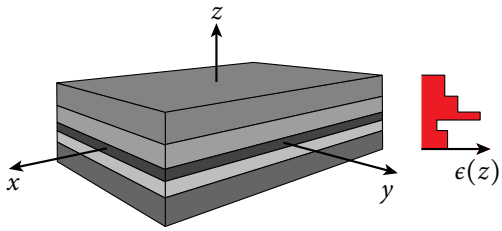

Figure 3.1: An example of a multilayered dielectric structure. The corresponding dielectric dispersion profile $\epsilon(z)$ is plotted on the right.

the transfer matrix formalism. We study the propagation of time-harmonic electromagnetic wave through a *stratified medium* comprising successive thin plane-parallel films. Each film consists of a homogeneous dielectric layer whose thickness and dielectric constant differ from film to film. The overall medium is neutral, nonconducting and nonmagnetic. A sketch of a sample structure is shown in Fig. 3.1, where the z-axis of a Cartesian reference system has been taken along the stratification direction. The time-harmonic electromagnetic wave is solution of the Maxwell equations in frequency-space (Jackson, 1999)

$$\begin{aligned} \nabla \cdot \boldsymbol{B}(\omega, \boldsymbol{r}_\parallel, z) &= 0, \\ \nabla \times \boldsymbol{E}(\omega, \boldsymbol{r}_\parallel, z) - i\omega \boldsymbol{B}(\omega, \boldsymbol{r}_\parallel, z) &= 0, \\ \nabla \cdot \boldsymbol{D}(\omega, \boldsymbol{r}_\parallel, z) &= \rho(\omega, \boldsymbol{r}_\parallel, z), \\ \nabla \times \boldsymbol{H}(\omega, \boldsymbol{r}_\parallel, z) + i\omega \boldsymbol{D}(\omega, \boldsymbol{r}_\parallel, z) &= \boldsymbol{J}(\omega, \boldsymbol{r}_\parallel, z), \end{aligned} \tag{3.1}$$

where the electric field $\boldsymbol{E}(\omega, \boldsymbol{r}_\parallel, z)$, the electric displacement $\boldsymbol{D}(\omega, \boldsymbol{r}_\parallel, z)$, the magnetic induction $\boldsymbol{B}(\omega, \boldsymbol{r}_\parallel, z)$ and the magnetic field $\boldsymbol{H}(\omega, \boldsymbol{r}_\parallel, z)$ are expressed in term of the frequency ω, the in-plane position vector $\boldsymbol{r}_\parallel$ and the position along the growth axis z.

We note that we do not loose generality by merely considering $\mathrm{e}^{i\omega t}$ time-dependent wave, because an arbitrary solution can be built any time by Fourier superposing equations 3.1. Considering that the dielectric layers are nonmagnetic — $\boldsymbol{H}(\omega, \boldsymbol{r}_\parallel, z) = \mu_0 \boldsymbol{B}(\omega, \boldsymbol{r}_\parallel, z)$ —, nonconducting — *the current density* $\boldsymbol{J}(\omega, \boldsymbol{r}_\parallel, z) = 0$ — and neutrally charged — *the charge density* $\nabla \rho(\omega, \boldsymbol{r}_\parallel, z) = 0$

—, Maxwell equations can be combined into a coupled equations for $\boldsymbol{E}$ and $\boldsymbol{D}$

$$\nabla^2 \boldsymbol{E}(\omega, \boldsymbol{r}_\parallel, z) - \frac{\omega^2}{\epsilon_0 c^2} \boldsymbol{D}(\omega, \boldsymbol{r}_\parallel, z) = 0. \tag{3.2}$$

We shall first solve this equation for a single homogenous dielectric film. Then we shall introduce transfer matrices and use them to express the propagation of electromagnetic wave at an interface between two consecutive films. Finally we will demonstrate how those matrices can be combined to calculate analytically the mode of the whole stratified medium.

3.1.1 Homogenous dielectric films

For a homogenous dielectric medium, the electric and displacement fields are linearly dependent $\boldsymbol{D}(\omega, \boldsymbol{r}_\parallel, z) = \epsilon(\omega)\boldsymbol{E}(\omega, \boldsymbol{r}_\parallel, z)$. Eq. (3.2) takes the form of a Helmholtz wave equation for $\boldsymbol{E}(\omega, \boldsymbol{r}_\parallel, z)$

$$\left(\nabla^2 + \frac{\omega^2}{c^2}\frac{\epsilon(\omega)}{\epsilon_0}\right)\boldsymbol{E}(\omega, \boldsymbol{r}_\parallel, z) = 0. \tag{3.3}$$

The dielectric dispersion $\epsilon(\omega)$ may very well be complex. Because it is constant, the electromagnetic field is invariant under in-plane translations (Bloch theorem) and solutions of (3.3) are plane-waves

$$\boldsymbol{E}_{\boldsymbol{k}_\parallel}(\omega, \boldsymbol{r}_\parallel, z) = \boldsymbol{\epsilon}_{\boldsymbol{k}_\parallel} u_{\boldsymbol{k}_\parallel}(\omega, z) \mathrm{e}^{i\boldsymbol{k}_\parallel \cdot \boldsymbol{r}_\parallel}. \tag{3.4}$$

Here $\boldsymbol{k}_\parallel$ is the in-plane wave vector and $\boldsymbol{\epsilon}_{\boldsymbol{k}_\parallel}$ the polarization vector. After substitution into (3.3), we are left with a one-dimensional problem for the mode function $u_{\boldsymbol{k}_\parallel}(\omega, z)$

$$\frac{\mathrm{d}^2 u_{\boldsymbol{k}_\parallel}(\omega, z)}{\mathrm{d}z^2} + \left(\frac{\omega^2}{c^2}\frac{\epsilon(\omega)}{\epsilon_0} - k_\parallel^2\right) u(\omega, z) = 0. \tag{3.5}$$

The solution represents two counter-propagating waves

$$u(\omega, \boldsymbol{k}_\parallel, z) = E_l(\boldsymbol{k}_\parallel)\mathrm{e}^{-ik_z z} + E_r(\boldsymbol{k}_\parallel)\mathrm{e}^{ik_z z}, \tag{3.6}$$

$$k_z = \sqrt{\frac{\omega^2}{c^2}\frac{\epsilon(\omega)}{\epsilon_0} - k_\parallel}. \tag{3.7}$$

The coefficient E_l and E_r are two complex coefficient that have to be determined by imposing Maxwell boundary conditions at the interface between adjacent layers. Let us note that if $\epsilon(\omega)$ is imaginary then k_z is imaginary as well and the solutions are evanescent waves.

3.1.2 Transfer matrix principle

In the framework of the one-dimensional problem (3.5) we define for each position z in space a two-dimensional vector containing the two coefficients in (3.6)

$$\boldsymbol{Q} = \begin{bmatrix} E_r \\ E_l \end{bmatrix}. \tag{3.8}$$

For a given structure, we would like to express the relation between coefficient vectors $\boldsymbol{Q}^{(1)}$ at z_1 and $\boldsymbol{Q}^{(2)}$ at z_2. Because Maxwell equations are linear,

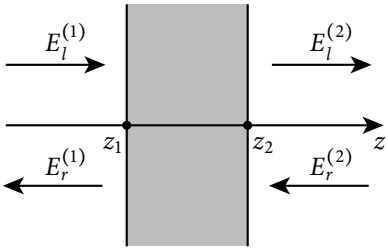

Figure 3.2: Electrical fields at the boundary z_1 and z_2 of a plane layer.

Maxwell boundary conditions will result in a linear relation, which we write as

$$\boldsymbol{Q}^{(2)} = \boldsymbol{M}\boldsymbol{Q}^{(1)}. \tag{3.9}$$

The 2×2 complex matrix $\boldsymbol{M}$ thus defined is called the *transfer* or *propagation matrix*. The most important property of transfer matrices is that they can be composed. Knowing the propagation matrix $\boldsymbol{M}_1$ from z_1 to z_2 and $\boldsymbol{M}_2$ from z_2 to z_3, the propagation matrix from z_1 to z_3 will be $\boldsymbol{M} = \boldsymbol{M}_2\boldsymbol{M}_1$. This procedure can be immediately generalized to the overall structure.

If z_1 and z_2 were to be found in the same homogenous layer, from (3.6) the transfer matrix would simply be

$$\boldsymbol{M}_{\text{hom}} = \begin{bmatrix} \mathrm{e}^{ik_z(z_2-z_1)} & 0 \\ 0 & \mathrm{e}^{-ik_z(z_2-z_1)} \end{bmatrix}. \tag{3.10}$$

The calculation of transfer matrices for more complicated problems might be difficult. We will now demonstrate that the transfer matrix of a given medium can simply be expressed in terms of its reflection and transmission coefficients.

3.1.3 Transfer matrix in terms of reflection and transmission coefficients

The Maxwell boundary conditions are invariant under time reversal. This means that the complex coefficient of a transfer matrix M do not change if we reverse the time evolution (Savona, 1999). Mathematically, we write this as

$$\boldsymbol{M} = \hat{T}\boldsymbol{M}\hat{T}^{-1}, \tag{3.11}$$

where $\hat{T}$ is the time reversal operator. We would like to calculate $\hat{T}\boldsymbol{Q}$. We remind that the amplitude of the electric field is given by the real part of its representation in terms of complex exponentials

$$E(\omega, \boldsymbol{k}_\parallel, \boldsymbol{r}_\parallel, z, t) = \Re\left[\left(E_l \mathrm{e}^{-ik_z z} + E_r \mathrm{e}^{ik_z z}\right) \mathrm{e}^{i\boldsymbol{k}_\parallel \cdot \boldsymbol{r}_\parallel} \mathrm{e}^{-i\omega t}\right].$$

The time reversal operator then acts as

$$\begin{aligned} \hat{T}E(\omega, \boldsymbol{k}_\parallel, \boldsymbol{r}_\parallel, z, t) &= E(\omega, \boldsymbol{k}_\parallel, \boldsymbol{r}_\parallel, z, -t) \\ &= \Re\left[\left(E_r^* \mathrm{e}^{-ik_z z} + E_l^* \mathrm{e}^{ik_z z}\right) \mathrm{e}^{-i\boldsymbol{k}_\parallel \cdot \boldsymbol{r}_\parallel} \mathrm{e}^{-i\omega t}\right]. \end{aligned}$$

Thus, $\widehat{T}$ reverse the sign of $\boldsymbol{k}_\parallel \to -\boldsymbol{k}_\parallel$ and acts on $\boldsymbol{Q}$ as

$$\widehat{T}\begin{bmatrix} E_r \\ E_l \end{bmatrix} = \begin{bmatrix} E_l^* \\ E_r^* \end{bmatrix}. \tag{3.12}$$

The time reversal invariance let us express the transfer matrix of a stratified medium in terms of its complex reflectivity and transfer coefficients. We consider the case of a unitary wave which is arriving on the left, reflected in

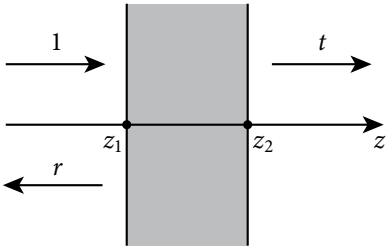

Figure 3.3: Electrical fields at the boundary z_1 and z_2 of a plane layer for a normalized incoming plane-wave.

the opposite direction with a wave amplitude r and transmitted to the right with an amplitude t. Then

$$\begin{bmatrix} t \\ 0 \end{bmatrix} = \begin{bmatrix} M_{11} & M_{12} \\ M_{21} & M_{22} \end{bmatrix} \begin{bmatrix} 1 \\ r \end{bmatrix} \tag{3.13}$$

By applying the time reversal operator $\hat{T}$ on both side of the equality we get a second system of equations

$$\begin{bmatrix} 0 \\ t^* \end{bmatrix} = \begin{bmatrix} M_{11} & M_{12} \\ M_{21} & M_{22} \end{bmatrix} \begin{bmatrix} r^* \\ 1 \end{bmatrix}. \tag{3.14}$$

Noting that in terms of r and t, the reflectivity and transmissivity are $R = |r|^2$ and $T = \alpha_{12}^{-1}|t|^2$ with

$$\alpha_{12} = \begin{cases} \Re\left[k_z^{(1)}\right] / \Re\left[k_z^{(2)}\right] & \text{for TE polarization} \\ \Re\left[k_z^{(1)}\right] n_2^2 / \Re\left[k_z^{(2)}\right] n_1^2 & \text{for TM polarization} \end{cases}, \tag{3.15}$$

we solve the system of linear equations (3.13) and (3.14) and obtain

$$M = \alpha_{12}^2 \begin{bmatrix} \dfrac{1}{t^*} & -\dfrac{r^*}{t^*} \\ -\dfrac{r}{t} & \dfrac{1}{t} \end{bmatrix}. \tag{3.16}$$

We can use Eq. (3.16) here above to calculate the transfer matrix at an interface between two homogenous layers (Born and Wolf, 1999). We obtain

the two transfer matrices for TE and TM polarization

$$\boldsymbol{M}^{\mathrm{TE}} = \alpha_{12}^{\mathrm{TE}} \begin{bmatrix} \dfrac{k_z^{(1)} + k_z^{(2)}}{2k_z^{(1)}} & \dfrac{k_z^{(1)} - k_z^{(2)}}{2k_z^{(1)}} \\ \dfrac{k_z^{(1)} - k_z^{(2)}}{2k_z^{(1)}} & \dfrac{k_z^{(1)} + k_z^{(2)}}{2k_z^{(1)}} \end{bmatrix} \tag{3.17}$$

and

$$\boldsymbol{M}^{\mathrm{TM}} = \alpha_{12}^{\mathrm{TM}} \begin{bmatrix} \dfrac{\epsilon^{(2)} k_z^{(1)} + \epsilon^{(1)} k_z^{(2)}}{2\sqrt{\epsilon^{(1)}\epsilon^{(2)}}\, k_z^{(1)}} & \dfrac{\epsilon^{(2)} k_z^{(1)} - \epsilon^{(1)} k_z^{(2)}}{2\sqrt{\epsilon^{(1)}\epsilon^{(2)}}\, k_z^{(1)}} \\ \dfrac{\epsilon^{(2)} k_z^{(1)} - \epsilon^{(1)} k_z^{(2)}}{2\sqrt{\epsilon^{(1)}\epsilon^{(2)}}\, k_z^{(1)}} & \dfrac{\epsilon^{(2)} k_z^{(1)} + \epsilon^{(1)} k_z^{(2)}}{2\sqrt{\epsilon^{(1)}\epsilon^{(2)}}\, k_z^{(1)}} \end{bmatrix}. \tag{3.18}$$

These expression are quite general and are valid for complex dielectric constants as well. Combining those two matrices with the propagation matrix (3.10) we are able to calculate the electromagnetic modes in any multilayered structure.

3.2 Optical wave in quantum wells

The optical properties of excitons in quantum wells have been derived for homogenously (Tassone *et al.*, 1990, 1992) and inhomogeneously broadened resonances (Andreani *et al.*, 1998). Building on previous work, we propose a more general derivation that is valid for any kind of optical resonance (exciton, trion), as long as we know the linear susceptibility of the quantum well.

The transfer matrix approach introduced in the previous section presumes that the material is described by a frequency-dependent complex dielectric tensor $\epsilon(\omega)$. Close to a resonance, this is not valid any more (Hyzhnyakov *et al.*, 1975) and the displacement field $\boldsymbol{D}(\omega, \boldsymbol{k}_\parallel, z)$ of an inhomogenous material with translational symmetry broken in the z-direction does not depend on the value of the electric field only at the point z, but rather on an average of the electric field over a certain small volume centered at z (Mills and Burnstein, 1974). A *spatial dispersion* occurs and the general form of the displacement field can be expressed in terms of the nonlocal susceptibility $\epsilon(\omega, \boldsymbol{k}_\parallel, z, z')$ as

$$\boldsymbol{D}(\omega, \boldsymbol{r}_\parallel, z) = \int_{-\infty}^{\infty} \mathrm{d}z'\, \epsilon(\omega, \boldsymbol{k}_\parallel, z, z')\boldsymbol{E}(\omega, \boldsymbol{r}_\parallel, z'). \tag{3.19}$$

This means that if we want to account for a particular resonance in the quantum well, we have to solve Eq. 3.2 with the displacement field 3.19. We assume that the susceptibility $\epsilon(\omega, \boldsymbol{k}_\parallel, z, z')$ can be written as

$$\epsilon(\omega, \boldsymbol{k}_\parallel, z, z') = \begin{cases} \epsilon(\omega)\,\delta(z-z') & \text{in the barrier} \\ \epsilon(\omega)\,\delta(z-z') + \chi_{QW}(\omega, \boldsymbol{k}_\parallel, z, z') & \text{in the well} \end{cases} \tag{3.20}$$

with

$$\chi_{QW}(\omega, \boldsymbol{k}_\parallel, z, z') = \chi_{QW}(\omega, \boldsymbol{k}_\parallel)\rho(z)\rho(z') \tag{3.21}$$

where $\rho(z) = \zeta_e(z)\zeta_h(z)$ is the product of the confinement functions for electrons and holes in the well. The confinement functions will be defined in a later chapter (6.7). An explicit expression for the dielectric susceptibility of the quantum well $\chi_{QW}(\omega)$ will be given later. We assumed the same homogenous local background dielectric dispersion $\epsilon(\omega)$ for the quantum well and the barriers. This is clearly not the case, but interface transfer matrices (3.17 and 3.18) can be applied a posteriori to our result.

We propose to first solve Eq. 3.2 for a quantum well of with width L when TE polarized light propagates in the barrier. The electric field is along the y-axis and (3.2) becomes

$$(\partial_z^2 + k_z^2)E_y + k^2\chi(\omega)\rho(z)\int_{-L/2}^{L/2} \mathrm{d}z'\,\rho(z')E_y(z') = 0 \tag{3.22}$$

with $k = \sqrt{\epsilon(\omega)/\epsilon_0}\,\omega/c$. As $\rho(z)$ is even for optical allowed transitions, it is convenient to treat separately solutions of the problem with definite parity under inversion of the z coordinate.

For odd E_y symmetry, the integral in 3.22 is zero and there is no polarization contribution from the quantum well. The reflectivity takes the simple form

$$r_{\mathrm{TE}}^{(\mathrm{odd})} = -e^{ik_z L}. \tag{3.23}$$

For even E_y symmetry, the solution of the second order differential equation (3.22) is

$$E_y = A(\omega, k_z)\cos(k_z z) + \int \mathrm{d}z'\,G(z, z')\rho(z'). \tag{3.24}$$

In this expression, the first term is the general even solution of the problem $(\partial_z^2 + k_z^2)E_y = 0$, with $A(\omega, k_z)$ a constant to be determined. The second term is a particular solution of (3.22) and was simply built from the definition of the Green function $(\partial_z^2 + k_z^2)G(z, z') = \delta(z - z')$. We choose

$$G(z, z') = -\frac{1}{2k_z}\sin(k_z|z - z'|) \tag{3.25}$$

which has the advantage to yield an even solution of E_y. Replacing (3.24) into (3.22) gives

$$A(\omega, k_z) = \chi(\omega)^{-1} - P(k_z)/Q(k_z) \tag{3.26}$$

$$Q(k_z) = \int_{-L/2}^{L/2} \mathrm{d}z\, \rho(z)\cos(k_z z) \tag{3.27}$$

$$P(k_z) = \int_{-L/2}^{L/2}\int_{-L/2}^{L/2} \mathrm{d}z\,\mathrm{d}z'\, \frac{1}{2k_z}\sin(k_z|z - z'|)\rho(z)\rho(z') \tag{3.28}$$

We consider Maxwell boundary condition at the interface $z = -L/2$. On the left side of the quantum well, we know that there are two counter-propagating plane waves propagating in the barrier given by Eqs. 3.4 and 3.6. The Maxwell boundary conditions give

$$\begin{aligned}
&(E_y^{(l)} + E_y^{(r)})\big|_{z=-L/2^-} = E_y\big|_{z=-L/2^+} \\
&\partial_z(E_y^{(l)} + E_y^{(r)})\big|_{z=-L/2^-} \\
&\qquad = ik_z(E_y^{(l)} - E_y^{(r)})\big|_{z=-L/2^-} = \partial_z E_y\big|_{z=-L/2^+}
\end{aligned} \tag{3.29}$$

Substituing Eq. 3.24 in those two equation, we obtain the reflectivity for the even solution:

$$\begin{aligned}
r_{\mathrm{TE}}^{(\mathrm{even})} = \frac{E_y^{(r)}}{E_y^{(l)}} &= \left.\frac{E_y - \frac{1}{ik_z}\partial E_y}{E_y + \frac{1}{ik_z}\partial E_y}\right|_{z=-L/2^+} = e^{ik_z L}\frac{A(\omega, k_z) - iQ(k_z)/2k_z}{A(\omega, k_z) + iQ(k_z)/2k_z} \\
&= e^{ik_z L}\frac{1 - \chi(\omega, k_z)(i\alpha(k_z) + P(\omega, k_z))}{1 + \chi(\omega, k_z)(i\alpha(k_z) - P(\omega, k_z))}
\end{aligned} \tag{3.30}$$

where $\alpha(k_z) = Q(k_z)^2/2k_z$. The total reflectivity is given by the mean of the odd 3.23 and even reflectivity 3.30:

$$r_{\mathrm{TE}} = \tfrac{1}{2}\left(r_{\mathrm{TE}}^{(\mathrm{even})} + r_{\mathrm{TE}}^{(\mathrm{odd})}\right) = \frac{-i\alpha(k_z)\chi(\omega, k_z)e^{ik_z L}}{1 + \chi(\omega, k_z)(i\alpha(k_z) - P(\omega, k_z))} \tag{3.31}$$

The same kind of calculation apply for the transmissivity, which reads

$$t_{\mathrm{TE}} = \tfrac{1}{2}\left(t_{\mathrm{TE}}^{(\mathrm{even})} - t_{\mathrm{TE}}^{(\mathrm{odd})}\right) = \frac{(1 - P(\omega, k_z)\chi(\omega, k_z))e^{ik_z L}}{1 + \left[i\alpha(k_z) - P(\omega, k_z)\right]\chi(\omega, k_z)} \tag{3.32}$$

If we now suppose that the quantum well has an infinite potential, the calculation of α and P functions becomes trivial. We obtain $\alpha \to 1$ and $P \to 0$. We are left with the simple reflectivity and transmissivity

$$r_{\mathrm{TE}} = e^{ik_z L}\frac{-i\chi(\omega, k_z)/2k_z}{1 + i\chi(\omega, k_z)/2k_z} \tag{3.33}$$

$$t_{\mathrm{TE}} = e^{ik_z L}\frac{1}{1 + i\chi(\omega, k_z)/2k_z} = 1 + r_{\mathrm{TE}} \tag{3.34}$$

When used in Eq. 3.16, these two expressions give the transfer matrix of a quantum well. The only information that is required to simulate the linear optical spectrum of our quantum well is the susceptibility.

3.3 Linear Susceptibility in modulation-doped quantum wells

In order to be able to calculate the transfer matrix of the quantum well, we need to write an expression for the susceptibility. As a starting point, we chose to use the linear susceptibility proposed by Esser *et al.* (2001) in the framework of density matrix theory. It includes both exciton and trion contributions, has a rather simple form and takes into account the non zero momentum of the excess electron in the quantum well used in the process of trion photogeneration. We emphasize that it neglects any scattering with the electrons. It reads

$$\chi(\omega) = \chi^X(\omega) + \chi^T(\omega), \tag{3.35}$$

where $\chi^X(\omega)$ and $\chi^T(\omega)$ are the contributions to the exciton and trion susceptibility. They are given by

$$\chi^X(\omega) = f_X \frac{|\phi_X(0)|^2}{\omega - \omega_X - i\gamma_X}, \tag{3.36}$$

$$\chi^T(\omega) = f_T \int \mathrm{d}\boldsymbol{q}\, n_e(\boldsymbol{q}) \frac{|M^T(\boldsymbol{q})|^2}{\omega - \omega_T + W_{\boldsymbol{q}} - i\gamma_T}. \tag{3.37}$$

	a	b	c	d	s	R_0
X^-	1.1723	0.5471	0.4809	0.0682	0.0013	1.1614
X^+	1.1774	0.4294	2.3943	0.08431	0.26173	0.7393

Table 3.1: Variational parameters for Sergeev and Suris' trion variational function

where ω_X (ω_X) is the exciton resonance energy, f_X (f_T) a contribution to the exciton (trion) oscillator strength, and γ_X (γ_T) the exciton (trion) homogenous broadening mainly due to phonons; $n_e(\boldsymbol{q})$ is the Fermi-Dirac distribution of the electrons and $W_{\boldsymbol{q}} = \hbar^2 q^2 M_X / 2 m_e M_T$ is a correction to the trion resonance that comprises trion c.o.m. energy and electron initial momentum $\boldsymbol{q}$, with m_e, M_X and M_T the electron, exciton and trion effective mass, respectively. For a given initial electron momentum, the strength of the integrant is weighted by the optical matrix element

$$M^T(\boldsymbol{q}) = \int \mathrm{d}\boldsymbol{\rho}_2 \, \psi_{1s}^T(0, \boldsymbol{\rho}_2) e^{i\eta \boldsymbol{q}\boldsymbol{\rho}_2} \tag{3.38}$$

where $\eta = M_X/M_T$ and $\psi_{1s}^T(\boldsymbol{\rho}_1, \boldsymbol{\rho}_2)$ is the trion 1s wavefunction, with $\boldsymbol{\rho}_1 = \boldsymbol{r}_{1e} - \boldsymbol{r}_h$ the relative position of the first electron to the hole and $\boldsymbol{\rho}_2 = \boldsymbol{r}_{2e} - \boldsymbol{r}_h$ from the second electron to the hole.

For the trion wavefunction, we relied on a simpler variational function (Sergeev and Suris, 2001), given by

$$\psi_T(\boldsymbol{\rho_1}, \boldsymbol{\rho_2}) = \left(e^{-a\rho_1 - b\rho_2} + e^{-a\rho_2 - b\rho_1}\right)(1 + cR) \frac{e^{-sR}}{1 + d(R - R_0)} \tag{3.39}$$

where $\boldsymbol{R} = \boldsymbol{r}_{1e} - \boldsymbol{r}_{2e}$. The variational parameters a, b, c, d, s, R_0 were obtained by fitting the numerical solution of the Schrödinger equation (Esser *et al.*, 2000b). They are given in Table 3.1 for both positive and negative trion in units of the bulk CdTe bulk Bohr radius (7.75 nm). The overlap with the numerical wave function is excellent (0.9981 for X^-).

Even if this variational function is analytical, its Fourier transform is not. To speed up calculations, we resorted to a simpler Chandrashekar's wave function (Chandrasekhar, 1944) with only two variational parameters λ = 6.8 nm and $\lambda' = 15$ nm. It is given by

$$\psi_T(\rho_1, \rho_2) = \mathcal{N}_T \left(e^{\rho_1/\lambda - \rho_2/\lambda'} + e^{\rho_1/\lambda' - \rho_2/\lambda} \right), \tag{3.40}$$

Where $\mathcal{N}_T$ is the normalization factor. With this approximation, the light coupling element $M(\boldsymbol{q})$ becomes

$$M_T(\boldsymbol{q}) = 4\mathcal{N}_T \left(\frac{\lambda_T}{\lambda'_T} \frac{1}{(1+(\lambda_T \boldsymbol{k})^2)^{3/2}} + \lambda_T \leftrightarrow \lambda'_T \right). \tag{3.41}$$

We evaluated the error induce by using the Chandrashekar's wavefunction. In Fig. 3.4, we compare the result obtained with variational functions 3.39 and 3.40. They do not differ much and we conclude that Eq. 3.41 is a reliable approximation.

Exciton and trion resonance may also be inhomogenously broadened, due to quantum well interface roughness. Building on Andreani *et al.* (1998) work, we supposed that the broadening can be described by a Gaussian distribution function. Thus, for excitons, we substituted the dielectric susceptibility (3.36)

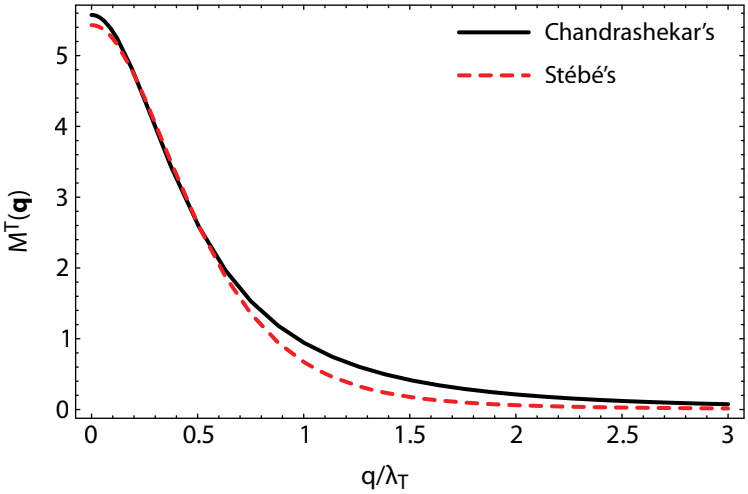

Figure 3.4: Trion optical coupling as a function of the momentum $\boldsymbol{q}$ of the initial electron.

by the convolution function

$$\widetilde{\chi}^X(\omega) = \frac{1}{\sqrt{\pi}} \int \mathrm{d}\nu\, \chi^X(\omega - \nu) \exp\left[-\left(\frac{\nu - \omega_X}{\Gamma^X_{\mathrm{inhom}}} \right)^2 \right]$$
$$= \frac{i\pi f_X |\phi_X(0)|^2}{\Gamma^X_{\mathrm{inhom}}} w\left(\frac{\omega - \omega_X - i\gamma_X}{\Gamma^X_{\mathrm{inhom}}} \right), \tag{3.42}$$

where w is the complex error function (Schreier, 1992) and $\Gamma^X_{\mathrm{inhom}}$ the exciton inhomogenous broadening constant. For trions the same kind of equation holds, except the convolution is performed before integrating over $\boldsymbol{q}$:

$$\widetilde{\chi}^T(\omega) = \frac{i\pi f_T}{\Gamma^T_{\mathrm{inhom}}} \int \mathrm{d}\boldsymbol{q}\, n_e(\boldsymbol{q}) |M^T(\boldsymbol{q})|^2 w\left(\frac{\omega - \omega_T + W_{\boldsymbol{q}} - i\gamma_T}{\Gamma^T_{\mathrm{inhom}}} \right) \tag{3.43}$$

3.4 Experimental Results

We performed the CW reflectivity experiments described in the previous chapter (Sec. 2.1.2). Fig. 3.5 shows the reflectivity spectra obtained for different electron densities. For increasing electron densities, we clearly observe a blue shift of the exciton resonance as reported in the literature (Huard *et al.*, 2000; Kossacki *et al.*, 1999; Yusa *et al.*, 2000). It is due to the filling of the conduction band by electrons. Electron-hole pairs can only be photo-generated above the Fermi level. To a good approximation, the shift is linear in the Fermi energy E_F. Thus the exciton-trion energy difference is given by

$$E = E_0^T + \alpha E_F, \tag{3.44}$$

where E_0^T is the trion binding energy and α is an empirical parameter. For CdTe quantum wells, $\alpha = 1.07$ (Huard *et al.*, 2000). Assuming that $E_0^T = 1.7$ meV, Eq. 3.44 was used to estimate the electron concentrations in the quantum well for each spectrum in Fig. 3.5. The densities that we obtained range from 4.3×10^{10} cm^{-2} to 1.7×10^{11} cm^{-2}.

Using the transfer matrix formalism described previously in this chapter, we calculated the mode of the field for our sample structure. The refractive index and absorption of the CdMgTe barriers (Choi *et al.*, 1997; Andre and Dang, 1997), CdTe quantum well[1], CdTe buffer (Benhlal *et al.*, 1999; Hlidek

[1] Régis André in Grenoble, measured a CdTe quantum well index of 4 (private communication).

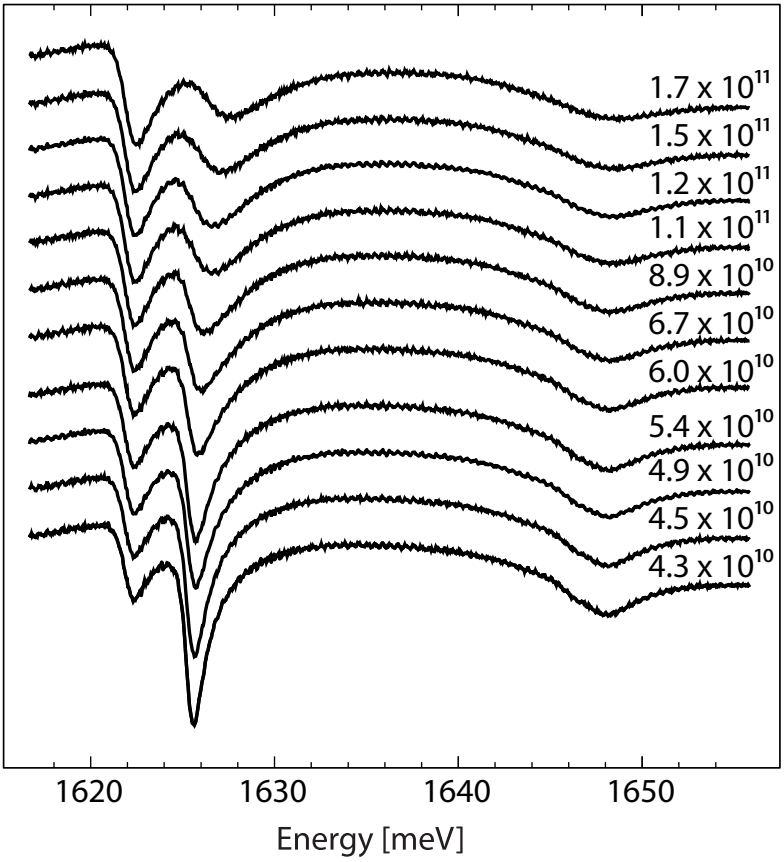

Figure 3.5: CW reflectivity spectra obtained at 5 K for different electron densities ranging from 4.3×10^{10} cm^{-2} to 1.7×10^{11} cm^{-2}.

et al., 2001), GaAs substrate and iodine dopant were all implemented. For each resonance, we used the following fitting parameters: spectral position, oscillator strength, homogenous linewidth and inhomogeneous linewidth. We fitted three densities: 4.9×10^{10}, 6.7×10^{10}, 1.2×10^{11} cm^{-2}. Results are shown in Fig. 3.6 and the value of the corresponding fitting parameters in Table 3.2.

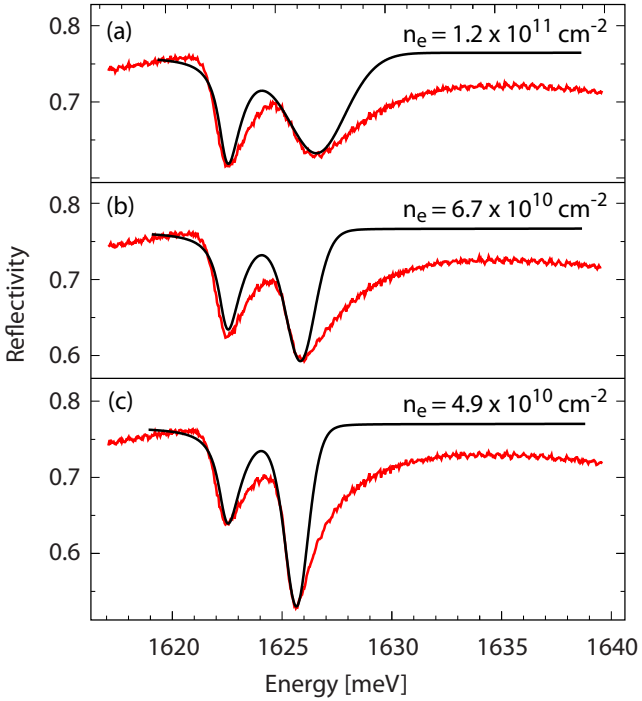

Figure 3.6: CW reflectivity spectra measured at 5 K and for electron densities of 4.9×10^{10}, 6.7×10^{10} and 1.2×10^{11} cm^{-2}. We show the best fit obtained.

From the fits in Fig. 3.6, we see that it is impossible to reproduce both low energy and high energy tail of exciton and trion resonance because of their strong asymmetry.

The high-energy tail of the exciton resonance is commonly acknowledge in the literature and attributed to electron-exciton collisions (Honold *et al.*, 1989; Capozzi *et al.*, 1993). Since we did not take them into account in our susceptibility, we obviously cannot reproduce the correct lineshape for the exciton. As for the high-energy broadening of the trion line, it has, to our knowledge, not been reported yet. We note that in our experiment, the low-energy tail of the trion resonance predicted by Esser *et al.* (2002) is marginal

	n_e [cm^{-2}]	E [meV]	Γ_{hom} [meV]	Γ_{inhom} [meV]
X	4.9×10^{10}	1623.9	0.25	0.1
X	6.7×10^{10}	1624.1	0.15	0.1
X	1.2×10^{11}	1624.4	0.10	0.1
X^-	4.9×10^{10}	1621.9	0.2	0.05
X^-	6.7×10^{10}	1621.9	0.3	0.05
X^-	1.2×10^{11}	1622.1	0.3	0.10

Table 3.2: Fitting parameters of the reflectivity spectra for three electron densities n_e. f is proportional to the exciton (trion) oscillator strength. The homogenous broadening Γ_{hom} is essentially due to phonon interaction and corresponds to γ_X for excitons and γ_T for trions (see Eq. 3.36 and 3.37). The inhomogenous broadering is defined in Eqs. 3.42 and 3.42.

and can be fairly well reproduced by our fit. In the next section, we will propose a model of trion-electron interaction that will perfectly explain the high-energy broadening.

3.5 Neutral and charged exciton scattering with electrons

A complete theory of neutral and charged exciton electron scattering has been proposed by Ramon *et al.* (2003). They investigated both elastic and inelastic scattering in GaAs quantum wells. They were able to fit the high energy line shape of excitons, but failed to check the validity of their result on the high energy tail of trions because in GaAs, at low temperature, exciton and trion lines are not well separated.

We applied their method to calculate the linewidth broadening due to the exciton-electron scattering in our CdTe quantum well. Here, we summarize the principles and show the results.

Exciton-electron scattering An electron of momentum $\boldsymbol{k}_e$ can interact elastically with an exciton $\boldsymbol{k}_X$. In that case, a momentum $\boldsymbol{q}$ is transferred from the electron to the exciton

$$(\boldsymbol{k}_X, \boldsymbol{k}_e) \longrightarrow (\boldsymbol{k}_X + \boldsymbol{q}, \boldsymbol{k}_e - \boldsymbol{q}). \tag{3.45}$$

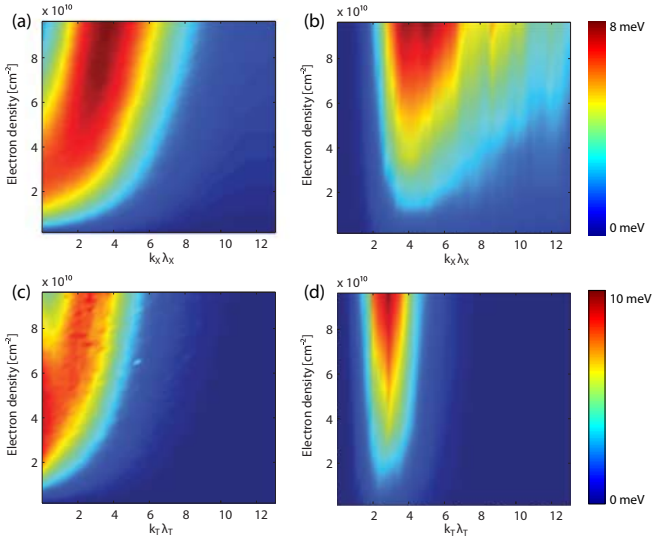

Figure 3.7: Top row: exciton-electron (a) elastic and (b) inelastic scattering. Bottom row: trion-electron (c) elastic and (d) inelastic scattering.

In the process, the electron bound in the exciton can be exchanged with the free electron. The exchange scattering matrix element is very strong compared to direct Coulomb interaction. Using Fermi's golden rule, it is possible to calculate the scattering rate of the process 3.45. Summing over all final exciton states, results — in the first Born approximation — in the exciton linewidth $\Gamma_{X-e}^{\text{elastic}}(k_X)$ due to elastic scattering, as a function of its initial momentum.

Fig. 3.7(a) shows the computed values of $\Gamma_{X-e}^{\text{elastic}}(\boldsymbol{k}_X)$ as a function of the exciton initial energy and the electron density. The large linewidth obtained for relatively low electron density reflects the high efficiency of the electron-scattering mechanism. This should be compared to an exciton linewidth of $\sim$ 0.1 meV for acoustic phonon scattering at T=5 K. It is explained by the exciton-electron interaction matrix elements that favor small energy-transfer transitions. At higher densities the effect of the phase-space filling becomes noticeable and effectively enlarges the exciton Bohr radius. Increasing the electron density further results in a shift of the maximum linewidth from

$k_X = 0$ to higher momenta.

During the scattering process, the exciton can also ionized into a free electron-hole pair. The exciton linewidth $\Gamma_{X-e}^{\text{inelastic}}(\boldsymbol{k}_X)$ due to this inelastic scattering is represented in Fig. 3.7(b). Although the magnitude of $\Gamma_{X-e}^{\text{inelastic}}(kx)$ is of the same order as $\Gamma_{X-e}^{\text{elastic}}(kx)$, its functional dependence on the exciton in-plane momentum is very different. In particular, we note that the maximal linewidth is obtained at a very large momentum. This is due to the fact that in order for an exciton with initially small k_X to be ionized, it must scatter on an electron with energy large enough to overcome its binding energy. At zero temperature this is only possible above the Fermi energy.

The two scattering processes that we described above contribute to admix states with $k_X > 0$ to the $k_X = 0$ state. This admixture can be easily included in our previous calculation of the absorption by convoluting the imaginary part of the exciton susceptibility (3.36) with a Lorentzian function whose broadening is given by the sum $\Gamma_{X-e}(k_X) = \Gamma_{X-e}^{\text{elastic}}(k_X) + \Gamma_{X-e}^{\text{inelastic}}(k_X)$ (Fig. 3.8). It becomes

$$\text{Im}\left[\chi_{QW}(\omega)\right] = \int_0^\infty \mathrm{d}\omega' \,\text{Im}\left[\chi_X(\omega - \omega')\right] \mathscr{L}(\omega', \Gamma_{X-e}(\omega')) \quad (3.46)$$

Use of the Kramers-Kronig relations yields the real part of the dielectric function. Since $\Gamma_{X-e}(k_X)$ is a decreasing function of k_X, the Lorentzian peak is shifted to higher exciton energies. This is seen as the electron density increases.

Trion-electron scattering For trions, the charge of the trion results in a divergence of its matrix elements in the limit of zero transferred momentum. This divergence, originating from the infinite range of the Coulomb potential, is treated by applying the Lindhard model for the potential screening. We use the Chandrashekar's variational function introduced above to perform the calculation. As for excitons, the broadening comes from direct and exchange scattering. The broadening $\Gamma_{X^- - e}(k_T)$ obtained is shown in Fig. 3.7c.

3.6 Electron scattering corrections

Using the CdTe exciton-electron and trion-electron scattering calculation performed in the previous section, we were able to fit the three cw reflectivity spectra considered in Fig. 3.6. For each resonance (exciton and trion), the free parameters were the spectral line position, the oscillator strength, the

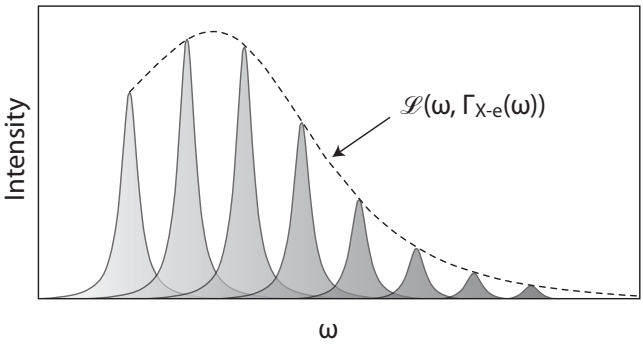

Figure 3.8: A schematic picture of the convolution resulting from electron scattering. The solid lines represent various exciton initial line shapes $\mathrm{Im}(\chi_Q W(\omega - \omega'))$. The contributions of states with $k_X > 0$ to the $k_X = 0$ state are weighted by the value of the Lorentzian function $\mathscr{L}_{x-e}[\omega, \Gamma_{x-e}(\omega)]$, given by the dashed line

electron density, the homogenous and the inhomogeneous linewidth. The fits are shown in Fig. 3.9 and the parameters of the fit in Table 3.3.

The fits we obtained are exceptionally good. Only a very small inhomogenous broadening had to be included, which is consistent with the high quality of our quantum well. The homogenous broadening γ_X and γ_T attributed to phonons remained quite small and more or less constant over the densities. This shows that we accounted for almost all electron induced broadening in our simple model. Had it been perfect, we would have expected the exciton and trion energy parameters to stay constant for all densities. Unfortunately, we could not get a perfect match of the spectrum lineshape by keeping the shift constant. Our model accounts for part of the shift but not all. We remind that it is a simple first order perturbation model and that we might expect higher order contributions to play a role. The density obtained remained quite close to those calculated with a simpler model in Sec. 3.4.

As for the oscillator strength, not much can be said, since we did not include any dependence on the electron density in our model. We did so intentionally because current theoretical models conclude that the trion oscillator strength depends on the volume of the sample (Esser *et al.*, 2002). We think

	n_e [cm^{-2}]	E [meV]	Γ_{hom} [meV]	Γ_{inhom} [meV]
X	4.9×10^{10}	1623.9	0.25	0.1
X	6.7×10^{10}	1624.1	0.20	0.05
X	1.2×10^{11}	1624.4	0.20	0.05
X^-	4.9×10^{10}	1621.9	0.2	0.05
X^-	6.7×10^{10}	1621.9	0.3	0.05
X^-	1.2×10^{11}	1622.1	0.3	0.10

Table 3.3: Fitting parameters

that it is a failure of the three-particle oversimplified trion model which is, strictly speaking, only correct in quantum dots. A correct description of the trion resonance should take into account the interaction of the excitons with all electron in the system. Such approach seems to lead to trion oscillator strength that do not depend on the volume (Dupertuis, 2006).

3.7 Conclusion

We conclude by some general remark on the validity of our model. Although it is surprisingly good at predicting the lineshape of the optical spectrum we resorted to strong approximations. First, we did not consider screening of excitons by electrons, but it was proved not be of much importance (Ramon *et al.*, 2003). Then the kinetic energy of the exciton was neglected, which may be of some importance (Rochat *et al.*, 2000). Finally we used a mean field theory that may eventually fail. Our results show that these three assumptions, that are the current subject of much debate, do not dramatically influence quantitative predictions on the linear optical spectrum in modulation-doped quantum wells. Theoretical work should then focus on the description of the oscillator strength intensity ratio between excitons and trions.

As far as we are concerned, we demonstrated that electrons play an important role on both exciton and trion resonance. This will be fundamental for the interpretation of the non-linear properties of modulation-doped quantum wells in the next chapter.

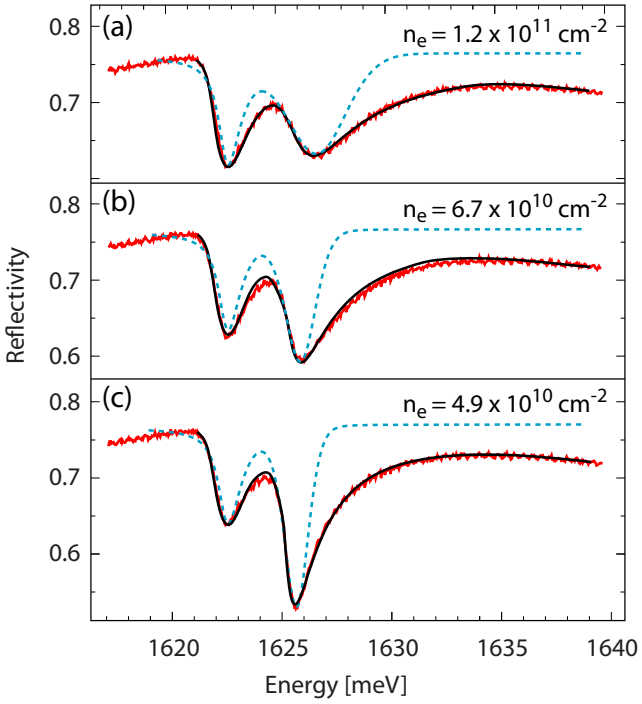

Figure 3.9: (red solid) cw reflectivity spectra measured at 5 K and for electron densities of 4.9×10^{10}, 6.7×10^{10} and 1.2×10^{11} cm^{-2}. Best fit obtained with electron scattering (black solid) and without (blue dashed).

4 Many-body interactions within an electron gas

Many-body interactions are the main source of nonlinear optical properties in condensed matter physics, and more particularly in semiconductors. Coulomb interaction gives rise to excitons and higher-order exciton states, such as biexcitons, that play a crucial role in determining the optical properties near the band edge. Although Coulomb correlations have been extensively studied in undoped quantum wells (Chemla and Shah, 2001), similar work in doped quantum wells is surprisingly sparse if not existing. Yet, in Chap. 3, we saw that electrons dramatically affect the near band edge spectrum, inducing a trion resonance and strongly modifying the exciton and trion lineshape. The exciton broadening due to electron-exciton scattering is even up to ten times more important that the well known exciton-exciton collisional broadening (Honold *et al.*, 1989). Consequently, we suspect that electrons also affect nonlinearities induced by excitons and trions and yield novel nonlinearities of much interest for the general understanding of many-body interactions in semiconductors. For this kind of investigations, our CdTe modulation-doped quantum well provides an excellent model system in which electrons, excitons and charged excitons cohabit in the same well. The many-body interactions among electrons excitons and trions may be probed through the non-linear behavior of trion and exciton optical resonances.

In this chapter, we perform pump and probe experiments (see Sec. 2.1.3) where the pump excites selectively the exciton or trion resonance. We investigate dynamical nonlinear optical properties of trions and excitons in modulation-doped quantum wells. We evidence high-order exciton Coulomb correlations in the presence of electrons, that lead to the formation of biexcitons. We observe crossover from excitons to biexcitons and biexciton redshift. We attest correlated behavior of excitons and trions under excitation which manifests itself by crossed trion-exciton effects. We observe a wealth of phenomena encompassing bleaching, crossed bleaching, induced-absorption and

energy shifts of the resonances. Significant differences are found between the nonlinear optical effects induced by an exciton and a trion population. The main source of these distinct differences is proposed to come from the Pauli exclusion-principle, which is at the origin of phase-space filling and short-range fermion exchange. We finally bring more insight on the role of electron interactions.

This chapter is structure the following way. In Sec. 4.1, we discuss the Pauli blocking of excitons. In Sec. 4.2 we show that third- and higher-order exciton Coulomb correlations occur in the presence of an electron gas. The crossed exciton-trion correlations are investigated in Sec. 4.3, while the time evolution of the different non-linearities is analyzed in Sec. 4.4. In Sec. 4.5, the effect of electrons on the trion nonlinearities is investigated.

4.1 Exciton Pauli blocking

In Fig. 4.1(a) and (c), we plot a set of differential reflectivity spectra, obtained when pumping selectively at the exciton resonance for different pump intensities. Both pump and probe are σ^+ polarized. Fig. 4.1(a) show the results obtained for zero delay time between pump and probe. Although discussion will focus on zero delay spectra, we shall have to keep in mind that coherence affect measurements (Chapter 5). Thus, for information, we also present results obtained in the same conditions at 4 ps delay time (Fig. 4.1(c)) when coherence is lost.

These differential spectra all evidence a clear blue-shift of the exciton line. This renormalization of the exciton resonance has been extensively studied in undoped-semiconductor quantum wells (Peyghambarian *et al.*, 1984; Schmitt-Rink *et al.*, 1985; Hulin *et al.*, 1986) and, is attributed to short-range exchange (Schmitt-Rink *et al.*, 1985) having its origin in the Pauli exclusion-principle acting on the Fermi particles forming the excitons of same spin. This is a repulsive electron-electron and hole-hole interaction. It does not show up in 3D systems because it is compensated almost exactly by the attractive long-range correlations. The latter corresponds to the first Coulomb interaction in the exciton gas and would induce a red-shift on the exciton resonance. The exciton blue-shift appears in two dimensional semiconductors (Hulin *et al.*, 1986) because the long-range Coulomb correlation effect is strongly reduced (Schmitt-Rink *et al.*, 1985). This means that, in our sample, the existence of the exciton blue-shift, due to the generation of an exciton population, is the

signature that the long-range Coulomb correlation has an effect that we can neglect to first order compared to the more efficient short-range exchange interaction.

In order to better understand the origin of the blue shift, we performed a calculation of the exciton-exciton exchange energy Ciuti *et al.* (1998); Tassone and Yamamoto (1999), similarly to what has been done for exciton-electron exchange in the previous chapter. Consider the collision of two excitons with wavevectors $\boldsymbol{k}_X$ and $\boldsymbol{k}'_X$. During the scattering process the momentum $\boldsymbol{q}$ will be transferred from one exciton to the other:

$$(\boldsymbol{k}_X, \boldsymbol{k}'_X) \rightarrow (\boldsymbol{k}_X + \boldsymbol{q}, \boldsymbol{k}'_X - \boldsymbol{q}). \tag{4.1}$$

The exchange of a single carrier lead to the most important contribution to the shift of the resonance. The exchange energy was calculated for both single

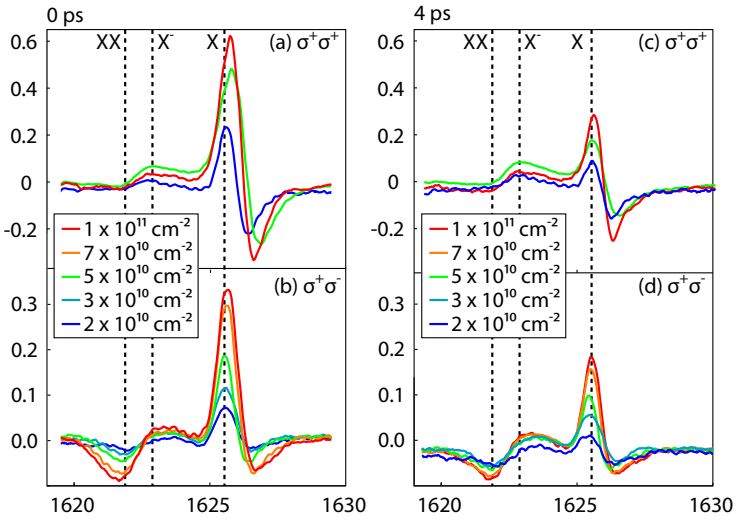

Figure 4.1: Differential reflectivity spectra obtained at (a), (b) 0 ps and (c), (d) 4 ps for different σ^+ pump intensities. The estimated concentration of photogenerated excitons are 2×10^{10}, 3×10^{10}, 5×10^{10}, 7×10^{10} and 1×10^{11} cm^{-2}. The probe is (a), (c) σ^+ polarized or (b), (d) σ^- polarized. The sample had a temperature of 5 K.

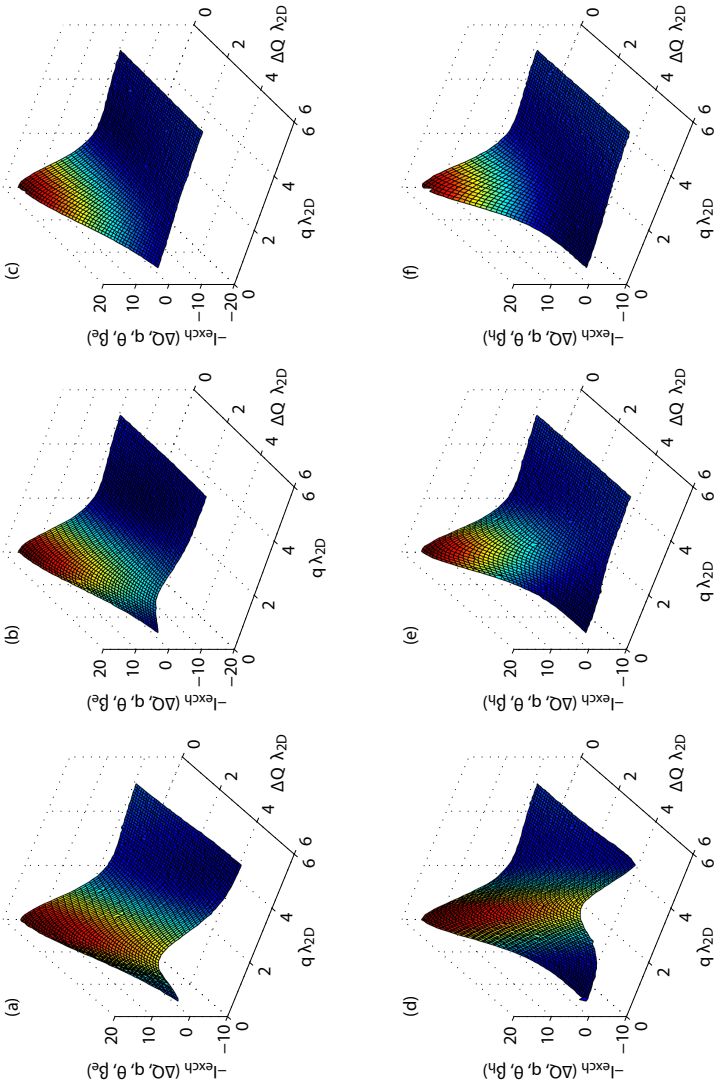

Figure 4.2: Exciton-exciton exchange energy as a function of the relative momentum ΔQ and transfer momentum q. (a) to (c) electron exchange. (d) to (f) hole exchange. The calculation was performed for the relative momentum angle $\theta = 0$ in (a) and (d), $\pi/2$ in (b) and (e), π in (c) and (f).

electron and single hole exchange. The results are plotted in Fig. 4.2 as a function of the initial relative momentum magnitude $\Delta k_X = |\boldsymbol{k}_X - \boldsymbol{k}'_X|$ and the transferred momentum amplitude q for three different relative momentum angle θ. We see that the exchange is positive and maximum for small Δk_X and small q. At large q, the exchange energy drop and can even become negative. The shift that we measure originates from the superposition of all q contributions and is therefore clearly positive.

The excitons that we photogenerate at $k_X = 0$ undergo strong exciton-electron scattering. After some time, the k_X distribution should broaden. However at 5 K, this broadening is not large enough to significantly modify the weight of the exchange energy terms in the exciton shift calculation. Therefore we expect the blueshift to remain important as long as exciton are present in the well. This is corroborated experimentally and the blueshift is clear up to 100 ps.

In Fig. 4.3, we also show the results obtained for cross-linear pump and probe. In this case, we generate both σ^+ and σ^- exciton population. Expectedly, a blueshift of the exciton is observed as in the presence of a pure σ^+ exciton population.

4.2 High-order exciton correlations within an electron gas

Fig. 4.1(b) and (d) show differential spectra obtained at the exciton resonance for $\sigma^+\sigma^-$ configuration. In that case, neither Pauli blocking nor first-order Coulomb-induced nonlinearity lead to a coupling among the subspaces of different exciton spin state (Meier *et al.*, 2000). Nevertheless, we observe nonlinearities on the exciton resonance that are the same order of magnitude as in the $\sigma^+\sigma^-$ case; a blueshift of the exciton resonance is clearly visible as well as a bleaching of the absorption line. This evidence high-order Coulomb correlation between excitons and makes the observation of two excitons bound states likely. Thus, we associate to a biexitonic signature the induced absorption that shows up about 4 meV below the exciton resonance, for it matches the biexciton binding energy in CdTe QW's (Birkedal *et al.*, 1996) and respects the selection rules for biexciton formation: it is neither observed for same circular polarization $\sigma^+\sigma^+$ (Fig. 4.1b), nor for orthogonal linear polarization (Adachi *et al.*, 1997) (Fig. 4.3). A full proof of the biexciton stability will be performed

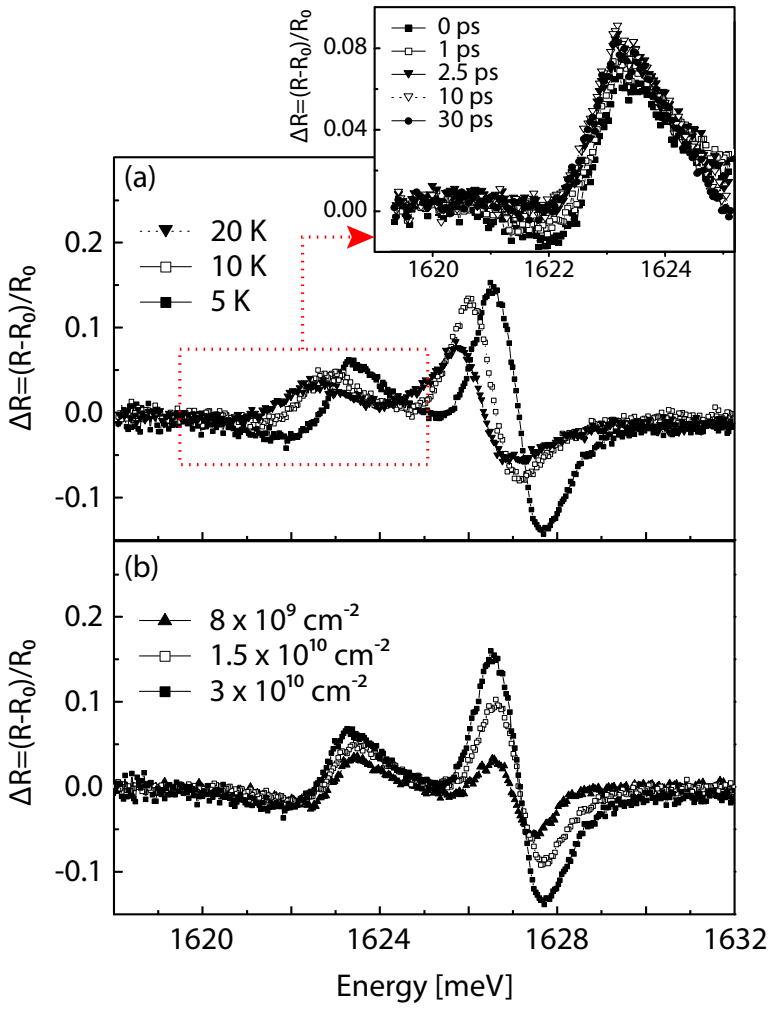

Figure 4.3: Differential spectra obtained for cross-linear pump and probe. The pump is tuned on the exciton resonance. (a) The exciton density is constant (3×10^{10} cm^{-2}) but the temperature varies (5, 10 and 20 K). Inset: time evolution at 5 *K*.
(b) Excitons are generated with densities of 8×10^9, 1.5×10^{10} and 3×10^{10} cm^{-2}.

in Chapter 5.

The relative strength of high-order Coulomb correlations relatively to Pauli blocking in the presence of electrons is very much comparable to the one observed in neutral quantum wells (Meier *et al.*, 2000). This demonstrates that electrons do not strongly affect high-order correlations.

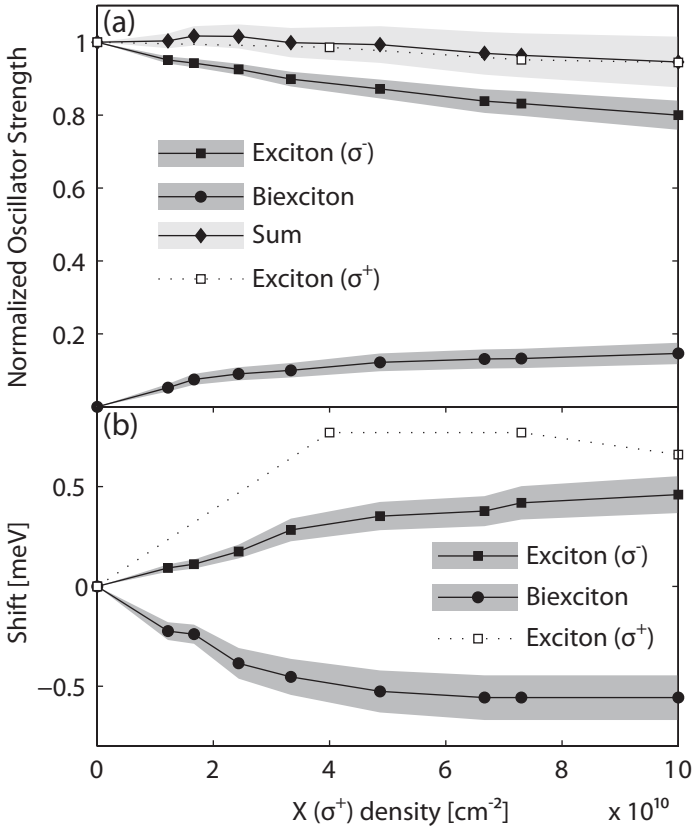

Figure 4.4: (a) Normalized oscillator strength of the σ^+ exciton, σ^- exciton, biexciton as a function of the σ^+ exciton density. The sum of the σ^- exciton and biexciton oscillator strength is also given represented. (b) Shift of the σ^+ exciton, σ^- exciton and biexciton as a function of the σ^+ exciton density.

In Fig. 4.4(b), we plot the shift of the σ^+-exciton, σ^--exciton and biexciton as a function of the σ^+ exciton concentration at 2.5 ps. At this delay time, coherent effects are negligible (see Chap. 5) and trion population is still weak. Results clearly exhibit a redshift of the biexciton resonance as the exciton population rises. The redshift grows up to 0.6 meV at 5×10^{10} cm^{-2} and saturates for higher exciton densities. Observations of such a redshift in neutral quantum wells (Maute *et al.*, 2003) evidenced a linear dependence on the pump excitation but the authors did neither specify explicitly what populations they were working at. We point out that the biexciton resonance can only redshift if the biexciton binding energy increases with the exciton density strongly enough to overcompensate the exciton blueshift. Even if, to our knowledge, no explanation has been proposed, an intuitive picture of this mechanism can be given. As the exciton density generated by the pump increases, they grow more promiscuous and are subject to stronger Pauli exclusion (they blueshift). On the other side, excitons photogenerated by the probe feel stronger Van der Waals attraction (they redshift). As the power law of both interactions is different, it is not surprising that the effects do not compensate. A thorough theoretical description would however require to better understand the density dependence of all exciton and biexciton shifts.

The saturation of the biexciton redshift happens well below the saturation regime of exciton absorption in the quantum well that would more likely occur above 3×10^{11} cm^{-2} exciton population density in CdTe quantum wells. We point out that it happens at the same exciton density as the σ^+ and σ^- exciton blue shift. Since high-order exciton correlations play an important role, it likely that this transition correspond to the transition from a third-order regime to a fifth-order regime. Both experiments and calculations performed by Meier *et al.* (2000) have demonstrated that third order correlations induced a blueshift of the exciton, while fifth-order correlation yielded a redshift. When the exciton density increases, the contribution from fifth-order exciton correlations manifests and consequently diminish the increase of the shift.

In Fig. 4.4a, we show that for increasing σ^+ exciton density, the oscillator strength of the biexciton transition grows at the expense of that of σ^- exciton density. The sum of both oscillator strength is constant which witness this exciton to biexciton cross-over and corroborate results obtained in microcavities Saba *et al.* (2000). The exciton to biexciton crossover is driven by three-exciton Coulomb correlations, which once again demonstrate that even in the presence of electrons, high-order exciton correlation are not affected. This explains why we observe a bleaching of the σ^- exciton resonance in Fig. 4.1(b).

4.3 Phase-space sharing by excitons and trions

We now return to the $\sigma^+\sigma^+$ experiments performed with the pump tuned to the exciton resonance. The novelty in our investigations is that the photo-generated σ^+-exciton population induces also nonlinear effects on the trion resonance. We observe a bleaching of the σ^+-trion resonance, which depends on temperature (Fig. 4.5b) and exciton density (Fig. 4.1(a)). As evidenced in Fig. 4.1(a), both crossed effects already occur at zero delay time. The trion bleaching increases with excitation density and broadens with temperature. In the inset of Fig. 4.5, we show the time evolution of the nonlinear trion signal. It is important to note that the trion bleaching signal does not increase with time, as would be expected if this bleaching was only due to a trion population. However, at 5 K, the trion formation from an exciton population takes place within about 10 ps (Portella-Oberli *et al.*, 2003). Consequently, at short delay after excitation, only a small amount of trions (less than 10%) is formed in the quantum well. The almost constant value of the trion bleaching over about 10 ps evidences that this bleaching evolves according to two opposite contributions of the same order of magnitude: the contribution due to the trion population which increases with time, and that due to the exciton population which decreases with time. Thus, we attribute the trion bleaching, at short times, to the phase-space filling of the optically-accessible k-space by the photo-generated excitons, resulting into a blocking of the trion transition. This result evidences that excitons and trions share the same k-space and originate from the same ground state.

After showing that the creation of an exciton population induces large effects on the trion resonance, let us turn to the effect of a trion population on the trion and exciton resonances. The nonlinear optical effects in the reflectivity spectrum for resonantly created trions are notably different from those induced by an exciton population (Fig. 4.5). The trion resonance is bleached without any shift in energy and we find an induced absorption of the exciton line. Figure 4.5 displays the time evolution of the differential reflectivity spectrum for cross linear polarization, when the sample is excited at the trion resonance, at 5 K. We note that the result are perfectly similar for $\sigma^+\sigma^+$ pump and probes (not shown). We evaluated the trion and exciton oscillator strength variations by using the transfer matrix calculation of Chap. 3. In Fig. 4.6, they are plotted as a function of time, for several excitation powers. These results show that: (a) as trions are created in the well, the induced absorption gained by excitons reaches similar amplitude as the bleaching experienced by

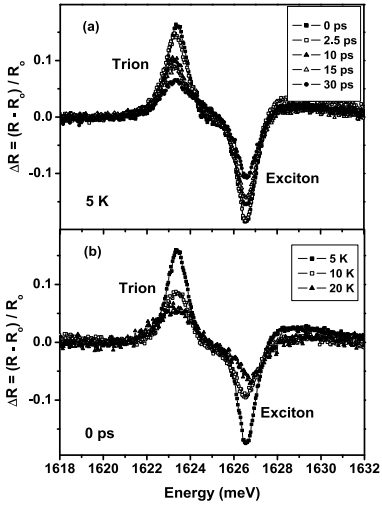

Figure 4.5: Cross-polarized differential reflectivity spectra obtained by pumping at the trion resonance for (a) different delay times a 5 K, (b) different temperatures at zero delay time.

trions and (b) the induced absorption of excitons decays with trion bleaching. These evidence correlated effects acting on both signals. The bleaching of the trion line obviously originates from phase-space filling of trions. The induced absorption on excitons is not an expected effect. Since excitons have been observed to block the trion transition due to phase-space filling, the presence of trions should block the exciton transition by the same phase-space filling argument. Thus, it is expected that the presence of trions should induce a loss in the exciton oscillator strength. In our experiment we obtain on the contrary an increase of the excitonic absorption when the electron population is transformed into a trion population because not only trions are created in the process but also electrons are removed.

In chapter 3, we already studied the effect of a variation of electron concen-

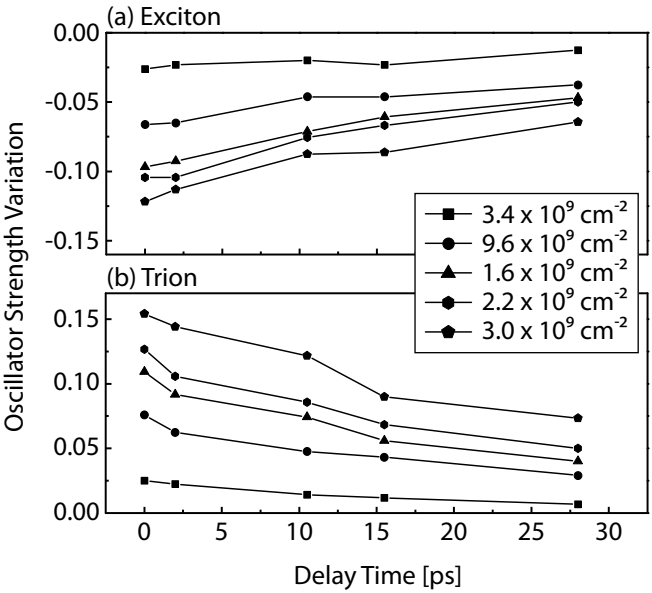

Figure 4.6: (a) Integrated induced absorption signal of excitons and (b) integrated bleaching signal of trions, as a function of delay time for several excitation powers at the trion resonance, at 5 K.

tration on the exciton resonance and we saw that excitons lose their oscillator strength, due to the presence of an electron gas (Kheng *et al.*, 1993). The reduction of the exciton oscillator strength in the presence of carriers has been attributed to the Pauli exclusion principle, due to both phase-space filling and short-range exchange interaction of the electron gas.[1] In the inset of Fig. 4.7, we plot the cw reflectivity spectra for two electron concentrations in the quantum well. We calculate their differential reflectivity and plot it in Fig. 4.7: this spectrum reveals the change in the reflectivity as the electron concentration is decreased by 1×10^{10} cm^{-2}. In this case, the trion bleaching and the induced absorption of excitons are purely due to the decreasing concentration of elec-

[1]First order Coulomb correlation may be neglected in our sample as discussed earlier. This validates that the reduction of excitons oscillator strength cannot result from such correlations (Schmitt-Rink *et al.*, 1985; Huang *et al.*, 1988; Zimmermann, 1988).

trons in the electron gas. We compare this differential spectrum with that recorded in the pump-probe experiment with a similar trion density of about 9.6×10^9 cm^{-2}. In this experiment, we also remove 9.6×10^9 cm^{-2} electrons from the well but additionally photogenerate 9.6×10^9 cm^{-2} trions. The difference between both differential spectra can be attributed to the phase-space filling by trions: in the same way excitons that have been observed to block the trion transition due to the phase-space filling (above), the presence of trions should block the exciton transition by the same phase-space filling argument. Although, screening effect on excitons by trions — much less important than that by electrons —, cannot be excluded. Further investigations are needed to get more accurate conclusions.

It is then necessary to invoke another effect to explain the increased absorption of excitons in our experiments. We attribute the gain of exciton oscillator strength, when trions are created, as resulting from the changes in the screening of excitons via short-range electron-electron exchange. It is worth noting that the exchange electron-electron interaction produces effects similar to that of the classical Coulomb interaction: the former also produces an 'exchange hole', by repelling all the electrons in the same spin state, just like the 'correlation hole' in the latter (Chemla and Miller, 1985). Therefore, this extra 'positive charge' generated from electron exchange process screens the exciton Coulomb potential. As trions are photo-generated, there are less electron in the electron gas to screen the exciton and the exciton gains back some oscillator strength. As a trion recombines, the electron is released back to the electron gas and is able again to screen excitons. Thus, we observe a recovery of the induced absorption signal of excitons with time (Figs. 4.5a). This result reveals that electrons interact much more efficiently among themselves than trions do, which suggests that excitons are more dynamically screened by electrons than by trions. Theoretical investigations in the field have been undertaken by Ciuti and Bastard (2004). We would like to stress that the similar amplitude of the signal changes of the trion and exciton resonances, comes from two distinct effects, which are both the consequence of Pauli exclusion principle: phase-space filling for trions and screening reduction for excitons. This is an intriguing result and we believe that only a theoretical description can explain it.

The above explanation in terms of more efficient screening of excitons by electrons than by trions is further corroborated by the absence of an energy shift of the trion resonance upon resonant pumping, which evidences the ineffectiveness of the trion-trion interaction. Note that, exciton-exciton

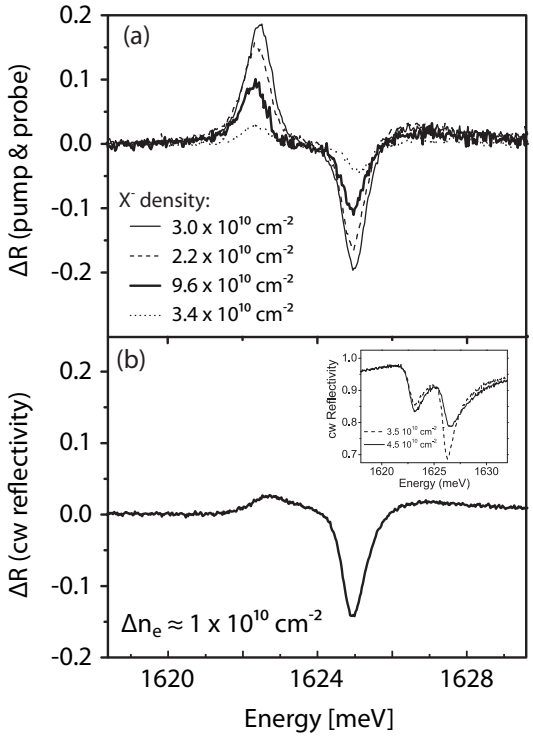

Figure 4.7: Differential cw reflectivity spectra obtained from reflectivity spectra shown in the inset. The variation of electron density between solid and dashed spectra is about 1×10^{10} cm^2. Temperature is 5 K

scattering is more effective since it induces a blue-shift in the exciton resonance. Therefore, we are led to assert that exciton-exciton exchange interaction is more efficient than that of trion-trion interaction. The elastic exciton-exciton Coulomb scattering in semiconductor quantum wells, considered earlier in this chapter, has shown that electron-electron and hole-hole exchange terms are the dominant ones, being much larger than the classical electrostatic dipole-dipole interaction as well as the direct exciton-exciton exchange. Furthermore, their computation shows that electron-electron and hole-hole exchange terms give

equal contributions to the interaction process (Fig. 4.2). In a simple minded approximation, we could expect that the inter-trion exchange interaction between carriers could be larger than that of inter-exciton exchange interaction, because trions are formed by three particles instead of two as excitons. In our knowledge, there is no theoretical investigation on the short-range exchange between trions, but our results suggest that the trion-trion exchange interactions are less efficient than the exchange interaction between excitons. The localization of trions may play an important role in this inefficient inter-trion exchange process. Trions have been indeed found to be more localized than excitons, at low temperature (Portella-Oberli *et al.*, 2002).

At higher temperatures, trions are no more localized[2] and thus, we could expect, when a trion population is generated, a blue shift of the trion line. We have performed experiments at 10 K and 20 K to test this premise (Fig. 4.5b). We found that there is no blue-shift of the trion resonance. Additionally, the induced absorption of excitons persists as a correlated effect between excitons and trions (Portella-Oberli *et al.*, 2004). This result shows that trion-trion interaction is always inefficient whether they are localized or not. As the temperature is increased, the main scattering process of trions is with acoustic-phonons via deformation potential, which is much more efficient than the exciton- (and electron-) acoustic phonon scattering because of the larger interaction potential of trions (Portella-Oberli *et al.*, 2002). This is evidenced by the broadening of the trion resonance with temperature (Fig. 4.5b). Both results together demonstrate, without ambiguity, that the trion-trion interaction is not the dominant scattering process for trions.

4.4 Exciton, trion and biexciton dynamics

Fig. 4.8(c) shows the time evolution of the biexciton and trion maximum intensity measured for the σ^+ and σ^- pump and probe experiment. At positive delay, the dynamics of the biexciton induced absorbtion signal is ruled by two time constants correlated to the exciton population decay. From zero delay time

[2]For low exciton density of 3×10^9 cm^{-2} and electron concentration (2×10^{10} cm^{-2}) the dephasing time is 10 ps at 2 K (Portella-Oberli *et al.*, 2002). For doubled density of excitons (6×10^9 cm^{-2}) the dephasing time is 8 ps. It has been reported that the interaction between excitons and electrons can be 8 to 10 times stronger than between excitons (Honold *et al.*, 1989). Therefore, the exciton dephasing time for an electron concentration of 4×10^{10} cm^{-2} can be estimated to be 1 ps or even less.

up to 10 ps, the biexciton induced absorbtion amplitude continuously diminishes because excitons quickly coalesce with electrons to form σ^+ trions. Once electrons are fully depleted, exciton and trion populations reach a thermodynamical equilibrium and deplete slowly through electron-hole recombination (Chap. 6). As we will see, trions need to spin-flip to efficiently bleach the trion resonance seen by the cross polarized probe. Consequently, the observed rise time of the trion bleaching should be delayed by the spin-flip time. The fact that there is hardly no delay — the rise time of the cross-polarized trion bleaching is equal to the σ^+ trion formation time (10 ps) — shows that the spin-flip is very fast and of the order of a few ps. Hole spin-flip relaxation for trion is mainly due to Bir-Aranov-Pikus mechanism (Bir *et al.*, 1976), which scatters preexisting electrons via the exchange interaction. The efficiency of this mechanism increases with the hole kinetic energy (Bastard and Ferreira, 1991). The extremely short spin-flip time show new light on the trion formation from a resonant exciton population: the energy conservation forces electrons and excitons to form trions with high k-vectors, which relax very quickly to other polarizations.

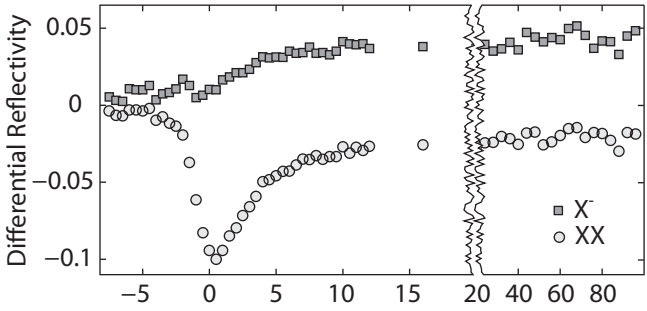

Figure 4.8: Co-polarized differential reflectivity spectra ($\sigma^+\sigma^+$) obtained by pumping at the exciton resonance, at 2 ps delay time between pump and probe pulses at 5 K. The exciton density was approximatively 3×10^{10}, 5×10^{10} and 9×10^{10} cm^{-2}

4.5 Electron gas heating

So far the effect of the exciton-electron and trion-electron scattering on the observed nonlinearities was not investigated. We now concentrate on this aspect. When we look closer at Fig. 4.3 which was obtained for cross-polarized pump and probe and excitation of the exciton resonance, we observe a slight induced absorption below the trion resonance. This effect can not be attributed to a renormalization of the trion transition due to trion population because, as we have seen above, a trion population does not induce a red-shift in the trion resonance and at short times, there are only electrons and the photogenerated excitons in the quantum well. We suggest that the most likely origin of this induced absorption is a change in the distribution of electrons due to the exciton-electron scattering. This results in an increase of the electron occupation at higher energies favoring the trion transitions at lower energies. In other words, it increases the spread of the trion red-tail discussed in Chap. 3. This induced absorption cannot be mistakenly attributed to biexcitons since, as we already mentioned, they cannot be observed for cross-linear pump and probes. The trion red-shift is then observed at short times (inset in Fig. 4.3) and, at later times, it is masked by the bleaching effect due to trion formation from the exciton population.

At higher temperatures, 10 K and 20 K, the red-shift of the trion resonance is not observed. At these temperatures, the homogeneous broadening of the electron distribution is essentially due to electron-acoustic phonon scattering, which is the dominant electron scattering process in this temperature range (Ciulin *et al.*, 2000b). Therefore, the exciton-electron interaction does not modify enough the electron distribution to induce an increase in the trion absorption at low energies. As a result, at higher temperatures, when excitons are created we only observe a broad bleaching of the trion resonance (Fig. 4.3(a)). This bleaching signal is the consequence of phase-space filling mainly by the excitons, at short times and, at longer times, is also attributed to trions while the thermal equilibrium between trion and exciton populations is reached (inset in Fig. 4.1).

In Fig. 4.9, we compare the differential spectra obtained for three different pumping energies (1628.39, 1625.76 and 1625.59 meV) at 0 ps and 4 ps and for both co- and counter-polarized pump and probes. When an exciton is photogenerated by pumping the high-energy tail of the exciton resonance, the electron gas is also heated in the process. We were hoping to be able to observe a change in the induced absorption below the trion as the pump is tuned to

the high-energy tail of the exciton. When the pump is tuned at 1628.39 meV —high-energy tail of the exciton—, the exciton absorption drops to about 10% and the nonlinear effects induced by such a low exciton concentration is hardly measurable at the exciton resonance. For $\sigma^+\sigma^+$ at 0 ps, we do not observe the expected induced absorption. This comes from the fact that σ^+ excitons only significantly scatter with σ^+ electrons and that σ^+ electrons only contribute to the red-tail of σ^- trions. At 4 ps, however, electrons thermalize and the low-energy trion absorption increases. For $\sigma^+\sigma^-$, the induced absorption should be obvious, unfortunately it cannot be easily discriminated from the biexciton signal.

When we pump the trion resonance at 1622.97 meV (Fig. 4.9) with a pump sufficiently strong to remove a significative amount of electrons in the quantum well, we strongly diminish scattering contributions from the electrons with the excitons and trions. Therefore, the trion high-energy tail shrinks significantly. Its line-shape changes and shifts towards lower energies (Chap. 3).

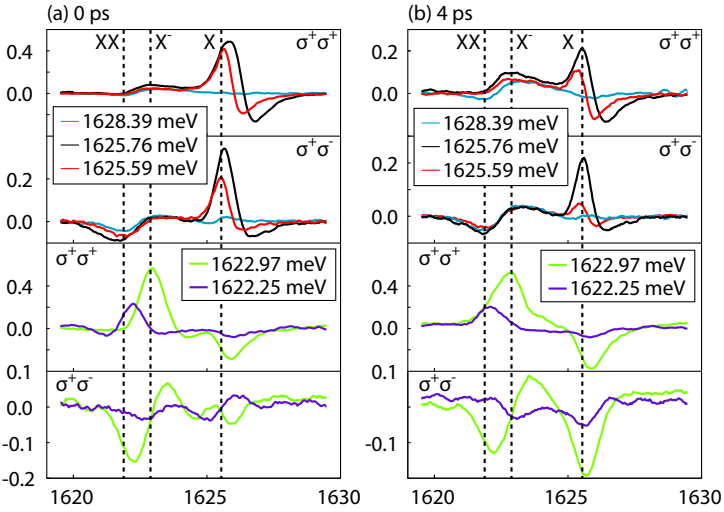

Figure 4.9: Differential reflectivity spectra obtained by tuning the pump at different energies for both co- and cross-polarized pump and probe. The results are presented for (a) zero delay and (b) 4 ps delay time.

This is evidence by the $\sigma^+\sigma^-$ pump and probe measurements in Fig. 4.9 which show a redshift. This redshift is not observed on $\sigma^+\sigma^+$ spectra because it is overwhelmed by the strong bleaching of the resonance.

4.6 Conclusion

In conclusion, we presented novel results which reveal that nonlinearities induced by trions and excitons are different and mutually correlated. For resonantly created excitons, a blue shift of the excitonic transition is observed due to repulsive exciton-exciton interactions while no energy shift was seen at the trion line when trions are generated on resonance. This result evidences the relative significance of the exciton-exciton and trion-trion interactions. Excitons and trions were shown to share the same phase-space.

Variation of the electron distribution or density were shown to strongly modify the exciton oscillator strength and alter the exciton and trion lineshape.

We also evidenced high-order exciton correlations, up to the fifth-order, in the presence of electrons.

5 Optical coherence within an electron gas

'[…] la cohérence pure, c'est du délire, c'est du délire abstrait.'

(Edgar Morin)

Much progress has been made in the controlled manipulation of light and matter using isolated atomic systems. Today, it is for instance possible to induce electromagnetically transparency in an otherwise opaque atom system (Harris *et al.*, 1990), enhance frequency conversion (Harris *et al.*, 1990; Hemmer *et al.*, 1995) and slow (Hau *et al.*, 1999) or even stop light (Liu *et al.*, 2001). However, the complex environment of a solid-state system makes it significantly more challenging to achieve a similar degree of control.

The extensive study of coherent optical properties of excitons in neutral nanostructures has allowed to evidence such fundamental results as ac Stark splitting (Quochi *et al.*, 2000) and Rabi oscillations (Saba *et al.*, 2000), which witness to the strong coupling between exciton and photons. It has also been demonstrated that high order Coulomb correlations between excitons play an important role in multi-level coherent process (Chemla and Shah, 2001) such as electromagnetically induced transparency (EIT) (Fleischhauer *et al.*, 2005) and optical Stark shift (Joffre *et al.*, 1989). In modulation-doped semiconductor quantum wells, many-body interactions tend to be more complicated, for excess carriers coalesce with excitons to form trion quasi-particles, and all electrons, excitons and trions interact with their environment. Electrons, for instance, are known to strongly screen the exciton oscillator strength (Kheng *et al.*, 1993; Huard *et al.*, 2000) and to modify their linewidth and binding energy through exchange interactions (Ramon *et al.*, 2003). Yet the field remains mainly unexplored and the effect of electrons on exciton coherence needs to be studied in much more detail. Here, we address the following issue: can excitons still be strongly correlated within an electron gas?

To answer this question, we used femtosecond pump and probe experiments (Sec. 2.1.3) to investigate high-order exciton correlations in modulation-doped quantum wells. In this chapter, we show that the electron population does not qualitatively affect the nature of interaction between excitons and higher order exciton complexes, such as bound and unbound two-exciton states. All major non-linear effects involving excitons can be observed, proving that exciton correlations are much stronger than what could have been expected within an electron see. We demonstrate high order correlation between excitons of different spins and bring strong evidence of the existence of unbound and bound (stable) two-exciton states in the presence of electrons and trions. They lead to the observation of electromagnetically induced transparency (EIT) and optical Stark-shift of the excitons. We also observe excitonic ac Stark splitting with gain of the exciton resonance, evidencing coherent exciton-photon coupling. Finally, we show that all coherent processes involving excitons are observable in the presence of electrons, which may open new possibilities for the realization of hybrid electron-exciton quantum information processors.

This chapter is organized as follow. In Sec. 5.1, we first give an overview of the dressed atom theory for an ensemble of non-interacting two-level atoms. Then we inspect some of its most striking predictions: Optical Stark shift, ac Stark splitting, Mollow fluorescence triplet and gain without inversion. We finally examine Λ-kind three-level atoms and introduce the concepts of coherent dark states, Autler-Townes splitting and electromagnetically induced transparency. In Sec. 5.2 we expand these concepts to the optical coherence of excitons in semiconductors and discuss in what extent they are modified by Coulomb interactions between excitons. In Sec. 5.3, we present our experimental results and discuss optical coherent effects of excitons in semiconductor quantum wells filled with an electron sea.

5.1 Optical coherence of atoms

If we neglect Coulomb interactions between excitons, the electron-photon interaction couples one valence state to one conduction state. These states are not mixed up by Coulomb and the problem is totally equivalent to the system of a two-level dressed atom. The assumption is clearly in contradiction with the results of chapter 4 where we saw the importance of many-body effects on the exciton resonance. Still, many of the major trends of our experimental results are encompassed qualitatively by such a simplified model.

The theory of an atom gas driven coherently by a radiation field has the advantage to be very well known. Two approach are possible. In the first one, the driving laser field is treated classically and interact with the quantum states of the matter. The time-evolution of the system is described by the semiclassical Bloch equations. However, in the classical description of the light field, the Hamiltonian is time-dependent and no energy-level can be actually defined. Consequently, some notions such as the concept of ac Stark splitting and Autler-Townes splitting have, strictly speaking, no meaning. Conversely, in the second approach, the field is quantized and the Hamiltonian is time-independent. The system has well defined energy levels and stationary states. The atom is *dressed* by photons, accordingly to the terminology introduced by Cohen-Tannoudji and Haroche (1969) to describe atoms in a radiation field. Here, we use the second approach and briefly remind the basics of the dressed atom theory (Cohen-Tannoudji *et al.*, 1992) which describes the coherent effects of a laser radiation on a two-level atom.

5.1.1 Dressed atom model

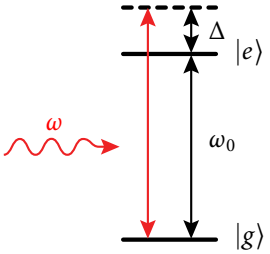

Figure 5.1: Interaction of a two-level quantum system with a single-mode laser field of frequency ω. The transition frequency from the ground state $|g\rangle$ to the excited state $|e\rangle$ is ω_0. The detuning between the pump and the probe is $\Delta = \omega - \omega_0$.

Consider the interaction of a single-mode quantized field of frequency ω with an atom, described by the Hamiltonian

$$\mathscr{H} = \mathscr{H}_A + \mathscr{H}_F + \mathscr{H}_1, \tag{5.1}$$

where $\mathscr{H}_A$ is the bear atom Hamiltonian, $\mathscr{H}_F$ the free field Hamiltonian and $\mathscr{H}_1$ the atom-field coupling. If ω closely matches one atom transition and is far apart from any other resonance, the atom can be safely modeled by a two level quantum system. Let $|e\rangle$ and $|g\rangle$ represent the upper and lower level states of such a system, i.e. they are the eigenstates of the unperturbed atom Hamiltonian

$$\mathscr{H}_A = \hbar\omega_e |e\rangle\langle e| + \hbar\omega_g |g\rangle\langle g| \tag{5.2}$$

with the eigenvalues $\hbar\omega_e$ and $\hbar\omega_g$, respectively. Let also ω_0 be the atom transition energy

$$\hbar\omega_0 = \hbar\omega_e - \hbar\omega_g. \tag{5.3}$$

In the single-mode case, the free field Hamiltonian $\mathscr{H}_F$ reduces to

$$\mathscr{H}_F = \hbar\omega\left(\hat{a}^\dagger\hat{a} + \frac{1}{2}\right), \tag{5.4}$$

where $\hat{a}^\dagger$ and $\hat{a}$ are creation and annihilation operators for a photon with frequency ω, polarization $\boldsymbol{\epsilon}$ and wavevector $\boldsymbol{k}$. The state of the free field $|f\rangle$ can be written in a very general way

$$|f\rangle = \sum_n \rho_n |n\rangle, \quad \rho_n = \langle n|f\rangle \tag{5.5}$$

where $|n\rangle$ is an eigenstate of $\mathscr{H}_F$ defined by

$$\mathscr{H}_F|n\rangle = n\hbar\omega|n\rangle. \tag{5.6}$$

If we neglect atom-field interactions, the eigenstates of the system are of the type $|g, n\rangle$ or $|e, m\rangle$, the corresponding energies being respectively $\hbar(\omega_g + n\omega)$ and $\hbar(\omega_e + m\omega)$. When the detuning

$$\Delta = \omega - \omega_0 \tag{5.7}$$

between the pump and the field is very small in comparison to the atom frequency ($|\Delta| \ll \omega_0$), the states $|g, n+1\rangle$ and $|e, n\rangle$ are nearly degenerate. We say that they are bunched in the manifold $\mathscr{E}_n$. The spectrum of $\mathscr{H}_0 = \mathscr{H}_A + \mathscr{H}_F$ can be then view as a sequence of two-dimensional manifolds $\mathscr{E}_n$ well separated in energy by $\hbar\omega$, each manifold consisting of the nearly degenerate doublet

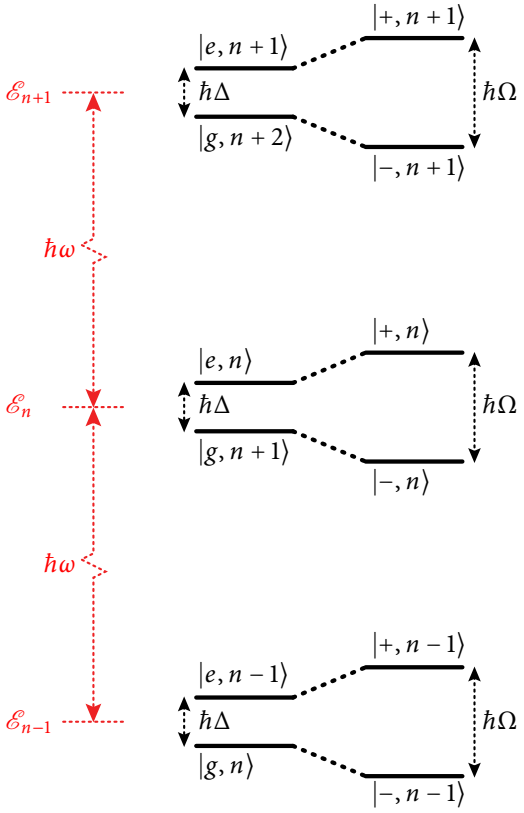

Figure 5.2: Dressed-atom energy diagram. (left-hand side) States of the combined atom-laser mode system without coupling, bunched in well-separated two-dimensional manifolds. (right-hand side) Dressed states.

$\{|g, n+1\rangle, |e, n\rangle\}$. On the left-hand side of Fig. 5.2, we sketch the bear states of the atom-laser system in the uncoupled basis.

The atom-field coupling $\mathscr{H}_1$ can be written in the electric-dipole approximation as

$$\mathscr{H}_1 = -\boldsymbol{d} \cdot \boldsymbol{E}_\perp, \tag{5.8}$$

where $\boldsymbol{d} = e\boldsymbol{r}$ is the atom dipole and $\boldsymbol{E}_\perp$ the field operator. In the bare atomic basis, the dipole reads

$$\boldsymbol{d} = \boldsymbol{\mu}(|g\rangle\langle e| + |e\rangle\langle g|), \tag{5.9}$$

where we assume (without loss of generality) that $\boldsymbol{\mu} = \langle g|\boldsymbol{d}|e\rangle = \langle e|\boldsymbol{d}|g\rangle$ is real. The field operator is defined as

$$\boldsymbol{E}_\perp = \hat{\boldsymbol{\epsilon}}\mathscr{E}(\hat{a} + \hat{a}^\dagger) \tag{5.10}$$

where $\mathscr{E} = (\hbar\omega/2\epsilon_0 V)^{1/2}$. With these definitions, the interaction Hamiltonian $\mathscr{H}_1$ takes the form

$$\mathscr{H}_1 = \hbar g(|g\rangle\langle e| + |e\rangle\langle g|)(\hat{a} + \hat{a}^\dagger) \tag{5.11}$$

where $g = -\boldsymbol{\mu}\cdot\hat{\boldsymbol{\epsilon}}\mathscr{E}/\hbar$ is a coupling constant.

The term $\hat{a}^\dagger|g\rangle\langle e|$ describes the process in which the atom is taken from the upper state into the lower state and a photon is created in the mode. The term $\hat{a}|e\rangle\langle g|$ describes the opposite process. The energy is conserved in both the processes. The term $\hat{a}|g\rangle\langle e|$ describes the process in which the atom makes a transition from the lower to the upper level and a photon is annihilated, resulting in the loss of $\hbar(\omega_0 + \omega)$ in energy. Similarly $\hat{a}^\dagger|e\rangle\langle g|$ results in the gain of $\hbar(\omega_0 + \omega)$. Dropping the energy non-conserving terms corresponds to the rotating-wave approximation. The resulting simplified Hamiltonian is

$$\mathscr{H}_1 = \hbar g[\hat{a}|g\rangle\langle e| + \hat{a}^\dagger|e\rangle\langle g|]. \tag{5.12}$$

It connects only the two-state in a given manifold $\mathscr{E}_n$ to each other. The coupling can be characterized by the Rabi frequency Ω_R

$$\tfrac{1}{2}\hbar\Omega_R = \langle e, n|\mathscr{H}_1|g, n+1\rangle = \hbar g\sqrt{n+1}. \tag{5.13}$$

As defined, the Rabi frequency should depend on n. However we can neglect this dependence by supposing that the laser beam is strong and initially coherent; it consequently has a Poison distribution for n, the width Δn of which is very small compared with the average number of photons:

$$n \gg \sqrt{n} \gg 1. \tag{5.14}$$

States in different manifolds are not coupled by Hamiltonian 5.12. Therefore the eigenvectors $|\pm, n\rangle$ of the dressed atom are a linear combinations of the states bunched in the same manifold $\mathscr{E}_n$:

$$|\pm, n\rangle = \alpha|g, n+1\rangle + \beta|e, n\rangle. \tag{5.15}$$

They must satisfy the Schrödinger equation $\mathscr{H}|\pm, n\rangle = E|\pm, n\rangle$, i.e. in the matrix form

$$\begin{pmatrix} \hbar\omega_e + (n+1)\hbar\omega & \hbar g\sqrt{n} \\ -\hbar g\sqrt{n} & \hbar\omega_g + n\hbar\omega \end{pmatrix} \begin{pmatrix} \alpha \\ \beta \end{pmatrix} = E \begin{pmatrix} \alpha \\ \beta \end{pmatrix}. \tag{5.16}$$

The eigenenergies and eigenstates are obtained by diagonalizing the matrix in Eq. 5.16. We obtain the eigenfrequencies

$$\omega_{\pm,n} = \tfrac{1}{2}\left[\omega_g + \omega_e + (2n+1)\omega\right] \pm \tfrac{1}{2}\Omega_n \tag{5.17}$$

where we introduced the generalized Rabi frequency $\Omega_n = \sqrt{\Delta^2 + 4ng^2}$. The corresponding dressed states are

$$|n+\rangle = \sin\theta|g, n+1\rangle + \cos\theta|e, n\rangle \tag{5.18}$$

$$|n-\rangle = \cos\theta|g, n+1\rangle - \sin\theta|e, n\rangle \tag{5.19}$$

where the angle θ is defined by

$$\cos 2\theta = -\frac{\Delta}{\Omega_n}. \tag{5.20}$$

At the approximation 5.14 the generalized Rabi frequency becomes

$$\Omega = \sqrt{\Delta^2 + \Omega_R^2}. \tag{5.21}$$

and the structure of the energy diagram of $\mathscr{H}$ is periodic. On the right-hand side of Fig. 5.2, we sketched the position of the dressed states, when we took the laser-atom coupling into account. They are separated in energy by $\hbar\Omega$. In Fig. 5.3 we plot the energy diagram as a function of the pump energy $\hbar\omega$. We see that the dressed states continuously go from the bear state $|e, n\rangle$ to the bear state $|g, n+1\rangle$. At zero detuning they are made of a linear superposition of the bear states, both having equal weights. The dressed states feature anti-crossing and the resonant splitting $\hbar\Omega_R$ is usually referred to as *ac Rabi splitting*. At large detuning, the dressed states asymptotically follow the light shift due to the laser coupling. In this limit we usually speak of an *optical Stark shift* and the shift is given by $\hbar\Omega \sim \Omega_R^2/\Delta$.

We finally note that the spectral splitting of the dressed states has its temporal counter part. If one assumes for $t < t_0$ that there is no interaction

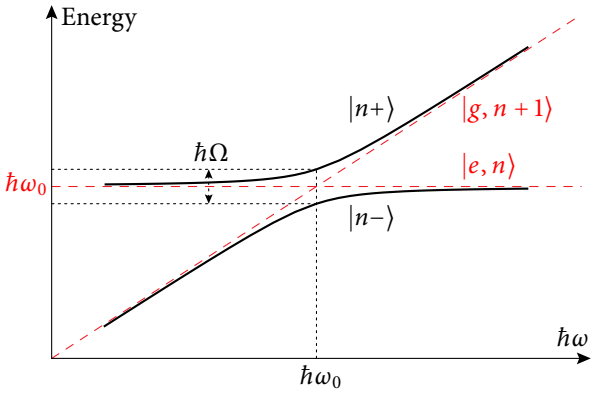

Figure 5.3: Variation with ω of the energies of the unperturbed states $|e, n\rangle$ and $|g, n+1\rangle$ (red dashed line) and of the dressed states $|n+\rangle$ and $|n-\rangle$ (black solid line).

between the atom and the field and that the atom is in its ground state, the state of the system for $t > t_0$ is given by

$$|\psi\rangle = \sum_n \left[\sin\theta e^{-i\omega_+(t-t_0)}|n_+\rangle + \cos\theta e^{-i\omega_-(t-t_0)}|n_-\rangle\right]. \tag{5.22}$$

The atomic population oscillates back and forth between the excited state and the ground state at the generalized Rabi frequency Ω. It is interesting to note that oscillations are still possible if no photons are present in the field ($n = 0$), because of vacuum fluctuations. In this model, the atom never decays to the ground state as observed experimentally. We show in the next section how this can be corrected.

5.1.2 Mollow triplet and gain without inversion

The Rabi flopping in Eq. 5.22 is not very realistic, because it does not feature decay to the ground state. This non realistic feature comes from the fact that we only considered coupling to a single mode and disregarded spontaneous emission to other (empty) modes. In the Weisskopf-Wigner approximation, it

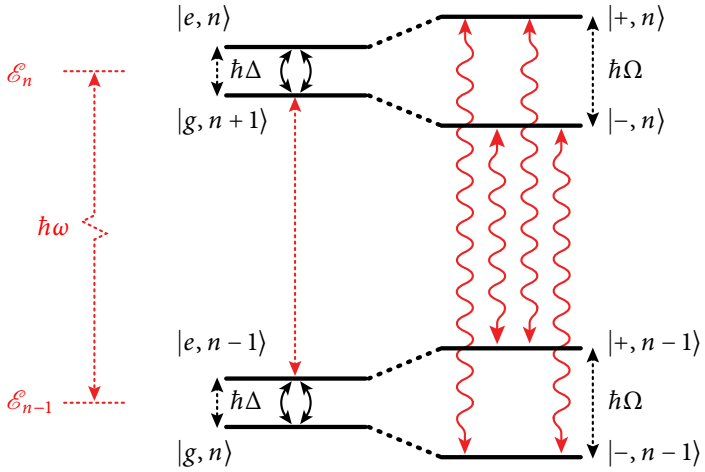

Figure 5.4: Spontaneous emission between unoccupied levels of the dressed atom. Allowed decay path between bear states (left-hand side) and dressed states (right-hand side) are indicated the red arrows.

is however possible to keep our single field description and to introduce non-Hermitian terms in the Hamiltonian 5.1 which take into account spontaneous emission to other modes through a decay rate Γ (for a detailed account, see e.g. Scully and Suhail Zubairy (1997)).

A photon of the dressed atom that was oscillating between its two bare states $|g,n+1\rangle$ and $|e,n\rangle$ in a manifold $\mathscr{E}_n$ can now leak out of the laser-atom system. During spontaneous emission, the dressed atom undergoes a transition from $|e,n\rangle$ to $|g,n\rangle$ and ends up in the manifold $\mathscr{E}_{n-1}$, where it will again start to oscillate between $|g,n\rangle$ and $|e,n-1\rangle$. Consequently, with spontaneous emission to an external reservoir of modes, the atom will cascade down from one manifold to another. The cascading time will be limited by the Rabi period, i.e. the characteristic time that is needed by the atom to absorb a laser photon and go from $|g,n+1\rangle$ (from which no spontaneous radiation is possible) to $|e,n\rangle$.

The fluorescence spectrum of the atom in a radiation field is then easily understood in terms of the dressed atomic states. Dressed states are a linear

superposition of both ground and excited bare states, thus all four transitions between the dressed states $|\pm, n\rangle$ and $|\pm, n-1\rangle$ of two contiguous manifold are possible. It is clear from Fig. 5.4 that there is one transition at $\omega - \Omega$, two at ω and one at $\omega + \Omega$. These three energies are often referred to as the *Mollow triplet* Mollow and Miller (1969) and show out in fluorescence spectra of dressed atoms Wu *et al.* (1975); Hartig *et al.* (1976); Grove *et al.* (1977).

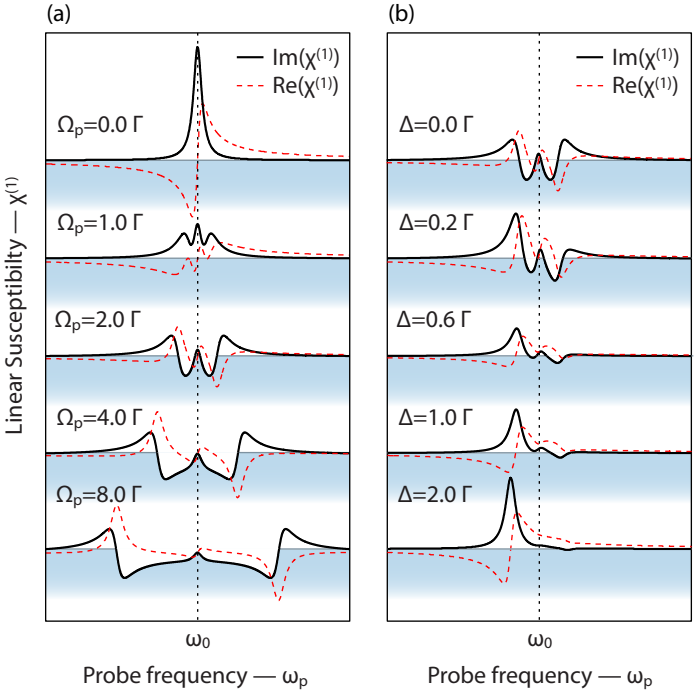

Figure 5.5: Mollow's absorption spectra of an atom driven by a laser field. (a) At zero detuning for Rabi frequency Ω_p/Γ = 0, 1, 2, 4 and 8. (b) For a Rabi frequency $\Omega_p = 2\Gamma$ and a detuning Δ/Γ = 0.0, 0.2, 0.6, 1.0, 2.0.

By solving master equations for the dressed atom, it is possible to calculate the steady state of the radiation cascade (as long as Δn is very large). This steady state appears after a time of the order of Γ^{-1} after which the contribution

coming from the manifold $\mathscr{E}_{n+1}$ compensate those going to the manifold $\mathscr{E}_{n-1}$. The populations of the states $|-,n\rangle$ and $|-,n-1\rangle$ ($|+,n\rangle$ and $|+,n-1\rangle$) are then equally populated. This has some importance when the dressed atom absorption spectrum is measured by a weak probe field. Transitions between $|-,n-1\rangle$ and $|-,n\rangle$ (or $|+,n-1\rangle$ and $|+,n\rangle$) should not affect the probe because in a steady state regime, they are equally populated. Contrarily to fluorescence no central line should be evidenced. Transitions from $|-,n-1\rangle$ to $|+,n\rangle$ and $|+,n-1\rangle$ to $|-,n\rangle$ are both possible yielding absorption or gain at $\omega-\Omega$ and $\omega+\Omega$. In our treatment, however, we only considered one-photon processes. If we relax this assumption, N-photons transitions between $|\pm,n\rangle$ and $|\pm,n-N\rangle$ are possible with various paths that interfere. A full quantum calculation becomes very difficult to perform in that case. Mollow (1972) performed a semiclassical calculation of the problem, in which the pump laser is implemented up to all orders and the probe remains a weak perturbation. In that case it can be demonstrated that a small gain might be observed at ω_0 even if there is properly speaking no inversion of the atom population. In Fig. 5.5, we used B. R. Mollow's results to plot the absorption (black solid line) and refractive index (red dashed line) at different pump intensities and pump detuning. We note that for large detuning, the dressed state tends asymptotically towards the bear states $|g,n+1\rangle$ and $|e,n\rangle$. Only one absorption line remains possible. For instance, a pump tuned below the resonance pushes the resonance up.

5.1.3 Electromagnetically induced transparency

In the previous section, a.c. Stark splitting could be observed when both coupling field and probe were exciting the same transition $|2\rangle \leftrightarrow |3\rangle$. We now consider the case in which the probe photons couples the upper state $|3\rangle$ to a third atomic state $|1\rangle$ as shown in Fig. 5.6(a). This is a typical Λ-level atom for which the upper level $|3\rangle$ is accessed by both coupling field (frequency ω_c) and probe field (frequency ω_p).

If the probe is very weak, we may think that it is possible to neglect any perturbation introduced by this beam on the atom dressed by the coupling field. Two transitions from the bear state $|1,n\rangle$ to the dressed states $|n+\rangle$ and $|n-\rangle$ are then possible and the absorption spectrum of the probe features two resonances called Autler-Townes doublet (Autler and Townes, 1955).

However, we misses some very important physics and the key features of electromagnetically induced transparency when treating the problem this way. A full three level calculation has to be performed in order to grasp them.

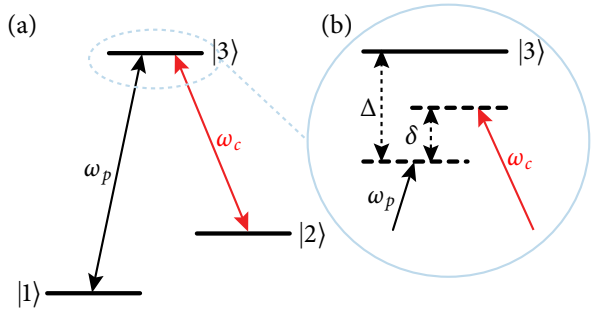

Figure 5.6: three-level Λ-type atom. (a) A coupling field of frequency ω_c drives the transition $|2\rangle \leftrightarrow |3\rangle$, while an auxiliary field of frequency ω_p probes the transition $|1\rangle \leftrightarrow |3\rangle$. (b) The detuning between the probe field and the upper level is given by Δ, while δ is the detuning between the coupling and the probe field.

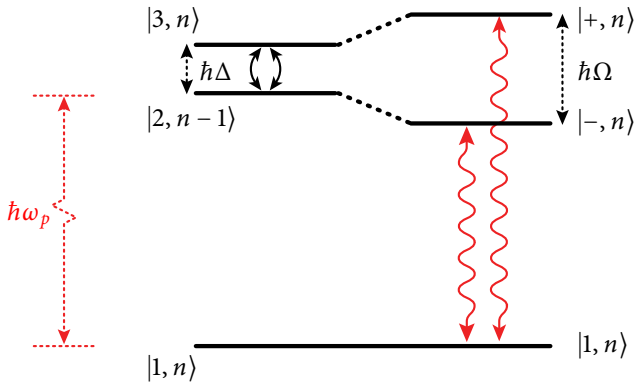

Figure 5.7: Autler-Townes doublet absorption scheme.

We therefore solve the Schrödinger equation in the case of a three-level atom. Similarly to the two-level atom, the eigenenergies and eigenstates are obtained by diagonalizing an Eq. 5.16-like Hamiltonian. In the rotating frame of the

probe, it reads

$$-\frac{\hbar}{2}\begin{pmatrix} 0 & 0 & \Omega_p \\ 0 & -2\delta & \Omega_c \\ \Omega_p & \Omega_c & -2\Delta \end{pmatrix}, \tag{5.23}$$

where Ω_c is the Rabi frequency of the coupling field and Ω_p of the probe field; δ is the two-photon detuning between the pump and the probe and Δ is the one-photon detuning between the probe and the level $|3\rangle$. We consider that transitions from $|2\rangle$ to $|1\rangle$ are forbidden. In the dressed atom formalism, we define the manifolds $\mathscr{E}_{n,m} = \{|1, n+1, m\rangle, |2, n, m+1\rangle, |3, n, m\rangle\}$, where n and m are the quantum number of the pump and probe field modes respectively. For two-photon condition $\delta = 0$, the eigenenergies of the Hamiltonian 5.23 have analytical values

$$\hbar\omega^{0,\pm} = \left\{0, \frac{1}{2}\left(-\Delta \pm \sqrt{\Delta^2 + \Omega_p^2 + \Omega_c^2}\right)\right\}. \tag{5.24}$$

The corresponding eigenstates are

$$|n, m, +\rangle = \sin\theta \sin\phi|1, n+1, m\rangle + \cos\theta \sin\phi|2, n, m+1\rangle \tag{5.25}$$

$$+ \cos\phi|3, n, m\rangle \tag{5.26}$$

$$|n, m, 0\rangle = \cos\theta|1, n+1, m\rangle - \sin\theta|2, n, m+1\rangle \tag{5.27}$$

$$|n, m, -\rangle = \sin\theta \cos\phi|1, n+1, m\rangle + \cos\theta \cos\phi|2, n, m+1\rangle \tag{5.28}$$

$$- \sin\phi|3, n, m\rangle. \tag{5.29}$$

where the mixing angles θ and ϕ are given by

$$\tan\theta = \frac{\Omega_p}{\Omega_c} \tag{5.30}$$

$$\tan 2\phi = \frac{\sqrt{\Omega_p^2 + \Omega_c^2}}{\Delta}. \tag{5.31}$$

We emphasize that the state $|n, m, 0\rangle$ has zero eigenenergy and is uncoupled from state $|3, n, m\rangle$ whatever the single-photon detuning Δ is. It is therefore a *dark state*. Once the atom is trapped in this state it cannot absorb any photon. In the limit of a perturbative probe field, $\Omega_p \ll \Omega_c$, $\sin\theta \to 0$ and $\cos\theta \to 1$, the dark state become identical to the state $|n, m, 0\rangle \sim |1\rangle$.

Similar to what has been done in the discussion about the Mollow triplet, it is possible to introduce anti-Hermitian terms in the Hamiltonian to take spontaneous emission into account. The Hamiltonian 5.23 then becomes

$$\mathscr{H} = -\frac{\hbar}{2}[\Omega_p|3\rangle\langle 1| + \Omega_c|3\rangle\langle 2| + H.c] + \hbar(\Delta - \frac{i}{2}\Gamma_3)|3\rangle\langle 3| + \hbar(\Delta - \frac{i}{2}\Gamma_3)|2\rangle\langle 2| \quad (5.32)$$

In the limiting case where $\Omega_p \to 0$, the real and imaginary part of the eigenvalue corresponding to the dark state $|1\rangle$ are the refractive index and absorption of the Λ-atom. The result of a direct numerical calculation in this limit is given in Fig. 5.8. We see that an induced transparency appears at the energy of the dark state. For $\Omega_c < \Gamma$, the width of this feature is match narrower than the linewidth of the resonance. Therefore, it is a clear quantum interference feature which is much more than a simple Autler-Townes splitting. We also note that at the transparency, the refraction is eliminated. This zero absorption and refraction is called ellectromagnetically induced transparency. For a full review of EIT and its applications, the best review was done by Fleischhauer *et al.* (2005).

5.2 Optical coherence of excitons

In the previous section, we neglected Coulomb interactions between excitons and argued that, in this limit, excitons were formerly equivalent to two-level atoms. We surveyed the major results of optical coherence in atoms. We now discuss the effect of Coulomb correlations between excitons and analyze in what respect it modifies the dynamical Stark effect and how it makes electromagnetically induced transparency of excitons feasible.

Because of Coulomb interactions, compound excitons states might form and have to be considered. Two-exciton states for instance couple to the pump field and play a dramatic role in the prediction of the optical Stark shift: wether they are bound (positive binding energy) or diffusive (negative binding energy) two-exciton may, in certain conditions, modify the direction of the shift. Thanks to two-exciton states, we will see that electromagnetically induced transparency of excitons can be observed.

5.2.1 Off resonant Stark effect of excitons

If the detuning is large compared with the exciton binding energy, the Coulomb interaction becomes a small perturbation value which can even be neglected

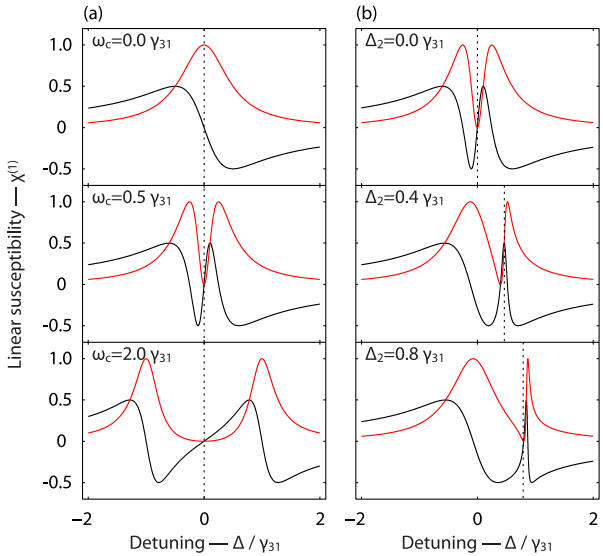

Figure 5.8: First order susceptibility $\chi^{(1)}$ as a function of the probe detuning Δ to the atomic resonance transition $|1\rangle \leftrightarrow |3\rangle$ for an EIT system. The imaginary part (red solid line) characterize the absorption, while the real part (black solid line) determines the refractive properties of the medium. (a) Resonant coupling field of various intensities $\Omega_c = 0.0\gamma_{31}, 0.5\gamma_{31}, 1.0\gamma_{31}$. (b) Coupling field $\Omega_c = 0.5\gamma_{31}$ at various detuning $delta = 0.0\gamma_{31}, 0.4\gamma_{31}, 0.8\gamma_{31}$

compared to the electron-photon interaction. The Coulomb interaction does not mix up the valence and conduction states and the problem reduces simply to a dressed two-level system (Fig. 5.9). The shift of the exciton state $|X_j\rangle$ is then simple to understand. On one hand, the ground state $|0\rangle$ is coupled to all exciton states $|X_i\rangle$, $i = 1, N$, pushing apart each $|0\rangle$ and $|X_i\rangle$ pair by $\hbar\Omega$: the ground state moves down by $N\hbar\Omega/2$ while all excitons X_i moves up by $\hbar\Omega/2$. On the other hand, due to exclusion principle, the particular one-exciton state $|X_1\rangle$ is coupled to only $N-1$ two-excitons states ($|X_1\rangle$ already occupy one state in momentum space). It pushes down $|X_1\rangle$ by $(N-1)\hbar\Omega/2$. The shift of the ground to one-exciton state $|X_1\rangle$ transition is finally given by

$[1-(N-1)-(-N)]\hbar\Omega/2 = \hbar\Omega$ which is the same shift as for the dressed state.

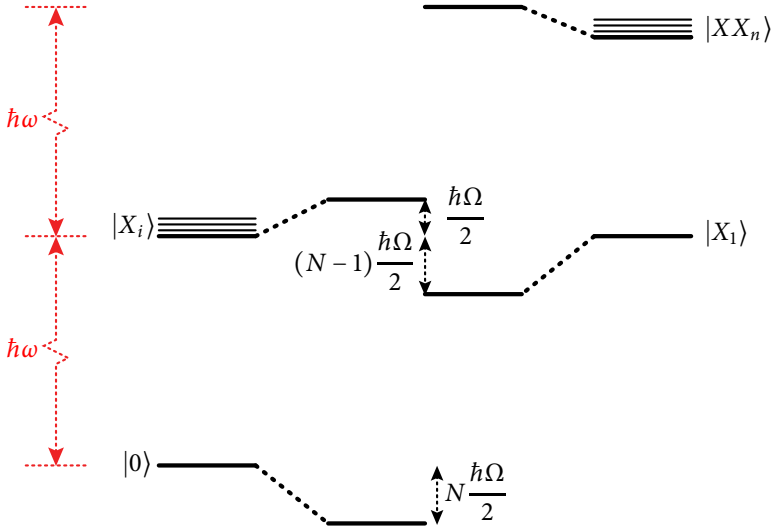

Figure 5.9: Dressed-atom energy diagram. (left-hand side) States of the combined atom-laser mode system without coupling, bunched in well-separated two-dimensional manifolds. (right-hand side) Dressed states.

First order perturbation theory can be used to calculate corrections to the dressed-atom model for weak Coulomb interaction. The shift is then given by

$$\delta\omega = \left\{ \frac{|\langle 0|U|X_1\rangle|^2}{\omega_{X_1} - \omega_p} - \sum_n \frac{|\langle XX_n|U^\dagger|X_1\rangle|^2}{\omega_{XX_n} - \omega_{X_1} - \omega_p} \right\} + \sum_i \frac{|\langle X_i|U^\dagger|0\rangle|^2}{\omega_{X_i} - \omega_p}. \quad (5.33)$$

where U and $U^\dagger$ are the operator corresponding to the creation and destruction of one electron-hole pair; $\hbar\omega_{X_i}$, $\hbar\omega_{XX_n}$ and $\hbar\omega_p$ being the energy of the states $|X_i\rangle$, $|XX_n\rangle$ and of the pump.

A thorough analysis of each term in Eq. 5.33 has been performed by Combescot and Combescot (1989). They demonstrated that at large detuning the main corrections to the dressed atom shift $\hbar\Omega$ originates from Pauli exclusion principle. At small detuning, the corrections come mainly from Coulomb

interactions between two excitons. It can also be shown that for a pump close to the exciton-biexciton resonance one find a redshift of the exciton if and only if the biexciton is bound. Otherwise a blue shift is observed.

We stress that in order to obtain these results the Coulomb interaction has to be kept exactly to all orders, forcing us to treat the electron-photon interaction as a perturbation. A simplification of the Coulomb interaction as would be done in the Hartree-Fock approximation only gives a correct shift in the regime where the Coulomb interaction is unimportant, i.e. at large detuning.

5.2.2 On resonant Stark effect of excitons

At the resonance, a perturbative approach of the pump and probe coupling is impossible. One approach is to use the dressed semiconductor Bloch equations in the Hartree-Fock approximation Haug and Koch (1990). In this approach, many-body interactions are averaged, which means neglecting all real and virtual, bound and unbound states. At first sight, this may seem a very crude approximation, especially when we know that a correct description of the non-resonant Stark shift requires two-exciton states. Nevertheless, a theoretical contribution in which the Coulomb scattering was treated in the second Born approximation showed that the light dressing is found to significantly decrease the Coulomb collision rates: Coulomb scattering is not strong enough to quench the coherent saturation effects due to phase space filling (**?**). Calculations show a dynamical Stark splitting in the absorption spectrum of a weak probe beam that is hardly different from Stark effect calculated in the Hartree-Fock approximation.

5.2.3 Electromagnetically induced transparency of exciton spin states

Electromagnetically induced transparency in exciton systems has been demonstrated for excitonic systems in neutral quantum wells (Phillips and Wang, 2002). Fig. 5.10(a) schematically depicts a first possible scheme for its observation. Exciton spin coherence is induced via Coulomb correlations between excitons with opposite spins ($|+\rangle$, $|-\rangle$), including correlations associated with unbound and bound exciton pairs. A coherent superposition of exciton states is produced by coupling $|-\rangle$ to $|XX_{\text{unbound}}\rangle$ with a strong σ^+ polarized pump

and $|+\rangle$ to $|XX_{\text{bound}}\rangle$ or $|XX_{\text{unbound}}\rangle$ with a weak σ^- probe. Thus a typical Λ-type three-level system is formed that may lead to electromagnetically induced transparency as discussed in previous section.

Another possible scheme is to couple the $|-\rangle$ to the $|XX_{\text{bound}}\rangle$ with a strong σ^+ pump and to the ground state with a σ^- probe as shown in Fig. 5.10(b). This form a ladder-type three-level system which is equally suited for electromagnetically induced transparency.

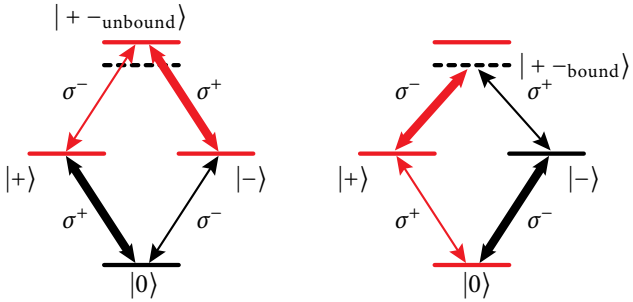

Figure 5.10: EIT schemes for excitons. (a) Ladder scheme. (b) Λ scheme.

5.3 Optical coherence of excitons within an electron sea

We performed the pump and probe experiments described in Sec. 2.1.3. When both pump and probe overlap we are in a coherent regime which corresponds to the situations described in Sec. 5.2, the pump being the coupling field and the probe the weak measurement field. By changing the pump detuning to the exciton resonance as well as its polarization, we can investigate ac Stark splitting, electromagnetically induced transparency or optical Stark shift in the presence of electrons.

5.3.1 On resonant exciton excitation

Circularly co-polarized pump and probe. First, we studied the effect of a pump tuned on the exciton resonance and worked in $\sigma^+\sigma^+$ configuration. As

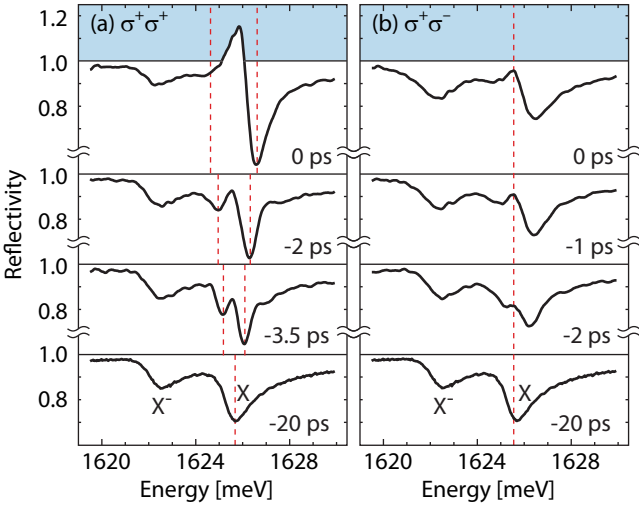

Figure 5.11: Reflectivity spectra collected at various delay times for a σ^+ pump tuned to the exciton resonance (1625.7 meV). The vertical scale is the same for all spectra. a) The probe is co-polarized and the red dashed-lines indicate the position of the Stark split modes. b) The probe is counter-polarized and the red dashed-line indicates the position of the EIT.

the probe delay changed, at negative delay, from −5 ps to 0 ps, we monitored the build up of the picosecond pump field and its effect on near band gap resonances. Fig. 5.11(a) shows that the exciton resonance of the unexcited reflectivity spectrum splits up as the pump intensity builds up: the side modes grow apart with the square root of the pump intensity. This dependence is a clear signature of the *ac Stark splitting*, observed in microcavities (Quochi *et al.*, 2000) and in single quantum wells (Schülzgen *et al.*, 1999; Saba *et al.*, 2000). The Rabi energy (half the spectral separation between the two side bands) is comparable to the exciton linewidth. This result indicates that nonlinear exciton-photon coupling dominates the many-body interactions which induce exciton decoherence. We also point out that the original exciton spectral position becomes increasingly transparent. At zero delay time (highest pump intensity), the effect reaches its maximum: the transparency turns into gain (20%). This is the gain without inversion predicted by Mollow (1972), discussed in Sec. 5.1.2 and calculated in Fig. 5.5. The robustness of the exciton ac Stark splitting over exciton induced dephasing was already very surprising when first observed in neutral semiconductors, but the fact that it can be observed in a see of electrons which is known to accelerate the exciton decoherence by exciton-electron scattering (Schultheis *et al.*, 1986) is astonishing.

Of course, the pump field is eventually absorbed, which creates excitons. At zero delay, the density of the photogenerated σ^+ polarized exciton gas is estimated at 5×10^{10} cm^{-2}. Excitons repel each other due to Pauli exclusion principle through exchange of their constituent carriers. The exciton resonance blueshifts (Schmitt-Rink *et al.*, 1985), making the intensity of the exciton Stark split states asymmetric. The build up of the exciton blueshift is clearer on differential reflectivity spectra (Fig. 5.12(a)). The role of electrons on exciton-exciton correlation of same spin through exchange interaction is not preponderant. Still, the presence of electrons is very clear at positive delay times. Electrons coalesce with excitons to form trions within 10 ps (Portella-Oberli *et al.*, 2003). As we have shown in Chap. 4, the blueshift of the excitons diminishes accordingly and the trion line is bleached because excitons and trions share the same phase-space (Portella-Oberli *et al.*, 2004).

Building on the observation of Mollow's absorption spectrum we now confidently turn to cross-polarized pump and probe measurements in order to investigate three-level atom-like coherence.

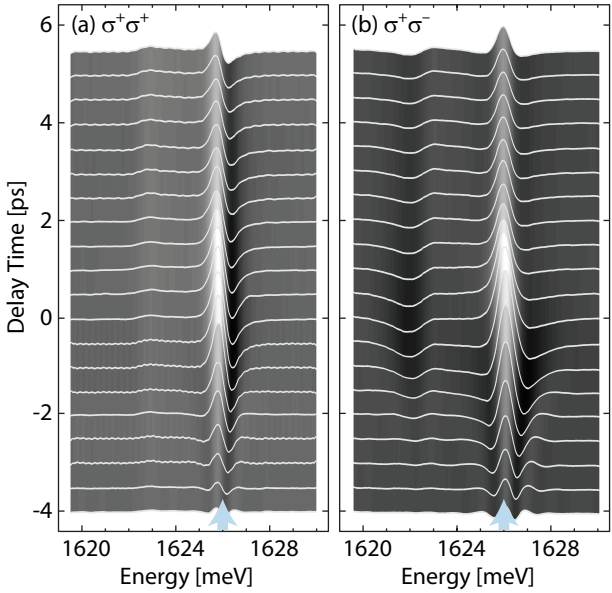

Figure 5.12: Collected differential reflectivity spectra as a function of the delay time for (a) $\sigma^+\sigma^+$ and (b) $\sigma^+\sigma^-$ pump and probe. The σ^+ pump (blue arrow) is tuned to the exciton resonance (1626 meV).

Circularly cross-polarized pump and probe. Since the σ^+ pump field only couples to excitons with angular momentum +1, ac Stark splitting should not be observed for $\sigma^+\sigma^-$ pump and probes (Saba *et al.*, 2000). Yet, as the pump field builds up, a spectral dip appears at the pump energy (see Fig. 5.11(b)). Around zero delay time, the sample even becomes fully transparent at this wavelength. As we slightly tune the pump around the exciton resonance (not shown), we observe that the dip follows the pump. This is typical of *electromagnetically induced transparency* (EIT) (Harris *et al.*, 1990; Phillips and Wang, 2002). EIT may be explained in terms of a three-level system. If excitons with opposite spins are correlated, they can form bound and unbound two-exciton states. Although σ^+ and σ^- transitions share no common states, the σ^+ pump coherently couples σ^- exciton states to two-exciton states. Coherent interferences then appear on the σ^- probe transition, which lead to transparency of

the resonance. In our case, since EIT occurs at the pump energy, it may be traced back to coherent interferences between transitions from both σ^+ and σ^- one-exciton states to the two-exciton states. Therefore, even within a gas of electrons, excitons with opposite spin states are sufficiently correlated to induce robust quantum coherence.

More insight on these correlations is gained by looking at the differential spectra in Fig. 5.12(b). The observed nonlinearities on the exciton resonance at short positive delay times, when all coherent processes have decayed away, are very much comparable in intensity to the ones observed for $\sigma^+\sigma^+$ pump and probe; a blueshift of the exciton resonance is clearly visible as well as a strong bleaching of the absorption line. Yet, neither Pauli blocking nor first-order Coulomb-induced nonlinearity lead to a coupling among the subspaces of different exciton spin state. Thus, the observed correlations evidence high-order Coulomb correlation between excitons (Meier *et al.*, 2000). Their strength make the observation of two-exciton bound states likely and we associate the induced absorption that shows up about 4 meV below the exciton line to a bound two-exciton (biexciton) resonance for the following reasons. First, it matches the exciton-biexciton transition energy in CdTe QW's (Birkedal *et al.*, 1996). Then, it respects the selection rules for biexciton formation: it is neither observed for same circular polarization $\sigma^+\sigma^+$, nor for orthogonal linear polarization (Portella-Oberli *et al.*, 2004; Adachi *et al.*, 1997). Finally, it is a real population effect that manifests well after the pump excitation and whose intensity is correlated to the exciton population. From 0 ps to 10 ps it decays very quickly because exciton merge with electrons to form trions (Portella-Oberli *et al.*, 2003). Afterwards, excitons and trions reach a thermodynamical equilibrium (Chapter 6)) and excitons deplete slowly by electron-hole recombination. The biexciton induced absorbtion decreases accordingly.

5.3.2 Off resonant exciton excitation

Circularly cross-polarized pump and probe. Since bound two-exciton states can be formed within an electron gas, we can now determine if, equally to unbound two-exciton states, they take part into coherent processes and yield EIT (Phillips *et al.*, 2003). Fig. 5.13(a) was obtained by tuning the pump close to the biexciton resonance in $\sigma^+\sigma^-$ configuration. When off resonant, nonlinearities are small and it is more convenient to assess them through the study of the differential reflectivity spectra. At exciton resonance and negative delay times differential spectra evidence an EIT signal similar to the one observed

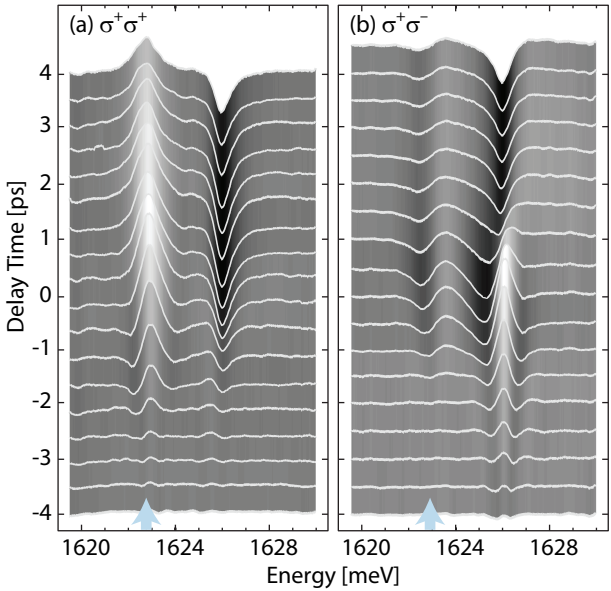

Figure 5.13: Collected differential reflectivity spectra as a function of the delay time for (a) $\sigma^+\sigma^+$ and (b) $\sigma^+\sigma^-$ pump and probe. The σ^+ pump (blue arrow) is tuned slightly above the biexciton resonance (1622.7 meV) as explained in the text.

in Fig. 5.12(b). Despite the electron population, biexcitons participate to coherent processes and quantum interference between the ground state and bound two-exciton states is possible.

In the same $\sigma^+\sigma^-$ configuration and at zero delay time, the exciton resonance redshifts. It has been observed (Mysyrowicz *et al.*, 1986; Von Lehmen *et al.*, 1986; Joffre *et al.*, 1989) and demonstrated theoretically (Combescot and Combescot, 1988) that when a direct band-gap semiconductor is irradiated in the transparency region, the exciton line shifts. This so-called *optical Stark shift* of the exciton is due to a coupling between the exciton and all virtual two-exciton states, bound and unbound. At large detuning of the pump relatively to the exciton-biexciton binding energy, this coupling is mainly due to statistical interactions, i.e. Pauli exclusion principle. It induces a blue-shift of the exciton resonance. At small detuning, when the pump is tuned close to biexciton energy, Coulomb interaction provides the leading term, and, for counter-polarized pump and probe, leads to a red-shift of the exciton line if and only if the biexciton is stable (Combescot and Combescot, 1989). Therefore, in the absence of stable two-exciton bound states only a blue-shift of the exciton resonance can be observed. The red-shift of the exciton line shows clearly the stability of biexcitons within an electron gas. We note that, in order to optimize the intensity of the redshift and of the EIT, we had to slightly tune the pump off the biexciton resonance towards the exciton. This corroborates previous observations of the optical induced Stark shift (Joffre *et al.*, 1989) and EIT (Phillips and Wang, 2004).

Circularly co-polarized pump and probe. For $\sigma^+\sigma^+$ pump and probe, only a blueshift appears up to 0 ps. This is the signature of the *optical Stark shift* for circular polarized pump and probe when biexcitons cannot be formed. In this configuration quantum coherence cannot possibly be established and therefore no EIT at the exciton resonance is observed. Since the pump and the trion resonance overlap inevitably, we generate involuntary a population of 2×10^{10} cm^{-2} trions that dramatically affects the exciton resonance and notably masks any potential optical Stark shift at 0 ps. The observed trion induced nonlinearities were described in details in Chapter 4. It is extremely interesting to see that even if electrons efficiently screen excitons and strongly attenuate their oscillator strength, exciton-exciton correlation are omnipresent and quantum coherence still possible when electrons are present.

5.4 Conclusion

As a conclusion, we have demonstrated that exciton correlations remain very strong within an electron gas. They yield unbound and stable bound two-exciton pairs that play an important role in quantum coherent processes as *electromagnetically induced transparency* and *optical Stark shift*. We also evidenced that exciton coupling to the incident field remains sufficiently robust in the presence of electrons to observe *ac Stark splitting*. The fact that coherent control of excitons and fundamental exciton-exciton correlations are not hindered by electrons opens may very promising opportunities when it comes to combine spintronics and optoelectronics in view of possible quantum information processors.

6 Formation of the neutral and charged excitons

'Équilibre est synonyme d'activité.'

(Jean Piaget)

Positively and negatively charged excitons (X^+ and X^- trions) (Kheng *et al.*, 1993; Finkelstein *et al.*, 1995) are usually compared to their atomic counterparts He^+ and H^- respectively. The dynamics of the formation of these atomic ions is of great importance in astronomy (Frolov and Smith, 2003); H^- is the primary source of the continuum opacity in most stellar photospheres and contributes to the production of hydrogen and other elements in various parts of the universe. Additionally the abundance of free electrons in the solar atmosphere is indirectly measured in terms of H^- concentration. Lately, models describing the formation dynamics of He^+ and H^- have grown more sophisticated and take into account many-body effects resulting from Coulomb correlations and Pauli exclusion principle in partially or fully ionized plasma (Bi *et al.*, 2000). In semiconductor quantum wells, we have seen in Chapter 4 that trions are also subject to many-body effects; they are highly correlated with the excitons and the plasma of free carriers. Therefore, they offer the possibility to test a model of formation of three particle complexes in the limit of strong Coulomb interactions.

The formation process of neutral excitons (X) in quantum wells has been extensively investigated over the past two decades (Piermarocchi *et al.*, 1997; Siantidis *et al.*, 2001) and recently shown to be strongly density and temperature dependent (Szczytko *et al.*, 2004a); it is a bi-molecular process, in which an electron (e) and a hole (h) are bound by Coulomb interaction. Conversely, the formation process of trions has been much less studied. It is largely believed that trions can only be formed if a population of excess carriers is trapped in the well, producing exclusively trions with the same charge. Consequently existing models discriminate the formation channel yielding trions of opposite charge. Such an approach is questionable, especially at low excess carrier den-

sities, where experiments performed on very pure samples demonstrated that both negatively and positively charged excitons do coexist indeed (Glasberg *et al.*, 1999). Current models for trion formation (Jeukens *et al.*, 2002; Vanelle *et al.*, 2000) surmise that trions are exclusively formed through a bi-molecular process, i.e. the coalescence of an exciton and a charged free carrier. While this is conceivable at low densities, nothing attests that genuine formation of the trion from an unbound electron-hole plasma (tri-molecular formation) is negligible at higher densities.

In this chapter, we address this fundamental problem and propose a formation model that fully implements bi- and tri-molecular channels for both negatively and positively charged excitons. We investigate the trion binding dynamics by following separately the evolution of the exciton, trion and plasma luminescence, which is possible by using a time-resolved photoluminescence setup of increased sensitivity. We evidence the complexity of many body effects in the trion formation and demonstrate that all the assumptions made in our model are necessary to adequately describe experiments over a broad range of excess carrier densities. Moreover, we show that the higher the carrier concentration, the more important the tri-molecular process. These experimental results are corroborated qualitatively by a simple theoretical model. Our model suggest that the momentum conservation of carriers is important in the trion formation.

6.1 Time-resolved dynamics of the photoluminescence

In order to study the dynamics of the luminescence in different density domains, we performed the time-resolved photoluminescence experiment described in Chapter 2. We performed our experiments with a variety of absorbed photon densities ($\boldsymbol{N}_{h\nu} = 10^8 - 10^{10}$ cm^{-2}) at 5.0 K and 1.5072 eV excitation. Then, we recorded the time evolution of the exciton, trion and plasma luminescence intensities. We used spectra obtained under cw-excitation to resolve the exciton and trion overlapping transitions. The experimental results are reported as symbols in Fig. 6.1.

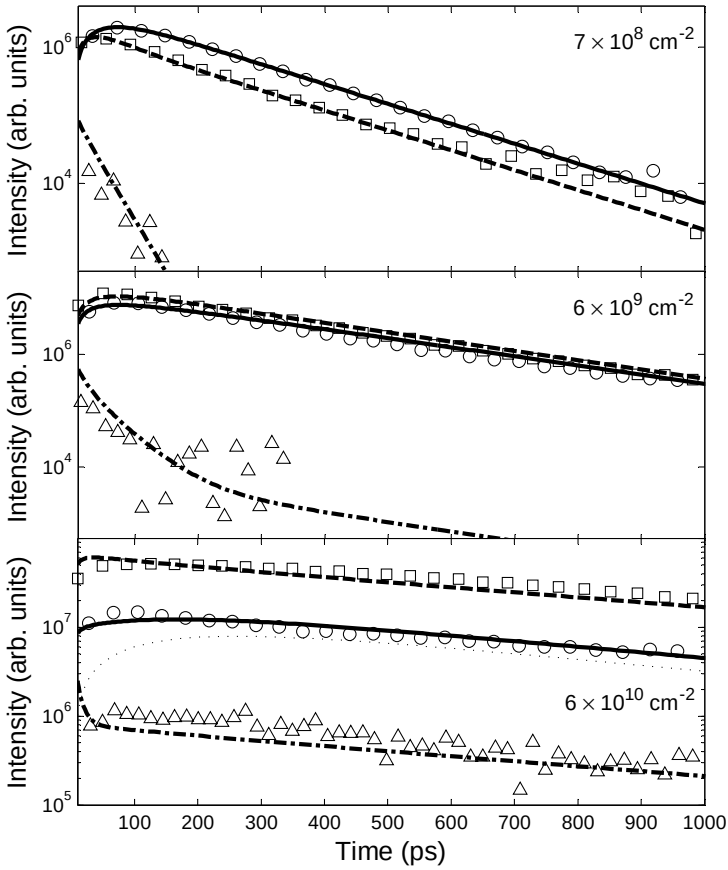

Figure 6.1: The intensity of the luminescence of trions (solid line, circles), excitons (dashed line, squares) and plasma (dashed-dotted line, triangles) calculated according to rate equations (lines) compared with experimental data (symbols) for 7×10^8, 6×10^9, 6×10^{10} cm^{-2} absorbed photon densities. At 6×10^{10} cm^{-2} density, the best fit for trions after artificially enforcing $A_3 = 0$ (thin dashed line). The excess of electron concentration is $N = 10^{10}$ cm^{-2}.

6.2 Trion formation model

The luminescence dynamics is governed by the temporal evolution of the population of free carriers, excitons and trions. We first make an inventory of all channels that couple those populations. Apart from the known bi-molecular reaction $e + h \leftrightarrow X$, we identify two bi-molecular reactions ($X + e \leftrightarrow X^-$, $X + h \leftrightarrow X^+$) and two tri-molecular reactions ($2e + h \leftrightarrow X^-$, $e + 2h \leftrightarrow X^+$) involving trions. The kinetics of these reactions is given in terms of five coupled rate equations:

$$
\begin{aligned}
\frac{d\boldsymbol{n}}{dt} &= -B\boldsymbol{n}\boldsymbol{p} - \frac{\boldsymbol{n}}{\tau_{\mathrm{nr}}} - F^X - F_2^{X^-} - F_3^{X^-} - F_3^{X^+} + \frac{\boldsymbol{X}^-}{\tau_{\mathrm{X}^-}} \\
\frac{d\boldsymbol{p}}{dt} &= -B\boldsymbol{n}\boldsymbol{p} - \frac{\boldsymbol{p}}{\tau_{\mathrm{nr}}} - F^X - F_2^{X^+} - F_3^{X^+} - F_3^{X^-} + \frac{\boldsymbol{X}^+}{\tau_{\mathrm{X}^+}} \\
\frac{d\boldsymbol{X}}{dt} &= F^X - \frac{\boldsymbol{X}}{\tau_{\mathrm{D}}} - F_2^{X^-} - F_2^{X^+} \\
\frac{d\boldsymbol{X}^-}{dt} &= F_2^{X^-} + F_3^{X^-} - \frac{\boldsymbol{X}^-}{\tau_{\mathrm{X}^-}} \\
\frac{d\boldsymbol{X}^+}{dt} &= F_2^{X^+} + F_3^{X^+} - \frac{\boldsymbol{X}^+}{\tau_{\mathrm{X}^+}},
\end{aligned}
$$

where the free carrier concentrations $\boldsymbol{n}$ (electrons) and $\boldsymbol{p}$ (holes) decay through — in order of appearance — the radiative and non-radiative recombination rates, the exciton formation rate F^X and the trion formation rates $F_2^{X^\alpha}$ (bi-molecular) and $F_3^{X^\alpha}$ (tri-molecular), $\alpha = \{-, +\}$. The term $\boldsymbol{X}^\alpha/\tau_{\mathrm{X}^\alpha}$ corresponds to the carriers recycled after the radiative decay of the trions. The exciton population $\boldsymbol{X}$ decays through radiative recombination and trion formation, while trion concentrations $\boldsymbol{X}^-$ and $\boldsymbol{X}^+$ decay through radiative recombination. The formation rates F_X, $F_2^{X^\alpha}$, $F_3^{X^\alpha}$ read

$$
\begin{aligned}
F^X &= \gamma C\boldsymbol{n}\boldsymbol{p} - \gamma C K_X \boldsymbol{X}, \\
F_2^{X^-} &= A_2^- \boldsymbol{X}\boldsymbol{n} - A_2^- K_2^- \boldsymbol{X}^-, \\
F_3^{X^-} &= A_3^- \boldsymbol{n}\boldsymbol{n}\boldsymbol{p} - A_3^- K_3^- \boldsymbol{X}^-, \\
F_2^{X^+} &= A_2^+ \boldsymbol{X}\boldsymbol{p} - A_2^+ K_2^+ \boldsymbol{X}^+, \\
F_3^{X^+} &= A_3^+ \boldsymbol{n}\boldsymbol{p}\boldsymbol{p} - A_3^+ K_3^+ \boldsymbol{X}^+,
\end{aligned}
$$

where the equilibrium coefficients K_X, K_2^α, K_3^α have been introduced to ensure the steady-state solution of the rate equations (Szczytko *et al.*, 2004a; Phillips *et al.*, 1996).

A few considerations allow us to reduce significantly the number of free parameters. The equilibrium coefficients can be calculated from a mass action law, exploiting the fact that the trion binding energies for both X^- and X^+ are equal (Glasberg *et al.*, 1999). The values of the bi-molecular plasma recombination rate B and bi-molecular exciton formation rate γC are known (Szczytko *et al.*, 2004a). Due to the high quality of the sample we assume very long non-radiative decay time τ_{nr}. Knowing the number of photons $\boldsymbol{N}_{h\nu}$ absorbed in our sample, we use the initial parameters $\boldsymbol{p} = \boldsymbol{N}_{h\nu}$ and $\boldsymbol{n} = \boldsymbol{N}_{h\nu} + \boldsymbol{N}$, where the excess electron concentration is estimated from impurity concentration: $\boldsymbol{N} = 10^{10}$ cm^{-2}. We have introduced the equations of formation for positive trions for sake of completeness. However, our present measurements are not sensitive to the X^+ population and we have decided to equate A_2^+ with A_2^- and A_3^+ with A_3^-. Once we have found an expression for the thermalized exciton and trion radiative decay times τ_D and τ_{X^α}, A_2 and A_3 will be the only parameters left.

We assume that excitons, trions and free carriers are thermalized and do share a same temperature T_c, different from the lattice temperature T_l. In our time resolved experiment, we use three electron-hole pair densities 7×10^8, 6×10^9, 6×10^{10} cm^{-2}. At the highest density, T_c is given by the exponential fit to the high energy tail of the free carrier luminescence. Tracing T_c over 1000 ps returns 35 K in average. At lower densities, the rapid plasma relaxation prevents us from measuring T_c that way. Yet, it can be trivially calculated if we depict the accumulated excess carriers trapped in the QW as a cold sea of electrons at T_l, in which the electron-hole pairs injected by the optical pump efficiently thermalize. We get 9 K and 16 K. At last, the temperature dependence of the radiative decay rates $\tau_{\mathrm{D}}(T_c)$ and $\tau_{\mathrm{X}^\alpha}(T_c)$ are most accurately described by the linear fits $\tau_{\mathrm{D}}(T_c) = 20 \times T_c$ [ps] and $\tau_{\mathrm{X}^\alpha} = 78 + 7 \times T_c$ [ps] (with T_c in [K]). Apart from a factor 1.5 attributed to the Bragg mirrors that enhances the coupling of the excitons and charged excitons to the field, and hence diminishes the radiative decay time, the agreement with the expected theoretical behavior is very good (Esser *et al.*, 2000a).

6.3 Experimental determination of the bi- and tri-molecular temperature dependence

We present the complete results of our calculations of excitonic, trion and plasma luminescence intensity dynamics in Fig. 6.1. The excitonic luminescence intensity given by $\boldsymbol{X}/\tau_{\mathrm{D}}$, is denoted by a dashed line. The luminescence intensities of X^- and X^+ are summed up ($X^-/\tau_{\mathrm{X}^-} + X^+/\tau_{\mathrm{X}^+}$) and denoted by solid lines. The free carrier luminescence $\boldsymbol{Bnp}$ is denoted by a dash-dotted line. Even with the necessary simplifications mentioned above, our rate equations provide a very good description of the observed time-resolved luminescence spectra. For instance for the smallest excitation densities the strongest transition comes from the trions, while for the larger densities the exciton transition dominates. Interestingly, for the lowest excitation density, trion and exciton dynamics are much faster than for the highest, in striking contrast with the exciton dynamics in undoped QWs (Szczytko *et al.*, 2004a). We may understand this fast luminescence dynamics in the low density regime: this is mostly the effect of the change of the temperature of carriers (and therefore of trions and excitons). If we impose the same temperature for all excitation densities, τ_{D} and τ_{X^α} then stay constant over the densities, and we get, as expected, slower dynamics for lower than for higher densities.

We report in Fig. 6.2 the parameters A_2 and A_3 derived from our calculations. We first notice that their temperature dependence better reminds the behavior of the bi-molecular recombination rate $B(T_c)$ than of the bimolecular formation rate $C(T_c)$. In our range of temperatures, $C(T_c)$ mostly depends on carrier-acoustic phonon interactions and thus stays constant (Piermarocchi *et al.*, 1997). The $1/T_c$ dependence of $B(T_c)$ comes from the momentum conservation of carriers. Our results strongly suggest that the momentum conservation of carriers play a very important role in both bi- and tri-molecular trion formation processes. This outcome yields new insight on trion formation process that should stimulate further theoretical investigations. Secondly, it turns out that both bi- and tri-molecular channels are essential to the generation of trions. At high carrier densities, i.e. short times or large densities, the tri-molecular process even dominates the bimolecular. This is evidenced by the thin-dashed fit in Fig. 6.1, calculated after having artificially eliminated the A_3 component. Finally, the trion formation time from an initial resonantly excited gas of exciton was measured in CdTe QWs for both X^- (Portella-Oberli *et al.*, 2003) and X^+ (Plochocka *et al.*, 2004) and turned out to be identical, which

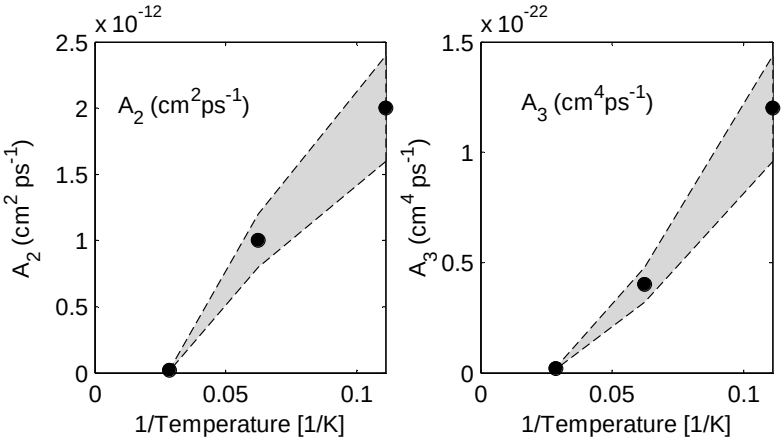

Figure 6.2: The bi- and tri- molecular trion formation coefficients A_2^α and A_3^α as a function of the inverse carrier temperature. The dark area states for the error. At 35 K, $A_2 \approx 2.0 \times 10^{-14}$ cm^{2}ps^{-1} and $A_3 \approx 4.0 \times 10^{-24}$ cm^{4}ps^{-1}.

comforts our assumption $A_2^- = A_2^+$. The bimolecular coefficient drawn from those experiments ($A_2 \approx 3 \times 10^{-12}$ cm^2/ps) matches ours. In next section, a theoretical derivation of both bi- and tri-molecular formation coefficients will confirm our hypothesis and qualitatively reproduce the temperature dependence in our experiments.

6.4 Theoretical derivation of the bi- and tri-molecular coefficients

In the previous section we were able to find experimentally the dependence of both bimolecular and tri-molecular formation coefficients. In this section, we propose a theoretical derivation of these coefficients. We first reproduce the results of Piermarocchi *et al.* (1997) on exciton formation. We then extend the formalism to the case of charged excitons.

6.4.1 Bimolecular formation of excitons

The dynamics of the exciton formation is considered in the framework of the Boltzmann equation for a system containing free electrons, free holes, and excitons. The residual Coulomb interaction between the free carriers is neglected, which is justified in the range of temperatures and densities considered. In this work we focus on the exciton formation mechanism and do not discuss the relaxation of the three species within their respective bands, the electron-hole scattering, and radiative recombination. We denote the occupation numbers for electrons, holes, and excitons by $f_e(\boldsymbol{k}_e)$, $f_h(\boldsymbol{k}_h)$, and $f_X(\boldsymbol{k}_X)$, respectively, where $\boldsymbol{k}_e$, $\boldsymbol{k}_h$, and $\boldsymbol{k}_X$ are the in-plane momenta for electrons, holes, and excitons. For the bimolecular formation, following Piermarocchi *et al.* (1997), the scattering terms in the Boltzmann equation process reads

$$\left(\frac{\mathrm{d}f_e(\boldsymbol{k_e})}{\mathrm{d}t}\right)_{form} = -\sum_{\boldsymbol{k_X},\boldsymbol{k_h}} w_{\boldsymbol{k_e},\boldsymbol{k_h}\to\boldsymbol{k_X}} f_h(\boldsymbol{k_h}) f_e(\boldsymbol{k_e}), \tag{6.1}$$

where $w_{\boldsymbol{k_e},\boldsymbol{k_h}\to\boldsymbol{k_X}}$ represents the probability per unit time for a free electron and a free hole to bind together and form an exciton. Free carriers thermalize very quickly in comparison to the exciton formation time, notably through fast carrier-carrier scattering (Knox, 1992). It is thus assumed that during the evolution of the system, the free electrons and holes are thermalized at the same temperature T_c. In the scattering term of Eq. (6.1), we use for $f_e(k_e)$, and $f_h(k_h)$ equilibrium Boltzmann distribution function at T_c. Consequently, by summing Eq. (6.1) over $\boldsymbol{k_e}$, we obtain an adiabatic equation for the evolution of the electronic density $n_e = \frac{1}{S}\sum_{\boldsymbol{k_e}} f_e(\boldsymbol{k_e})$

$$\frac{\mathrm{d}n_e}{\mathrm{d}t} = -\sum_{\boldsymbol{k_X}} F(\boldsymbol{k_X}) n_e n_h \equiv -C n_e n_h. \tag{6.2}$$

The coefficient C is the bimolecular formation coefficient, which depends on both T_c and the lattice temperature T_l through the term

$$F(\boldsymbol{k_X}) = \left(\frac{2\pi\hbar^2}{k_B T_c}\right)^2 \frac{1}{m_e m_h S} \sum_{\boldsymbol{k_e},\boldsymbol{k_h}} w_{\boldsymbol{k_e},\boldsymbol{k_h}\to\boldsymbol{k_X}} e^{-(E_e(\boldsymbol{k_e})+E_h(\boldsymbol{k_h}))/k_B T_c}, \tag{6.3}$$

where S denotes the QW surface area.

Free carriers are coupled to the exciton by a continuum of phonon states $(\boldsymbol{q}, q_z)$ through a carrier-phonon interaction Hamiltonian $\mathcal{H}_{e/h-ph}$. A phonon can be emitted (+) or absorbed (-) in the formation process of the exciton. We calculate both case separatly using the Fermi's golden rule

$$w^{\pm}_{\boldsymbol{k}_e,\boldsymbol{k}_h\to\boldsymbol{k}_X} = \frac{2\pi}{\hbar}\sum_{\boldsymbol{q},q_z}\left|\langle\boldsymbol{k}_X|\otimes\langle n_{\boldsymbol{q},q_z}\pm 1|\,\mathcal{H}_{e/h-ph}\,|n_{\boldsymbol{q},q_z}\rangle\otimes|\boldsymbol{k}_e\rangle\otimes|\boldsymbol{k}_h\rangle\right|^2 \times\delta\Big[E_e(\boldsymbol{k}_e)+E_h(\boldsymbol{k}_h)-E_X(\boldsymbol{k}_X)\mp\hbar\omega_{ph}(\boldsymbol{q},q_z)\Big], \quad (6.4)$$

with $E_e(\boldsymbol{k}_e)$, $E_h(\boldsymbol{k}_h)$ and $E_X(\boldsymbol{k}_X)$ the energy dispertion of the electrons, holes and excitons respectively, and $\hbar\omega_{ph}(\boldsymbol{q},q_z)$ the energy of the emitted (absorbed) phonon. We first build the bound and unbound electron-hole pair states $|\boldsymbol{k}_X\rangle$ and $|\boldsymbol{k}_e\rangle\otimes|\boldsymbol{k}_h\rangle$.

Bound and unbound exciton states. Let $(\boldsymbol{r}_{e\parallel},z_e)$ and $(\boldsymbol{r}_{h\parallel},z_h)$ be the electron and hole position vectors respectively and $\Phi^X[(\boldsymbol{r}_{e\parallel},z_e),(\boldsymbol{r}_{h\parallel},z_h)]$ the exciton wavefunction, where we have separated the coordinates in the QW plane (x-y) from the perpendicular coordinates (z). Denoting the electron (hole) in-plane momenta $\boldsymbol{k}_e$ ($\boldsymbol{k}_h$), we write the in-plane Fourier transform of this function

$$\Phi^X_{\boldsymbol{k}_e,\boldsymbol{k}_h}(z_e,z_h)=\frac{1}{S}\int \mathrm{d}\,r_{e\parallel}\mathrm{d}\,r_{h\parallel}\Phi^X[(\boldsymbol{r}_{e\parallel},z_e),(\boldsymbol{r}_{h\parallel},z_h)]\,e^{-i(\boldsymbol{k}_e\cdot\boldsymbol{r}_{e\parallel}+\boldsymbol{k}_h\cdot\boldsymbol{r}_{h\parallel})}, \quad (6.5)$$

where S denotes the QW surface area. Transforming to center-of-mass (CM) and relative coordinates in the QW plane — $\boldsymbol{R}_\parallel=\alpha_X\boldsymbol{r}_{e\parallel}+\beta_X\boldsymbol{r}_{h\parallel}$, $\boldsymbol{r}_\parallel=\boldsymbol{r}_{e\parallel}-\boldsymbol{r}_{h\parallel}$, where $\alpha_X=m_e/M_X$, $\beta_X=m_h/M_X$ and m_e, m_h, M_X are the electron, hole and exciton in-plane effective mass — we can apply Bloch's theorem and decompose the exciton wavefunction into a free motion part $e^{i\boldsymbol{k}_X\cdot\boldsymbol{R}_\parallel}$ related to the exciton in-plane momentum $\boldsymbol{k}_X$ and an envelope function. To facilitate the calculation, we use an envelope function separable in z and $r_\parallel$, although it is strictly justifiable only for narrow well structures,

$$\phi^X(r_\parallel,z_e,z_h)=\chi_e(z_e)\chi_h(z_h)\varphi^{\lambda_X}(r_\parallel). \quad (6.6)$$

The confinement functions $\chi_e(z_e)$ ($\chi_h(z_h)$) is taken to be the wavefunction of an electron (hole) in the ground state of a finite square quantum well (Bastard,

1988)

$$\chi_\alpha(z_\alpha) = \begin{cases} A_\alpha \cos\left(k_z^{w(\alpha)} z_\alpha\right) & \text{for} \quad |z_\alpha| < \frac{L_z}{2} \\ B_\alpha \exp\left(-k_z^{b(\alpha)}(|z_\alpha| - L_z/2)\right) & \text{for} \quad |z_\alpha| > \frac{L_z}{2}, \ \alpha = e, h, \end{cases} \tag{6.7}$$

and we use the simplest electron orbital function

$$\varphi^{\lambda_X}(r_\parallel) = \sqrt{\frac{2}{\pi\lambda_X^2}} e^{-r_\parallel/\lambda_X}, \tag{6.8}$$

whose in-plane Fourier transform is given by

$$\varphi_{\boldsymbol{k}}^{\lambda_X} = \sqrt{\frac{8\pi{\lambda_X}^2}{S}} \left[1 + (\lambda_X k)^2\right]^{-3/2}. \tag{6.9}$$

The variational parameter λ_X is associated with the Bohr radius of the exciton in the QW. Eq. (6.5) can be rewritten as

$$\begin{aligned} \Phi^X_{\boldsymbol{k}_e,\boldsymbol{k}_h}(z_e, z_h) =& \frac{1}{S} \int \mathrm{d}\, R_\parallel \mathrm{d}\, r_\parallel \phi^X(r_\parallel, z_e, z_h) \\ & \times e^{i\boldsymbol{k}_X\cdot\boldsymbol{R}_\parallel} e^{-i[\boldsymbol{R}_\parallel\cdot(\boldsymbol{k}_e+\boldsymbol{k}_h)+\boldsymbol{r}_\parallel\cdot(\beta_X\boldsymbol{k}_e-\alpha_X\boldsymbol{k}_h)]} \\ =& \delta_{\boldsymbol{k}_X-\boldsymbol{k}_e-\boldsymbol{k}_h} \phi^X_{\boldsymbol{k}_e-\alpha_X\boldsymbol{k}_X}(z_e, z_h), \end{aligned} \tag{6.10}$$

where $\phi^X_{\boldsymbol{k}}(z_e, z_h) = \chi_e(z_e)\chi_h(z_h)\varphi^{\lambda_X}_{\boldsymbol{k}}$ is the in-plane Fourier transform of the exciton envelope function. We can now construct the state of a single exciton with an in-plane momentum $\boldsymbol{k}_X$ in the Fermionic Hilbert space of electron-hole pairs. It is the superposition of wavefunctions (6.10) with all electron momenta $\boldsymbol{k}_e$ and all electron z_e and hole z_h coordinates, given by

$$|\boldsymbol{k}_X\rangle = \sum_{\boldsymbol{k}_e} \int \mathrm{d}z_e\, \mathrm{d}z_h\, \phi^{X*}_{\alpha_X\boldsymbol{k}_X+\boldsymbol{k}_e}(z_e, z_h)\, \hat{c}^\dagger_{-\boldsymbol{k}_e,z_e} \hat{d}^\dagger_{\boldsymbol{k}_X+\boldsymbol{k}_e,z_h} |0\rangle, \tag{6.11}$$

where $\hat{c}^\dagger_{\boldsymbol{k}_X,z_e}$ ($\hat{d}^\dagger_{\boldsymbol{k}_X,z_h}$) is the electron (hole) creation operator with in-plane momentum $\boldsymbol{k}_X$ and z_e (z_h) coordinate.

Similarly, we choose plane waves for the free carriers. Thus the in-plane Fourier transform $\psi^\alpha_{\boldsymbol{k}}(z)$ of the carrier wavefunction takes the simple form

$$\psi^\alpha_{\boldsymbol{k}}(z) = \chi_\alpha(z), \quad \alpha = e, h. \tag{6.12}$$

The unbound electron-hole pair then reads

$$|\boldsymbol{k}_e, \boldsymbol{k}_h\rangle = \int \mathrm{d}z_e\, \mathrm{d}\, z_h\, \psi^{e*}_{\boldsymbol{k}_e}(z_e)\, \psi^{h*}_{\boldsymbol{k}_h}(z_h) \hat{c}^\dagger_{\boldsymbol{k}_e,z_e} \hat{d}^\dagger_{\boldsymbol{k}_h,z_h} |0\rangle. \tag{6.13}$$

Carrier-phonon interaction Hamiltonian. We write the interaction Hamiltonian for a coupled electron-phonon system in the notation of the second quantization (Mahan, 2000)

$$\mathcal{H}_{\alpha-ph} = \sum_{\boldsymbol{q},q_z} V^{\alpha}_{\boldsymbol{q},q_z}\left(\hat{a}_{\boldsymbol{q},q_z} + \hat{a}^{\dagger}_{-\boldsymbol{q},-q_z}\right)\hat{\rho}_{\alpha}(\boldsymbol{q},q_z) \tag{6.14}$$

where $\hat{a}^{\dagger}_{\boldsymbol{q},q_z}$ is the phonon creation operator. The electron density operator $\hat{\rho}_{\alpha}(\boldsymbol{r}_{\parallel},z)$ and its counterpart in Fourier space $\hat{\rho}_{\alpha}(\boldsymbol{q},q_z)$ are expressed on the basis $\left\{\phi^{\sigma}_{\boldsymbol{k}}(\boldsymbol{r}_{\parallel},z,s) = e^{i\boldsymbol{k}\cdot\boldsymbol{r}_{\parallel}}\delta(z)\zeta_{\sigma}(s)\right\}$

$$\hat{\rho}^{\sigma}_{e}(\boldsymbol{r}_{\parallel},z) = \sum_{\boldsymbol{k},\boldsymbol{k}'}\hat{c}^{\sigma\dagger}_{\boldsymbol{k},z}\hat{c}^{\sigma}_{\boldsymbol{k}',z}e^{-i(\boldsymbol{k}-\boldsymbol{k}')\cdot\boldsymbol{r}_{\parallel}}, \tag{6.15}$$

$$\hat{\rho}^{\sigma}_{e}(\boldsymbol{q},q_z) = \sum_{\boldsymbol{k}}\int \mathrm{d}z\; e^{-iq_zz}\hat{c}^{\sigma\dagger}_{\boldsymbol{k}+\boldsymbol{q},z}\hat{c}^{\sigma}_{\boldsymbol{k},z},$$

$$\hat{\rho}^{\sigma}_{h}(\boldsymbol{r}_{\parallel},z) = -\sum_{\boldsymbol{k},\boldsymbol{k}'}\hat{d}^{\sigma\dagger}_{\boldsymbol{k},z}\hat{d}^{\sigma}_{\boldsymbol{k}',z}e^{-i(\boldsymbol{k}-\boldsymbol{k}')\cdot\boldsymbol{r}_{\parallel}}, \tag{6.16}$$

$$\hat{\rho}^{\sigma}_{h}(\boldsymbol{q},q_z) = -\sum_{\boldsymbol{k}}\int \mathrm{d}z\; e^{-iq_zz}\hat{d}^{\sigma\dagger}_{\boldsymbol{k}+\boldsymbol{q},z}\hat{d}^{\sigma}_{\boldsymbol{k},z}.$$

Spin states $\zeta_{\sigma}(s) = \langle\sigma|s\rangle$ have been intruduced for their will be necessary when we treat the trion formation.

Only longitudinal acoustical (LA) and longitudinal optical phonons (LO) couple significantly to careers. We express the coupling vertex functions $V^{\alpha}_{\boldsymbol{q},q_z}$ for both coupling

$$V^{\alpha\,(LA)}_{\boldsymbol{q},q_z} = ia_{\alpha}\sqrt{\frac{\hbar(|\boldsymbol{q}|^2+q_z^2)}{2\rho_0 V\omega_{\boldsymbol{q},q_z}}}, \quad V^{\alpha\,(LO)}_{\boldsymbol{q},q_z} = \sqrt{\frac{2\pi\hbar\omega_{\boldsymbol{q},q_z}e^2}{(|\boldsymbol{q}|^2+q_z^2)V}\left(\frac{1}{\epsilon_0}-\frac{1}{\epsilon_{\infty}}\right)}, \tag{6.17}$$

where ϵ_0 is the static dielectric constant and ϵ_{∞} is the *high frequency* dielectric constant. We use the notation a_{α} for the deformation-potential constant (assumed to be associated with a non-degenerate conduction or valence band), ρ_0 for the density of the crystal, e for the charge of the electron and V for the volume of the sample. We follow Einstein interpolation scheme, so that the dispersion is merely $\omega^{LA}_{\boldsymbol{q}} = v_s\sqrt{\boldsymbol{q}^2+q_z^2}$ for LA phonons and $\omega^{LO}_{\boldsymbol{q}} = \omega_{LO}$ for LO phonons, v_s standing for the Debye sound velocity and ω_{LO} for the reststrahl frequency.

Matrix element calculation. The matrix elements in Eq. (6.4) are calculated, making use of Eq. (6.11) and (6.13)

$$
\begin{aligned}
&\langle \boldsymbol{k}_X, n_{\boldsymbol{q},q_z} \pm 1| \, \mathcal{H}_{\text{e-ph}} + \mathcal{H}_{\text{h-ph}} \, |\boldsymbol{k}_e, \boldsymbol{k}_h, n_{\boldsymbol{q},q_z}\rangle \\
&= \sum_{\tilde{\boldsymbol{q}},\tilde{q}_z} \sum_{\boldsymbol{k},\boldsymbol{k}'_e} \int \mathrm{d}z_e \, \mathrm{d}z_h \, \mathrm{d}z'_e \, \mathrm{d}z'_h \, \mathrm{d}z \, \varphi^X_{\alpha \boldsymbol{k}_X + \boldsymbol{k}'_e} \\
&\quad \times \langle n_{\boldsymbol{q},q_z} \pm 1 | \hat{a}_{\pm\tilde{q},\tilde{q}_z} \hat{a}^\dagger_{-\tilde{\boldsymbol{q}},-\tilde{q}_z} | n_{\boldsymbol{q},q_z}\rangle \chi^*_e(z_e) \chi_e(z'_e) \chi^*_h(z_h) \chi_h(z'_h) e^{-i\tilde{q}_z z} \\
&\quad \times \Big\{ V^e_{\tilde{\boldsymbol{q}},\tilde{q}_z} \langle 0 | \hat{c}_{-\boldsymbol{k}'_e,z'_e} \hat{c}^\dagger_{\boldsymbol{k}+\tilde{\boldsymbol{q}},z} \hat{c}_{\boldsymbol{k},z} \hat{c}^\dagger_{\boldsymbol{k}_e,z_e} | 0\rangle \langle 0 | \hat{d}_{\boldsymbol{k}_X+\boldsymbol{k}'_e,z'_h} \hat{d}^\dagger_{\boldsymbol{k}_h,z_h} | 0\rangle \\
&\qquad\quad - V^h_{\tilde{\boldsymbol{q}},\tilde{q}_z} \langle 0 | \hat{c}_{-\boldsymbol{k}'_e,z'_e} \hat{c}^\dagger_{\boldsymbol{k}_e,z_e} | 0\rangle \langle 0 | \hat{d}_{\boldsymbol{k}_X+\boldsymbol{k}'_e,z'_h} \hat{d}^\dagger_{\boldsymbol{k}+\tilde{\boldsymbol{q}},z} \hat{d}_{\boldsymbol{k},z} \hat{d}^\dagger_{\boldsymbol{k}_h,z_h} | 0\rangle \Big\}.
\end{aligned}
$$

Applying operators on the ground state

$$
\begin{aligned}
\langle 0 | \hat{c}_{-\boldsymbol{k}'_e,z'_e} \hat{c}^\dagger_{\boldsymbol{k}+\tilde{\boldsymbol{q}},z} \hat{c}_{\boldsymbol{k},z} \hat{c}^\dagger_{\boldsymbol{k}_e,z_e} | 0\rangle &= \delta_{-\boldsymbol{k}'_e,\boldsymbol{k}+\tilde{\boldsymbol{q}}} \, \delta(z - z'_e) \, \delta_{\boldsymbol{k},\boldsymbol{k}_e} \, \delta(z - z_e) \\
\langle 0 | \hat{d}_{\boldsymbol{k}_X+\boldsymbol{k}'_e,z'_h} \hat{d}^\dagger_{\boldsymbol{k}_h,z_h} | 0\rangle &= \delta_{\boldsymbol{k}_h,\boldsymbol{k}_X+\boldsymbol{k}'_e} \, \delta(z_h - z'_h) \\
\langle 0 | \hat{c}_{-\boldsymbol{k}'_e,z'_e} \hat{c}^\dagger_{\boldsymbol{k}_e,z_e} | 0\rangle &= \delta_{\boldsymbol{k}_e,-\boldsymbol{k}'_e} \, \delta(z_e - z'_e) \\
\langle 0 | \hat{d}_{\boldsymbol{k}_X+\boldsymbol{k}'_e,z'_h} \hat{d}^\dagger_{\boldsymbol{k}+\tilde{\boldsymbol{q}},z} \hat{d}_{\boldsymbol{k},z} \hat{d}^\dagger_{\boldsymbol{k}_h,z_h} | 0\rangle &= \delta_{\boldsymbol{k}_X+\boldsymbol{k}'_e,\boldsymbol{k}+\tilde{\boldsymbol{q}}} \, \delta(z - z'_h) \, \delta_{\boldsymbol{k},\boldsymbol{k}_h} \, \delta(z - z_h) \\
\langle n_{\boldsymbol{q},q_z} \pm 1 | \hat{a}_{\tilde{\boldsymbol{q}},\tilde{q}_z} + \hat{a}^\dagger_{-\tilde{\boldsymbol{q}},-\tilde{q}_z} | n_{\boldsymbol{q},q_z}\rangle &= \sqrt{n_{\boldsymbol{q},q_z} + \tfrac{1}{2} \pm \tfrac{1}{2}} \, \delta_{\mp\tilde{\boldsymbol{q}},\boldsymbol{q}} \, \delta_{\mp\tilde{q}_z,q_z}
\end{aligned}
$$

we obtain

$$
\begin{aligned}
&\langle \boldsymbol{k}_X, n_{\boldsymbol{q},q_z} \pm 1| \, \mathcal{H}_{\text{e-ph}} + \mathcal{H}_{\text{h-ph}} \, |\boldsymbol{k}_e, \boldsymbol{k}_h, n_{\boldsymbol{q},q_z}\rangle \\
&= \sqrt{n_{\boldsymbol{q},q_z} + \tfrac{1}{2} \pm \tfrac{1}{2}} \, \delta_{\pm\boldsymbol{q},\boldsymbol{k}_e+\boldsymbol{k}_h-\boldsymbol{k}_X} \\
&\qquad \times \Big\{ V^e_{\boldsymbol{q},q_z} \varphi^X_{-\beta_X \boldsymbol{k}_X + \boldsymbol{k}_h} I_e(q_z) - V^h_{\boldsymbol{q},q_z} \varphi^X_{\alpha_X \boldsymbol{k}_X - \boldsymbol{k}_e} I_h(q_z) \Big\}, \qquad (6.18)
\end{aligned}
$$

where the integrals, in the orthogonal direction are given by

$$
I_\alpha(q_z) = \int \mathrm{d}z_\alpha \, |\chi_\alpha(z_\alpha)|^2 e^{i q_z z_\alpha}, \qquad \alpha = \{e, h\}. \qquad (6.19)
$$

Finally, if we choose the bound and unbound electron-hole pairs dispersion to be parabolic, the probability transition (6.4) reads

$$
\begin{aligned}
&w^{\pm}_{\boldsymbol{k}_e,\boldsymbol{k}_h\to\boldsymbol{k}_X} \\
&= \frac{2\pi}{\hbar}\sum_{\boldsymbol{q},q_z}\left(n_{\boldsymbol{q},q_z}+\tfrac{1}{2}\pm\tfrac{1}{2}\right)\left|V^{e}_{\boldsymbol{q},q_z}\varphi^{X}_{\beta_X\boldsymbol{k}_X-\boldsymbol{k}_h}I_e(q_z)-V^{h}_{\boldsymbol{q},q_z}\varphi^{X}_{\alpha_X\boldsymbol{k}_X-\boldsymbol{k}_e}I_h(q_z)\right|^2 \\
&\qquad\times\delta\left[\frac{\hbar^2k_e^2}{2m_e}+\frac{\hbar^2k_h^2}{2m_h}+E_b-\frac{\hbar^2k_X^2}{2M}\mp\hbar\omega_{ph}(\boldsymbol{q},q_z)\right]\delta_{\pm\boldsymbol{q},\boldsymbol{k}_e+\boldsymbol{k}_h-\boldsymbol{k}_X}.
\end{aligned}
\tag{6.20}
$$

LA phonons assisted formation Considering that the sample volume $V = L_zS$ is macroscopic the sum over the orthogonal phonon wavevectors may be replaced by the integral

$$
\sum_{q_z}\longleftrightarrow\quad\left(\frac{L_z}{2\pi}\right)\int \mathrm{d}q_z \tag{6.21}
$$

and reexpressing the Dirac distribution as

$$
\begin{aligned}
&\delta\left[\frac{\hbar^2k_e^2}{2m_e}+\frac{\hbar^2k_h^2}{2m_h}+E_b-\frac{\hbar^2k_X^2}{2M}\mp\hbar v_s\sqrt{\boldsymbol{q}^2+q_z^2}\right] \\
&=\frac{\sqrt{\boldsymbol{q}^2+q_z^2}}{|\hbar v_s q_z|}\left\{\delta\left[q_z-q_z^{(0)}(\boldsymbol{k}_e,\boldsymbol{k}_h,\boldsymbol{k}_X))\right]+\delta\left[q_z+q_z^{(0)}(\boldsymbol{k}_e,\boldsymbol{k}_h,\boldsymbol{k}_X)\right]\right\} \\
&\qquad\times\theta\left[\pm\left(\frac{\hbar^2k_e^2}{2m_e}+\frac{\hbar^2k_h^2}{2m_h}+E_b-\frac{\hbar^2k_X^2}{2M}\right)\right],
\end{aligned}
\tag{6.22}
$$

with

$$
q_z^{(0)}(\boldsymbol{k}_e,\boldsymbol{k}_h,\boldsymbol{k}_X)=\sqrt{\frac{1}{\hbar^2v_s^2}\left(\frac{\hbar^2k_e^2}{2m_e}+\frac{\hbar^2k_h^2}{2m_h}+E_b-\frac{\hbar^2k_X^2}{2M}\right)^2-q^2}, \tag{6.23}
$$

makes the integration (6.21) trivial for LA phonons:

$$
\begin{aligned}
w_{\boldsymbol{k}_e,\boldsymbol{k}_h\to\boldsymbol{k}_X} &= \frac{4\pi}{\hbar}\frac{L_z}{2\pi}\frac{\hbar}{2\rho V v_s}\frac{q^2+{q_z^{(0)}}^2}{|\hbar v_s q_z^{(0)}|} \\
&\times \left|a_e\varphi^X_{\beta_X\boldsymbol{k}_X-\boldsymbol{k}_h} I_e(q_z^{(0)}) - a_h\varphi^X_{\alpha_X\boldsymbol{k}_X-\boldsymbol{k}_e} I_h(q_z^{(0)})\right|^2 \\
&\times \left\{\left(n_{\boldsymbol{q},q_z^{(0)}}+1\right)\,\theta\left(\frac{\hbar^2k_e^2}{2m_e}+\frac{\hbar^2k_h^2}{2m_h}+E_b-\frac{\hbar^2k_X^2}{2M}\right)\right. \\
&\qquad \left. + n_{\boldsymbol{q},q_z^{(0)}}\,\theta\left(-\frac{\hbar^2k_e^2}{2m_e}-\frac{\hbar^2k_h^2}{2m_h}-E_b+\frac{\hbar^2k_X^2}{2M}\right)\right\}. \qquad (6.24)
\end{aligned}
$$

This expression already includes the sum over absorbed and emitted phonon contributions. The phonon in-plane momentum needs to be substituted by $\boldsymbol{q} = \boldsymbol{k}_e + \boldsymbol{k}_h - \boldsymbol{k}_X$.

LO phonons assisted formation In the case of interaction with LO phonons, Eq. 6.20 becomes

$$
\begin{aligned}
w_{\boldsymbol{k}_e,\boldsymbol{k}_h\to\boldsymbol{k}_X} &= \sum_{q_z}\frac{2\pi}{\hbar}\frac{\hbar\omega_{LO}e^2(1/\epsilon_\infty - 1/\epsilon_0)}{V(q^2+q_z^2)}n_{\boldsymbol{q},q_z} \\
&\times \left|\varphi^X_{\beta_X\boldsymbol{k}_X-\boldsymbol{k}_h} I_e(q_z) - \varphi^X_{\alpha_X\boldsymbol{k}_X-\boldsymbol{k}_e} I_h(q_z)\right|^2 \\
&\qquad \times \delta\left[\frac{\hbar^2k_e^2}{2m_e}+\frac{\hbar^2k_h^2}{2m_h}+E_b-\frac{\hbar^2k_X^2}{2M}+\hbar\omega_{LO}\right], \qquad (6.25)
\end{aligned}
$$

where we dropped the phonon absorption part, which is negligible up to room temperature. For the calculation of the exciton formation coefficient C, it is convenient to rewrite the Dirac distribution as

$$
\begin{aligned}
&\delta\left[\frac{\hbar^2k_e^2}{2m_e}+\frac{\hbar^2k_h^2}{2m_h}+E_b-\frac{\hbar^2k_X^2}{2M}+\hbar\omega_{LO}\right] \\
&\quad = \frac{M_X}{\hbar}\left\{\delta\left[k_X - k_X^{(0)}(\boldsymbol{k}_e,\boldsymbol{k}_h)\right) + \delta\left[k_X + k_X^{(0)}(\boldsymbol{k}_e,\boldsymbol{k}_h)\right]\right\}, \qquad (6.26)
\end{aligned}
$$

with

$$
k_X^{(0)}(\boldsymbol{k}_e,\boldsymbol{k}_h) = \sqrt{\frac{2M_X}{\hbar^2}\left(\frac{\hbar^2k_e^2}{2m_e}+\frac{\hbar^2k_h^2}{2m_h}+E_b-\hbar\omega_{LO}.\right)}, \qquad (6.27)
$$

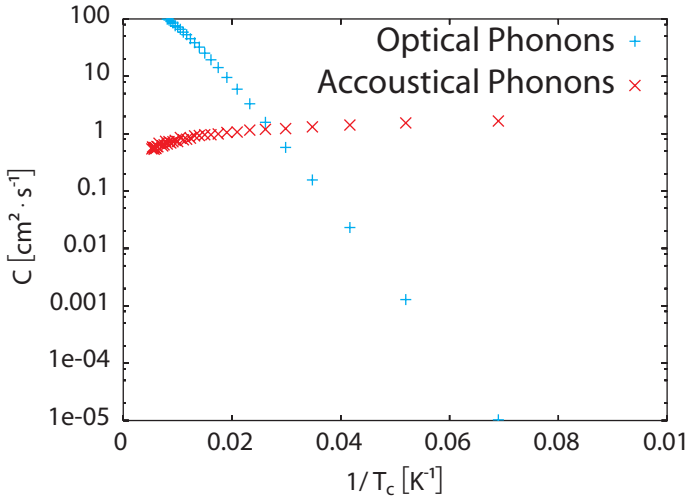

Figure 6.3: The exciton formation coefficient C as a function of the carrier temperature T_c, at a fixed lattice temperature $T_l = 10$ K. Other parameters are given in the text.

Numerical Results. If we change all the sum in Eq. 6.2, 6.3, 6.24 and 6.25 into integrals, the bimolecular formation coefficient C can be numerically calculated by Monte Carlo integration. In Fig. 6.3, we report C as a function of $1/T_c$ for a fixed lattice temperature $T_l = 5$ K, for a GaAs QW of 80 Å. The two contributions from the acoustic and optical phonons are shown separately. The acoustical phonon dominates for temperatures smaller than 40 K and does not depend on T_l. We see that these results perfectly match those published by Piermarocchi *et al.* (1997). We show in Table 6.1 the numerical value of the different parameters entering in the calculation.

Parameter	Symbol	Value	Unit
Band gap energy	E_g	1519	meV
Electron effective mass	m_e	0.08	m_0
Heavy hole effective mass	m_{hh}	0.17	m_0
LO phonon energy	$\hbar\omega_{LO}$	36	meV
Static dielectric constant	ϵ_0	12.85	
High frequency dielectric constant	ϵ_∞	10.88	
Crystal density	ρ	5.3162	$g{\cdot}cm^{-3}$
Sound velocity	v_s	4726.5	$m{\cdot}s^{-1}$
Conduction band deformation potential	a_e	−7.0	eV
Valence band deformation potential	a_h	3.5	eV
Exciton binding energy	E_T	6.5	meV
Trion binding energy	E_T	1.77	meV
Exciton Bohr radius	λ_X	11.0	nm
Trion variational parameter #1 (X^-)	λ_T	15	nm
Trion variational parameter #2 (X^-)	λ'_T	30.0	nm
Trion variational parameter #1 (X^+)	λ_T	16	nm
Trion variational parameter #2 (X^+)	λ'_T	25.0	nm

Table 6.1: GaAs Material Parameters

6.4.2 Bimolecular formation of trions

We now extend our formalism to the derivation of the bimolecular formation of trions. We restrict ourselves to negatively charged excitons and will give at the end of this work some indication on how to retrieve their positive counterpart.

We write the scattering term in the Boltzmann equation process for the bimolecular formation of trions:

$$\left(\frac{\mathrm{d}f_e(\boldsymbol{k_e})}{\mathrm{d}t}\right)_{form} = -\sum_{\boldsymbol{k_T},\boldsymbol{k_e}} F_{\boldsymbol{k_X},\boldsymbol{k_e}\to\boldsymbol{k_T}} f_X(\boldsymbol{k_X}) f_e(\boldsymbol{k_e}), \tag{6.28}$$

where $F_{\boldsymbol{k_h},\boldsymbol{k_e}\to\boldsymbol{k_T}}$ represents the probability per unit time for a bound electron-hole pair and a free electron to bind together and form an exciton. We assume that bound and unbound carriers are thermalized and use Boltzmann distribution function $f_X(k_X)$ and $f_e(k_e)$ for exciton and electron population, respectively. By summing Eq. (6.28) over $\boldsymbol{k_e}$, we obtain an adiabatic equation for the evolution of the electron density

$$\frac{\mathrm{d}n_e}{\mathrm{d}t} = -\sum_{\boldsymbol{k_T}} F(\boldsymbol{k_T}) n_X n_e \equiv -A_2^- n_X n_e. \tag{6.29}$$

The coefficient A_2^- is the bimolecular formation coefficient, which depends on both T_c and the lattice temperature T_l through the term

$$F(\boldsymbol{k_T}) = \left(\frac{2\pi\hbar^2}{k_B T_c}\right)^2 \frac{1}{m_X m_e S} \sum_{\boldsymbol{k_X},\boldsymbol{k_e}} w_{\boldsymbol{k_X},\boldsymbol{k_e}\to\boldsymbol{k_T}} e^{-(E_X(\boldsymbol{k_X})+E_e(\boldsymbol{k_e}))/k_B T_c}. \tag{6.30}$$

We calculate the formation rate using Fermi's golden rule

$$\begin{aligned} w^{\pm}_{\boldsymbol{k}_X,\boldsymbol{k}_e\to\boldsymbol{k}_T} = \frac{2\pi}{\hbar} \sum_{\boldsymbol{q},q_z} &\left|\langle \boldsymbol{k}_T| \otimes \langle n_{\boldsymbol{q},q_z} \pm 1| \mathcal{H}_{e/h-ph} |n_{\boldsymbol{q},q_z}\rangle \otimes |\boldsymbol{k}_X\rangle \otimes |\boldsymbol{k}_e\rangle\right|^2 \\ &\times \delta\left[E_X(\boldsymbol{k}_X) + E_e(\boldsymbol{k}_e) - E_T(\boldsymbol{k}_T) \mp \hbar\omega_{ph}(\boldsymbol{q}, q_z)\right], \end{aligned} \tag{6.31}$$

with $E_X(\boldsymbol{k}_X)$, $E_e(\boldsymbol{k}_e)$ and $E_T(\boldsymbol{k}_T)$ the energy dispertion of the electrons, holes and excitons respectively, and $\hbar\omega_{ph}(\boldsymbol{q}, q_z)$ the energy of the emitted (absorbed) phonon. We first build the bound and unbound electron-hole pair states $|\boldsymbol{k}_T\rangle$ and $|\boldsymbol{k}_X\rangle \otimes |\boldsymbol{k}_e\rangle$.

Trion state. The two electrons and the hole are positioned at $(\boldsymbol{r}_{1\parallel}, z_1)$, $(\boldsymbol{r}_{2\parallel}, z_2)$ and $(\boldsymbol{r}_{h\parallel}, z_h)$ respectively, while the center-of-mass (CM) and relative coordinates in the QW plane are now given by $\boldsymbol{R}_\parallel = \alpha_T(\boldsymbol{r}_{1\parallel} + \boldsymbol{r}_{2\parallel}) + \beta_T \boldsymbol{r}_{h\parallel}$ and $\boldsymbol{r}_{ih\parallel} = \boldsymbol{r}_{i\parallel} - \boldsymbol{r}_{h\parallel}$ $(i = 1, 2)$; $\alpha_T = m_e/M_T$, $\beta_T = m_h/M_T$ and M_T is the trion mass. We consider the same simple two parameter Chandrasekhar-type trial envelope function that was successively used to calculate trion-electron scattering in Chapter 3:

$$\begin{aligned}&\phi^T(r_{1h\parallel}, r_{2h\parallel}, z_1, z_2, z_h)\\ &= \mathcal{N}_T \chi_e(z_1)\chi_e(z_2)\chi_h(z_h)[\varphi^{\lambda_T}(r_{1h})\varphi^{\lambda'_T}(r_{2h}) \pm \varphi^{\lambda'_T}(r_{1h})\varphi^{\lambda_T}(r_{2h})],\end{aligned} \tag{6.32}$$

where the + (−) sign applies to the singlet (triplet) spin configuration and the trion wavefunction normalization factor is given by

$$\mathcal{N}_T = \frac{1}{\sqrt{2(1 \pm \kappa^2)}}, \tag{6.33}$$

with

$$\kappa = \frac{4\lambda\lambda'}{(\lambda + \lambda')^2}. \tag{6.34}$$

Its in-plane Fourier transform reads

$$\Phi^T_{\boldsymbol{k}_1, \boldsymbol{k}_2, \boldsymbol{k}_h}(z_1, z_2, z_h) = \delta_{\boldsymbol{k}_T - \boldsymbol{k}_1 - \boldsymbol{k}_2 - \boldsymbol{k}_h}\, \phi^T_{\alpha_T \boldsymbol{k}_T - \boldsymbol{k}_1, \alpha_T \boldsymbol{k}_T - \boldsymbol{k}_2}(z_1, z_2, z_h) \tag{6.35}$$

and the state of a single trion with an in-plane CM momentum $\boldsymbol{k}_T$ is constructed similarly to that of a single exciton

$$\begin{aligned}\left|\boldsymbol{k}_T^S\right\rangle = \sum_{\substack{\boldsymbol{k}_1, \boldsymbol{k}_2\\ s_1, s_2}} \int \mathrm{d}z_1\, \mathrm{d}z_2\, \mathrm{d}z_h\, \phi^{T*}_{\alpha_T \boldsymbol{k}_T + \boldsymbol{k}_1, \alpha_T \boldsymbol{k}_T + \boldsymbol{k}_2}(z_1, z_2, z_h)\\ \times\, \xi^*_S(s_1, s_2)\, \hat{c}^{s_1\dagger}_{-\boldsymbol{k}_1, z_1} \hat{c}^{s_2\dagger}_{-\boldsymbol{k}_2, z_2} \hat{d}^\dagger_{\boldsymbol{k}_T + \boldsymbol{k}_1 + \boldsymbol{k}_2, z_h} |0\rangle,\end{aligned} \tag{6.36}$$

where we have added the spin index to the electron creation operator and introduced $\xi_S(s_1, s_2) = \langle S|s_1, s_2\rangle$ the projection of a generic spin configuration of two electrons on the singlet spin configuration. The in-plane Fourier transform of the trion singlet wavefunction in Eq. (6.35) is given by

$$\phi^{T*}_{\boldsymbol{k}_1, \boldsymbol{k}_2}(z_1, z_2, z_h) = \mathcal{N}_T \chi_e(z_1)\chi_e(z_2)\chi_h(z_h)\left[\varphi^{\lambda_T}_{\boldsymbol{k}_1}\varphi^{\lambda'_T}_{\boldsymbol{k}_2} + \varphi^{\lambda'_T}_{\boldsymbol{k}_1}\varphi^{\lambda_T}_{\boldsymbol{k}_2}\right], \tag{6.37}$$

where $\varphi^{\lambda'_T}_{\boldsymbol{k}_1}$ has already been defined in Eq. 6.9. The exciton-free electron state is given by

$$|\boldsymbol{k}_X, \boldsymbol{k}_{e'}\rangle = \sum_{\boldsymbol{k}_e} \int \mathrm{d}z_e\, \mathrm{d}z_h\, \mathrm{d}z'_e\, \phi^*_{\alpha_X \boldsymbol{k}_X + \boldsymbol{k}_e}(z_e, z_h)\, \psi^*_{\boldsymbol{k}_{e'}}(z_{e'}) \times \hat{c}^\dagger_{-\boldsymbol{k}_e, z_e} \hat{d}^\dagger_{\boldsymbol{k}_X + \boldsymbol{k}_e, z_h} \hat{c}^\dagger_{\boldsymbol{k}_{e'}, z_{e'}} |0\rangle\,. \tag{6.38}$$

Matrix element calculation. We calculate the matrix elements in (6.31)

$$\begin{aligned}
&\langle \boldsymbol{k}^S_T; s'_h| \otimes \langle n_{\boldsymbol{q},q_z} \pm 1|\, \mathcal{H}_{e/h-ph}\, |n_{\boldsymbol{q},q_z} + 1\rangle \otimes |\boldsymbol{k}_X; s_1; s_h\rangle \otimes |\boldsymbol{k}_2; s_2\rangle \\
&= \sum_{\boldsymbol{k},s} \sum_{\boldsymbol{k}_1} \sum_{\boldsymbol{k}'_1, \boldsymbol{k}'_2} \sum_{s'_1, s'_2} \int \mathrm{d}z\; \mathrm{d}z_1\, \mathrm{d}z_2\, \mathrm{d}z_h\, \mathrm{d}z'_1\, \mathrm{d}z'_2\, \mathrm{d}z'_h \sqrt{n_{\boldsymbol{q},q_z} + 1} \\
&\times \xi^*_S(s'_1, s'_2) \phi^X_{\alpha_X \boldsymbol{k}_X + \boldsymbol{k}_1}(z_1, z_h) \psi_{\boldsymbol{k}_2}(z_2) \phi^{T*}_{\alpha_T \boldsymbol{k}_T + \boldsymbol{k}'_1, \alpha_T \boldsymbol{k}_T + \boldsymbol{k}'_2}(z'_1, z'_2, z'_h) e^{i q_z z} \\
&\times \Big[V^e_{\boldsymbol{q},q_z} \langle 0|\, \hat{c}_1\, \hat{c}_2 \hat{c}^\dagger_3 \hat{c}_4 \hat{c}^\dagger_5 \hat{c}^\dagger_6\, |0\rangle \langle 0|\, \hat{d}_7 \hat{d}^\dagger_8\, |0\rangle \\
&\qquad - V^h_{\boldsymbol{q},q_z} \langle 0|\, \hat{c}_1\, \hat{c}_2 \hat{c}^\dagger_5 \hat{c}^\dagger_6\, |0\rangle \langle 0|\, \hat{d}_7 \hat{d}^\dagger_3 \hat{d}_4 \hat{d}^\dagger_8\, |0\rangle \Big].
\end{aligned} \tag{6.39}$$

where we simplified the operators index using the following scheme

$$\begin{aligned}
&1 = (-\boldsymbol{k}'_1, z'_1, s'_1) && 2 = (-\boldsymbol{k}'_2, z'_2, s'_2) && 3 = (\boldsymbol{k} + \boldsymbol{q}, z, s) \\
&4 = (\boldsymbol{k}, z, s) && 5 = (-\boldsymbol{k}_1, z_1, s_1) && 6 = (\boldsymbol{k}_2, z_2, s_2) \\
&7 = (\boldsymbol{k}_T + \boldsymbol{k}'_1 + \boldsymbol{k}'_2, z'_h, s'_h) && 8 = (\boldsymbol{k}_X + \boldsymbol{k}_1, z_h, s_h)
\end{aligned}$$

Using the electron, holes anti-commutation relations, the Fermi vacuum expectation value of the operators read

$$\langle 0|\, \hat{c}_1\, \hat{c}_2 \hat{c}^\dagger_3 \hat{c}_4 \hat{c}^\dagger_5 \hat{c}^\dagger_6\, |0\rangle = \delta_{13}(\delta_{25}\delta_{46} - \delta_{26}\delta_{45}) - \delta_{23}(\delta_{15}\delta_{46} - \delta_{16}\delta_{45}) \tag{6.40}$$

$$\langle 0|\, \hat{d}_7 \hat{d}^\dagger_8\, |0\rangle = \delta_{78} \tag{6.41}$$

$$\langle 0|\, \hat{c}_1\, \hat{c}_2 \hat{c}^\dagger_5 \hat{c}^\dagger_6\, |0\rangle = \delta_{25}\delta_{16} - \delta_{15}\delta_{26} \tag{6.42}$$

$$\langle 0|\, \hat{d}_7 \hat{d}^\dagger_3 \hat{d}_4 \hat{d}^\dagger_8\, |0\rangle = \delta_{37}\delta_{48} \tag{6.43}$$

Using the later results in Eq. (6.39) gives

$$\begin{aligned}
&\langle \boldsymbol{k}_T^S; s_h'| \otimes \langle n_{\boldsymbol{q},q_z} \pm 1| \mathcal{H}_{e/h-ph} |n_{\boldsymbol{q},q_z}\rangle \otimes |\boldsymbol{k}_X; s_1; s_h\rangle \otimes |\boldsymbol{k}_2; s_2\rangle \\
&= \left[\xi_S^*(s_2,s_1) - \xi_S^*(s_1,s_2)\right] \delta_{s_h,s_h'} \sqrt{n_{\boldsymbol{q},q_z} + 1/2 \pm 1/2} \sum_{\boldsymbol{k}_1} \phi^X_{\alpha_X \boldsymbol{k}_X + \boldsymbol{k}_1} \\
&\times \Big\{ V^e_{\boldsymbol{q},q_z} I_e(q_z) [\phi^{T*}_{\alpha_T \boldsymbol{k}_T - \boldsymbol{k}_2, \alpha_T \boldsymbol{k}_T + \boldsymbol{k}_1 + \boldsymbol{q}} + \phi^{T*}_{\alpha_T \boldsymbol{k}_T - \boldsymbol{k}_2 + \boldsymbol{q}, \alpha_T \boldsymbol{k}_T + \boldsymbol{k}_1}] \\
&\qquad - V^h_{\boldsymbol{q},q_z} I_h(q_z) \phi^{T*}_{\alpha_T \boldsymbol{k}_T - \boldsymbol{k}_2, \alpha_T \boldsymbol{k}_T + \boldsymbol{k}_1} \Big\} \delta_{\boldsymbol{q}, \boldsymbol{k}_X + \boldsymbol{k}_2 - \boldsymbol{k}_T}. \qquad (6.44)
\end{aligned}$$

Finally, for parabolic electron, exciton and trion dispersion, the probability transition 6.31

$$\begin{aligned}
&w^{\pm}_{\boldsymbol{k}_X, \boldsymbol{k}_2 \to \boldsymbol{k}_T} \\
&= \frac{2\pi}{\hbar} \sum_{\boldsymbol{q}, q_z} (n_{\boldsymbol{q},q_z} + \tfrac{1}{2} \pm \tfrac{1}{2}) \\
&\times \left| \sum_{\boldsymbol{k}_1} V^e_{\boldsymbol{q},q_z} I_e(q_z) [\phi^{T*}_{\alpha_T \boldsymbol{k}_T - \boldsymbol{k}_2, \alpha_T \boldsymbol{k}_T + \boldsymbol{k}_1 + \boldsymbol{q}} + \phi^{T*}_{\alpha_T \boldsymbol{k}_T - \boldsymbol{k}_2 + \boldsymbol{q}, \alpha_T \boldsymbol{k}_T + \boldsymbol{k}_1}] \right. \\
&\qquad \left. - V^h_{\boldsymbol{q},q_z} I_h(q_z) \phi^{T*}_{\alpha_T \boldsymbol{k}_T - \boldsymbol{k}_2, \alpha_T \boldsymbol{k}_T + \boldsymbol{k}_1} \right|^2 \\
&\times \delta \left[\frac{\hbar^2 k_X^2}{2M_X} + \frac{\hbar^2 k_2^2}{2m_e} + E_T - \frac{\hbar^2 k_T^2}{2M_T} \mp \hbar \omega_{ph}(\boldsymbol{q}, q_z) \right] \delta_{\pm \boldsymbol{q}, \boldsymbol{k}_X + \boldsymbol{k}_2 - \boldsymbol{k}_T},
\end{aligned} \qquad (6.45)$$

where we averaged over the initial electron spin states and exciton angular momentum states.

6.4.3 Trimolecular formation of trions

Again, we write the scattering term in the Boltzmann equation process

$$\left(\frac{\mathrm{d} f_e(\boldsymbol{k}_e)}{\mathrm{d}t} \right)_{form} = - \sum_{\boldsymbol{k}_T, \boldsymbol{k}_e'} F_{\boldsymbol{k}_e, \boldsymbol{k}_e', \boldsymbol{k}_h \to \boldsymbol{k}_T} f_e(\boldsymbol{k}_e) f_e(\boldsymbol{k}_e') f_h(\boldsymbol{k}_h), \qquad (6.46)$$

where $F_{\boldsymbol{k}_e, \boldsymbol{k}_e', \boldsymbol{k}_h \to \boldsymbol{k}_T}$ represents the probability per unit time for two free electrons and one free hole to bind together and form an exciton. We assume

that bound and unbound carriers are thermalized and use Boltzmann distribution function $f_X(k_e)$ and $f_h(k_h)$ for exciton and electron population, respectively. By summing Eq. (6.46) over $\boldsymbol{k}_e$, we obtain an adiabatic equation for the evolution of the electron density

$$\frac{\mathrm{d}n_e}{\mathrm{d}t} = -\sum_{\boldsymbol{k}_T} F(\boldsymbol{k}_T) n_e^2 n_h \equiv -A_3^- n_e^2 n_h. \tag{6.47}$$

The coefficient A_3^- is the trimolecular formation coefficient, which depends on both T_c and the lattice temperature T_l through the term

$$F(\boldsymbol{k}_T) = \left(\frac{2\pi\hbar^2}{k_B T_c}\right)^3 \frac{1}{m_e^2 m_h S^{3/2}} \sum_{\boldsymbol{k}_e, \boldsymbol{k}'_e, \boldsymbol{k}_h} w_{\boldsymbol{k}_e, \boldsymbol{k}_e, \boldsymbol{k}'_h \to \boldsymbol{k}_T} e^{-(E_e(\boldsymbol{k}_e)+E_e(\boldsymbol{k}'_e)+E_h(\boldsymbol{k}_h))/k_B T_c}. \tag{6.48}$$

We calculate the formation rate using Fermi's golden rule

$$\begin{aligned} w^{\pm}_{\boldsymbol{k}_e, \boldsymbol{k}'_e, \boldsymbol{k}_h \to \boldsymbol{k}_T} = \frac{2\pi}{\hbar} \sum_{\boldsymbol{q}, q_z} \left| \langle \boldsymbol{k}_T | \otimes \langle n_{\boldsymbol{q}, q_z} \pm 1 | \, \mathcal{H}_{e/h-ph} \, | n_{\boldsymbol{q}, q_z} \rangle \otimes | \boldsymbol{k}_e \rangle \otimes | \boldsymbol{k}'_e \rangle \otimes | \boldsymbol{k}_h \rangle \right|^2 \\ \times \delta\big[E_e(\boldsymbol{k}_e) + E_e(\boldsymbol{k}'_e) + E_h(\boldsymbol{k}_h) - E_T(\boldsymbol{k}_T) \mp \hbar\omega_{ph}(\boldsymbol{q}, q_z)\big], \end{aligned} \tag{6.49}$$

with $E_X(\boldsymbol{k}_X)$, $E_e(\boldsymbol{k}_e)$ and $E_T(\boldsymbol{k}_T)$ the energy dispertion of the electrons, holes and excitons respectively, and $\hbar\omega_{ph}(\boldsymbol{q}, q_z)$ the energy of the emitted (absorbed) phonon. Finally, for parabolic electron, exciton and trion dispersion, the probability transition 6.49 becomes

$$\begin{aligned} & w^{\pm}_{\boldsymbol{k}_e, \boldsymbol{k}'_e, \boldsymbol{k}_h \to \boldsymbol{k}_T} \\ & = \frac{2\pi}{\hbar} \sum_{\boldsymbol{q}, q_z} \left(n_{\boldsymbol{q}, q_z} + \tfrac{1}{2} \pm \tfrac{1}{2}\right) \\ & \times \Big| V^e_{\boldsymbol{q}, q_z} I_e(q_z) [\phi^{T*}_{\alpha_T \boldsymbol{k}_T - \boldsymbol{k}_2, \alpha_T \boldsymbol{k}_T + \boldsymbol{k}_1 + \boldsymbol{q}} + \phi^{T*}_{\alpha_T \boldsymbol{k}_T - \boldsymbol{k}_2 + \boldsymbol{q}, \alpha_T \boldsymbol{k}_T + \boldsymbol{k}_1}] \\ & \qquad - V^h_{\boldsymbol{q}, q_z} I_h(q_z) \phi^{T*}_{\alpha_T \boldsymbol{k}_T - \boldsymbol{k}_2, \alpha_T \boldsymbol{k}_T + \boldsymbol{k}_1} \Big|^2 \\ & \times \delta\left[\frac{\hbar^2 k_e^2}{2m_e} + \frac{\hbar^2 k_e'^2}{2m_e} + \frac{\hbar^2 k_h^2}{2m_h} + E_T - \frac{\hbar^2 k_T^2}{2M_T} \mp \hbar\omega_{ph}(\boldsymbol{q}, q_z)\right] \delta_{\pm \boldsymbol{q}, \boldsymbol{k}_X + \boldsymbol{k}_2 - \boldsymbol{k}_T}, \end{aligned} \tag{6.50}$$

where we averaged over the initial electron spin states and exciton angular momentum states.

6.4.4 Numerical results

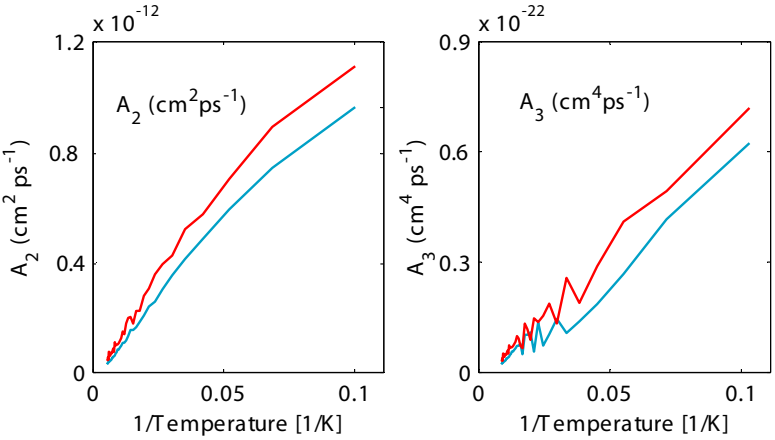

Figure 6.4: The bi- and tri- molecular trion formation coefficients A_2^α and A_3^α as a function of the inverse carrier temperature as calculated from our model for LA phonon assisted formation. The red curve indicates X^+ formation and the blue curve X^- formation.

In Fig. 6.4, we represent the results of our numerical calculation for LA phonon assisted formation. We stress the fact that the results for LO phonons are orders of magnitude smaller and consequently negligible for bi- and tri-molecular processes. This shows that the exclusive formation mechanism for trions is governed by LA phonon interaction. We correctly predict a decrease of the bi- or tri-molecular formation for raising temperatures. We also demonstrate that the bi and tri-molecular formation coefficients for negatively and positively charged excitons are approximatively equal ($A_2^+ = A_2^-$) and ($A_3^+ = A_3^-$), which validates the assumption made at the beginning of this chapter. However, the values are about 2 times smaller at 10 K and do not drop as sharply as in the experiment for increasing temperatures. A more accurate calculation should rely on a better trion wavefunction. The Chandrashekar variational function is

most likely to simple to yield quantitative results. We also argue, that in order to simplify our model, we neglected any dark state channel that may play a role in the overall dynamic of our system. However, we believe that our model is sufficient to predict the dynamics of the photoluminescence spectra for trions.

6.5 Predictions of our model

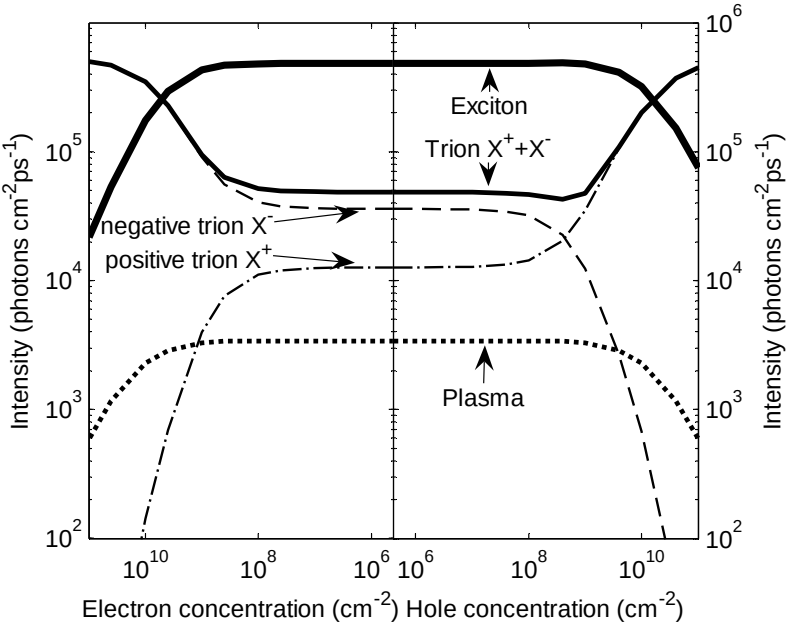

Figure 6.5: Exciton, trion (X^- and X^+) and plasma cw-luminescence intensities calculated as a function of the residual electron (left panel) and hole (right panel) concentrations at T_c=9.0 K. A 5×10^5 photons/(cm^{2}ps) density was assumed.[1]

We demonstrate the robustness of our model by some convincing predictions. In Fig. 6.5, we apply our rate equations model to the cw-luminescence of excitons, trions and free carriers in an InGaAs QW. In the absence of excess carriers ($\boldsymbol{n} = \boldsymbol{p}$), the trion luminescence is about 20 times weaker than the

exciton one, which is in very good agreement with experiments (Glasberg *et al.*, 1999). The difference in intensities of X^- and X^+ cw-luminescence shown in Fig. 6.5 are the consequence of the difference between K_2^α and K_3^α, imposed by the mass difference between positive and negative trions. The critical excess carrier concentration of about 10^{10} cm^{-2} at which trions start to dominate the luminescence spectrum, does correspond to many experiments (Kossacki, 2003). What is new however, is that the crossing of X^- and X^+ intensities, which has been observed experimentally (Glasberg *et al.*, 1999), does not occur at zero excess carrier density but is shifted toward some positive carrier density.

Applied to a system of excitons under resonant excitation, our model explains a very puzzling decay time of excitons, which is raised from 20 ps to 100 ps in the presence of an excess electron gas (Finkelstein *et al.*, 1998). Excitons and trions actually come into thermal equilibrium and decay together, which considerably stretches the decay time.

6.6 Conclusion

In summary, we have shown that both bi- and tri-molecular processes are necessary to describe trion formation. We could quantify both formation rates from the experiment and draw an empirical law for their temperature dependence. This law was confirmed by a simple formation model at low temperature. At high temperature, we argued that inelastic electron scattering contributes to trion ionization and should be taken into account. We obtained new insight on X^- and X^+ luminescence intensities at low excess carrier densities. The model turned out to be also perfectly applicable to other experiments.

7 Conclusion

In this thesis work, we carried on pioneering work on the dynamics of nonlinearities in modulation-doped quantum wells.

We demonstrated through cw linear optical measurements (Chapter 3) that electrons scatter with excitons and trions, affecting profoundly the shape of their resonance; the high energy tail of both trion and exciton resonance is broadened and the exciton oscillator strength is reduced. Electron scattering was shown to play an important role in non-linear pump and probe experiments (Chapter 4) as well as in the formation dynamics of trions from a free electron-hole plasma (6). In pump and probe experiments, a photogenerated exciton gas was shown to heat the excess electron gas and modify their scattering properties. The trion creation process removed electrons from the quantum well and strongly reduced the scattering.

We also evidenced correlated behavior of excitons and trions under excitation, which manifests itself by crossed trion-exciton effects. We observed a wealth of phenomena encompassing bleaching, crossed bleaching, induced-absorption and energy shifts of the resonances. Significant differences were found between the nonlinear optical effects induced by an exciton and a trion population. We also evidenced high-order exciton correlations, up to the fifth-order, in the presence of electrons.

These strong correlations lead to very interesting features in the coherent regime, that we would have never expected within a gas of electrons. We identified biexcitons and demonstrated their stability through coherent optical Stark measurements (Chapter 4). We proved that both ac Stark splitting with gain and electromagnetically induced transparency were observable within an electron gas, despite electron induced dephasing.

Finally, we demonstrated that the dynamics of exciton, trion and electron-hole plasma can be ruled by a simple rate equation model, in which we accounted for bimolecular formation of excitons from an electron-hole plasma, bimolecular formation of trions from excitons and free carriers and trimolecular formation from free carriers (Chapter 6).

Bibliography

Adachi, S., T. Miyashita, S. Takeyama, Y. Takagi, A. Tackeuchi, and M. Nakayama, 1997, Physical Review B **55**, 1654. 41, 76

Andre, R., and L. S. Dang, 1997, Journal of Applied Physics **82**(10), 5086. 28

Andreani, L. C., G. Panzarini, A. V. Kavokin, and M. R. Vladimirova, 1998, Phys. Rev. B **57**(8), 4670. 22, 27

Autler, S. H., and C. H. Townes, 1955, Phys. Rev. **100**(2), 703. 65

Bastard, G., 1988, *Wave mechanics applied to semiconductor heterostrutures* (Les éditions de physique, Les Ulis, France). 89

Bastard, G., and R. Ferreira, 1991, Surface Science **267**, 335. 51

Benhlal, J. T., K. Strauch, R. Granger, and R. Triboulet, 1999, Optical Materials **12**(1), 143. 28

Bi, S. L., M. P. Di Mauro, and J. Christensen-Dalsgaard, 2000, Astronomy and Astrophysics **364**, 879, and references therein. 81

Bir, G. L., A. G. Aronov, and G. E. Pikus, 1976, Soviet Physics JETP **42**, 7705. 51

Birkedal, D., J. Singh, V. G. Lyssenko, J. Erland, and J. M. Hvam, 1996, Physical Review Letters **76**, 572. 41, 76

Born, M., and E. Wolf, 1999, *Principles of Optics* (Cambridge University Press), 7th edition. 21

Brinkmann, D., J. Kudrna, P. Gillot, B. Hönerlage, A. Arnoult, J. Cibert, and S. Tarenko, 1999, Physical Review B **60**, 4474. 2

Brunhes, T., R. Andr, A. Arnoult, J. Cibert, and A. Wasiela, 1999, Physical Review B **60**, 11568. 2

Capozzi, V., L. Pavesi, and J. L. Staehli, 1993, Physical Review B **47**(11), 6340. 15, 30

Chandrasekhar, S., 1944, Astrophysical Journal **100**(2), 176. 26

Chemla, D. S., and D. A. B. Miller, 1985, Journal of the Optical Society of America B **2**(7), 1155. 1, 15, 48

Chemla, D. S., and J. Shah, 2001, Nature **411**, 6837, and references therein. 37, 55

Choi, S. G., Y. D. Kim, S. D. Yoo, D. E. Aspnes, I. Miotkowski, and A. K. Ramdas, 1997, Applied Physics Letters **71**(2), 249. 28

Ciulin, V., P. Kossacki, J. D. Ganière, S. Haacke, B. Deveaud, A. Moradi, and B. Stébé, 2000a, Physica Status Solidi A **178**, 495. 2

Ciulin, V., P. Kossacki, S. Haacke, J.-D. Ganière, B. Deveaud, A. Esser, M. Kutrowski, and T. Wojtowicz, 2000b, Phys. Rev. B **62**(24), R16310. 52

Ciuti, C., and G. Bastard, 2004, Solid State Communications **133**, 537. 48

Ciuti, C., V. Savona, C. Piermarocchi, A. Quattropani, and P. Schwendimann, 1998, Physical Review B **58**(12), 7926. 39

Cohen-Tannoudji, C., J. Dupont-Roc, and G. Grynberg, 1992 (Wiley-Interscience, New York). 57

Cohen-Tannoudji, C., and S. Haroche, 1969, J. Phys. (Paris) **30**. 57

Combescot, M., and R. Combescot, 1988, Physical Review Letters **61**, 115. 78

Combescot, M., and R. Combescot, 1989, Physical Review B **40**, 3788. 70, 78

Combescot, M., J. Tribollet, G. Karczewski, F. Bernardot, C. Testelin, and M. Chamarro, 2005, Europhysics Letters **71**(3), 431. 16

Cundiff, S. T., A. Knorr, J. Feldmann, S. W. Koch, E. O. Gobel, and H. Nickel, 1994, Physical Review Letters **73**(8), 1178. 1

Deveaud, B., F. Quochi, M. Saba, C. Ciuti, and J.-L. Staehli, 2001, Les Comptes rendus de l'Académie des sciences **t. 2, Srie IV**, 1439. 1

Dingle, R., A. C. G. H. L. Strömer, and W. Wiegmann, 1978, Applied Physics Letters **33**, 665. 1

Dupertuis, M.-A., 2006, private communication. 35

Esser, A., E. Runge, R. Zimmermann, and W. Langbein, 2000a, Physica Status Solidi A **178**, 489. 85

Esser, A., E. Runge, R. Zimmermann, and W. Langbein, 2000b, Physical Review B **62**(12), 8232. 16, 26

Esser, A., Y. Yayon, and I. Bar-Joseph, 2002, Physica Status Solidi B **234**, 266. 30, 34

Esser, A., R. Zimmermann, and E. Runge, 2001, Physica Status Solidi B **227**(2), 317. 16, 25

Feng, M., I. D'Amico, P. Zanardi, and F. Rossi, 2004, Europhysics Letters **66**, 14. 2

Ferrio, K. B., and D. G. Steel, 1998, Physical Review Letters **80**(4), 786. 1

Finkelstein, G., H. Shtrikman, and I. Bar-Joseph, 1995, Phys. Rev. Lett. **74**(6), 976. 2, 81

Finkelstein, G., V. Umansky, I. Bar-Joseph, V. Ciulin, S. Haacke, J.-D. Ganière, and B. Deveaud, 1998, Physical Review B **58**, 12637. 2, 104

Fleischhauer, M., A. Imamoglu, and J. P. Marangos, 2005, Reviews of Modern Physics **77**(2), 633. 55, 68

Frohlich, D., A. Nothe, and K. Reimann, 1985, Physical Review Letters **55**(12), 1335. 1

Frolov, A. M., and V. H. Smith, 2003, **119**, 3130. 81

Gilliot, P., D. Brinkmann, J. Kudrna, R. L. O. Grégut, A. Arnoult, J. Cibert, and S. Tatarenko, 1999, Physical Review B **60**, 5797. 2

Glasberg, S., G. Finkelstein, H. Shtrikman, and I. Bar-Joseph, 1999, Phys. Rev. B **59**(16), R10425. 82, 85, 104

Grove, R. E., F. Y. Wu, and S. Ezekiel, 1977, Physical Review A **15**(1), 227. 64

Harris, S. E., J. E. Field, and A. Imamoğlu, 1990, Physical Review Letters **64**(10), 1107. 55, 75

Hartig, W., W. Rasmussen, and H. Walther, 1976, Zeitschrift für Physik A **278**. 64

Hau, L. V., S. E. Harris, Z. Dutton, and C. H. Behroozi, 1999, Nature **397**, 594. 55

Haug, H., and S. W. Koch, 1990, *Quantum Theory of the Optical and Electronic Properties of Semiconductors* (World Scientific, Singapore). 71

Haug, H., and S. Schmitt-Rink, 1985, Journal of the Optical Society of America B **2**, 1135. 1

Heberle, A. P., J. J. Baumberg, and K. Köhler, 1995, Phys. Rev. Lett. **75**(13), 2598. 1

Hemmer, P. R., D. P. Katz, J. Donoghue, M. Cronin-Golomb, M. S. Shahriar, and P. Kumar, 1995, Optics Letters **20**, 982. 55

Hlidek, P., J. Bok, J. Franc, and R. Grill, 2001, Journal of Applied Physics **90**(3), 1672. 28

Honold, A., L. Schultheis, J. Kuhl, and C. W. Tu, 1989, Physical Review B **40**(9), 6442. 15, 30, 37, 50

Huang, D., H. Y. Chu, Y. C. Chang, R. Houdré, and H. Morko, 1988, Physical Review B **38**(2), 1246. 47

Huard, V., R. T. Cox, K. Saminadayar, A. Arnoult, and S. Tatarenko, 2000, Physical Review Letters **84**(1), 187. 15, 28, 55

Hulin, D., A. Mysyrowicz, A. Antonetti, A. Migus, W. T. Masselink, H. Morko, H. M. Gibbs, and N. Peyghambarian, 1986, Physical Review B **33**(6), 4389. 38

Hyzhnyakov, V. V., A. A. Maradudin, and D. L. Mills, 1975, Physical Review B **11**, 3149. 22

Jackson, J. D., 1999, *Classical Electrodynamics* (John Wiley & Sons, Inc., New York), 3rd edition. 17

Jeukens, C. R. L. P. N., P. C. M. Christianen, J. C. Maan, D. R. Yakovlev, W. Ossau, V. P. Kochereshko, T. Wojtowicz, G. Karczewski, and J. Kossut, 2002, Phys. Rev. B **66**(23), 235318. 82

Joffre, M., D. Hulin, J.-P. Foing, J.-P. Chambaret, A. Migus, and A. Antonetti, 1989, IEEE J. Quantum Electron. **25**, 2505. 55, 78

Kamada, H., H. Gotoh, J. Temmyo, T. Takagahara, and H. Ando, 2001, Physical Review Letters **87**, 246401. 2

Kheng, K., 1995, Annales de Physique **20**, C2. 2

Kheng, K., R. T. Cox, M. Y. d' Aubigné, F. Bassani, K. Saminadayar, and S. Tatarenko, 1993, PRL **71**(11), 1752. 1, 15, 47, 55, 81

Kleinman, D. A., and R. C. Miller, 1985, Physical Review B **32**, 2266. 1

Knox, W. H., 1992, *Optical Studies of Femtosecond Carrier Thermalization in GaAs* (Academic Press, San Diego), p. 313. 88

Kossacki, P., 2003, Journal of Physics: Condensed Matter **15**, R471. 104

Kossacki, P., J. Cibert, D. Ferrand, Y. M. d'Aubigne, A. Arnoult, A. Wasiela, S. Tatarenko, and J. A. Gaj, 1999, Physical Review B **60**(23), 16018. 15, 28

Liu, C., Z. Dutton, C. H. Behroozi, and L. Hau, 2001, Nature **409**, 490. 55

Lovisa, S., R. T. Cox, N. Magnea, and K. Saminadayar, 1997, Physical Review B **56**, R12787. 2

Mahan, G. D., 2000, *Many Particle Physics* (Springer), 3rd edition. 91

Maute, M., S. Wachter, H. Kalt, K. Ohkawa, and D. Hommel, 2003, Physical Review B **67**(16), 165323 (pages 4). 44

Meier, T., S. W. Koch, P. Brick, C. Ell, G. Khitrova, , and H. M. Gibbs, 2000, Physical Review B **62**, 4218. 41, 43, 44, 76

Mills, D. L., and E. Burnstein, 1974, Reports on Progress in Physics **37**, 817. 22

Mollow, B. R., 1972, Phys. Rev. A **5**(5), 2217. 65, 74

Mollow, B. R., and M. M. Miller, 1969, Annals of Physics **52**, 464. 64

Mysyrowicz, A., D. Hulin, A. Antonetti, A. Migus, W. T. Masselink, and H. Morko, 1986, Physical Review Letters **56**(25), 2748. 1, 78

Nazir, A., B. W. Lovett, S. D. Barrett, T. P. Spiller, and G. A. D. Briggs, 2004, Physical Review Letters **93**, 150502. 2

Nielsen, M., and I. Chuang, 2000, *Quantum Computation and Quantum Information* (Cambridge University Press, Cambridge). 2

Pazy, E., E. Biolatti, T. Calarco, I. D'Amico, P. Zanardi, F. Rossi, and P. Zoller, 2003, Europhysics Letters **62**, 175. 2

Peyghambarian, N., H. M. Gibbs, J. L. Jewell, A. Antonetti, A. Migus, D. Hulin, and A. Mysyrowicz, 1984, Physical Review Letters **53**(25), 2433. 38

Phillips, M. C., and H. Wang, 2002, Physical Review Letters **89**, 186401. 1, 71, 75

Phillips, M. C., and H. Wang, 2004, Physical Review B **69**, 115337. 78

Phillips, M. C., H. Wang, I. Rumyantsev, N. H. Kwong, R. Takayama, and R. Binder, 2003, Physical Review Letters **91**(18), 183602. 76

Phillips, R. T., G. C. Nixon, T. Fujita, M. Y. Simmons, and D. A. Ritchie, 1996, Solid State Communications **98**, 287. 85

Piermarocchi, C., F. Tassone, V. Savona, A. Quattropani, and P. Schwendimann, 1997, Phys. Rev. B **55**(3), 1333. 81, 86, 87, 88, 95

Plochocka, P., P. Kossacki, W. Maslana, J. Cibert, S. Tatarenko, C. Radzewicz, and J. A. Gaj, 2004, Physical Review Letters **92**(17), 177402 (pages 4). 86

Portella-Oberli, M. T., V. Ciulin, J. Berney, B. Deveaud, M. Kutrowski, and T. Wojtowicz, 2004, Physical Review B **69**, 235311. 50, 74, 76

Portella-Oberli, M. T., V. Ciulin, P. Kossacki, S. Haacke, M. Kutrowski, T. Wojtowicz, J.-D. Ganière, and B. Deveaud, 2002, Physica Status Solidi A **190**, 787. 2, 50

Portella-Oberli, M. T., V. Ciulin, M. Kutrowski, T. Wojtowicz, and B. Deveaud, 2003, Physica Status Solidi B **238**, 513. 45, 74, 76, 86

Puls, J., G. Mikhailov, F. Henneberger, D. R. Yakovlev, A.Waag, and W. Faschinger, 2002, Physical Review Letters **89**, 287402. 2

Quochi, F., M. Saba, C. Ciuti, R. P. Stanley, R. Houdré, U. Oesterle, J. L. Staehli, , B. Deveaud, A. Mura, and G. Bongiovanni, 2000, Physical Review B **61**, R5113. 55, 74

Ramon, G., A. Mann, and E. Cohen, 2003, Physical Review B **67**, 45323. 16, 31, 35, 55

Riva, C., F. M. Peeters, and K. Varga, 2000, Physical Review B **61**(20), 13873. 16

Rochat, G., C. Ciuti, V. Savona, C. Piermarocchi, A. Quattropani, and P. Schwendimann, 2000, Phys. Rev. B **61**(20), 13856. 35

Ruckenstein, A. E., S. Schmitt-Rink, and R. C. Miller, 1986, Physical Review Letters **56**, 504. 1

Saba, M., F. Quochi, C. Ciuti, D. Martin, J.-L. Staehli, B. Deveaud, A. Mura, and G. Bongiovanni, 2000, Physical Review B **62**, R16322. 44, 55, 74, 75

Sanvitto, D., F. Pulizzi, A. J. Shields, P. C. M. Christianen, S. N. Holmes, M. Y. Simmons, D. A. Ritchie, J. C. Maan, and M. Pepper, 2001, Science **294**(5543), 837. 2

Savona, V., 1999, in *Confined photon systems: Fundamentals and applications* (Springer Verlag, Berlin, New York), pp. 173–242. 20

Schmitt-Rink, S., D. S. Chemla, and D. A. B. Miller, 1985, Physical Review B **32**, 6601. 38, 47, 74

Schmitt-Rink, S., D. S. Chemla, and D. A. B. Miller, 1989, Advances in Physics **38**, 89. 1

Schreier, F., 1992, Journal of Quantitative Spectroscopy & Radiative Transfer **48**(5-6), 743. 28

Schultheis, L., J. Kuhl, A. Honold, and C. W. Tu, 1986, Physical Review Letters **57**(13), 1635. 15, 74

Schülzgen, A., R. Binder, M. E. Donovan, M. Lindberg, K. Wundke, H. M. Gibbs, G. Khitrova, and N. Peyghambarian, 1999, Physical Review Letters **82**(11), 2346. 74

Scully, M. O., and M. Suhail Zubairy, 1997, *Quantum Optics* (Cambridge University Press, Cambridge). 63

Sergeev, R. A., and R. A. Suris, 2001, Physics of the Solid State **43**(4), 746. 26

Siantidis, K., V. M. Axt, and T. Kuhn, 2001, Physical Review B **65**, 035303. 81

Stebe, B., G. Munschy, L. Stauffer, F. Dujardin, and J. Murat, 1997, Physical Review B **56**(19), 12454. 16

Stebe, B., and L. Stauffer, 1989, Superlattices and Microstructures **5**(3), 451. 15

Stievater, T. H., X. Li, D. G. Steel, D. Gammon, D. S. Katzer, D. Park, C. Piermarocchi, and L. J. Sham, 2001, Physical Review Letters **87**, 133603. 2

Suris, R. A., V. P. Kochereshko, G. V. Astakhov, D. R. Yakovlev, W. Ossau, J. Nurnberger, W. Faschinger, G. Landwehr, T. Wojtowicz, G. Karczewski, and J. Kossut, 2001, Physica Status Solidi B-Basic Research **227**(2), 343. 16

Szczytko, J., L. Kappei, J. Berney, F. Morier-Genoud, M. T. Portella-Oberli, and B. Deveaud, 2004a, Physical Review Letters **93**(13), 137401. 81, 85, 86

Szczytko, J., L. Kappei, J. Berney, F. Morier-Genoud, M. T. Portella-Oberli, and B. Deveaud, 2005, Physical Review B **71**(19), 195313. 12

Szczytko, J., L. Kappei, F. Morier-Genoud, T. Guillet, M. T. Portella-Oberli, and B. Deveaud, 2004b, (238), 493. 12

Tassone, F., F. Bassani, and L. C. Andreani, 1990, Nuovo Cimento della Societa Italiana di Fisica D **12**, 1673. 22

Tassone, F., F. Bassani, and L. C. Andreani, 1992, Physical Review B **45**, 6023. 22

Tassone, F., and Y. Yamamoto, 1999, Phys. Rev. B **59**(16), 10830. 39

Thilagam, A., 1997, Physical Review B **55**(12), 7804. 16

Tribollet, J., F. Bernardot, M. Menant, G. Karczewski, C. Testelin, and M. Chamarro, 2003, Physical Review B **68**(23), 235316. 2

Vanelle, E., M. Paillard, X. Marie, T. Amand, P. Gillot, D. Brinkmann, R. Lévy, J. Cibert, and S. Tatarenko, 2000, Physical Review B **62**, 2696. 2, 82

Von Lehmen, A., D. S. Chemla, J. E. Zucker, and J. P. Heritage, 1986, Opt. Lett. **11**, 609. 1, 78

Wagner, H. P., H.-P. Tranitz, and R. Schuster, 1999, Physical Review B **60**, 15542. 2

Wojtowicz, T., M. Kutrowski, G. Karczewski, and J. Kossut, 1998, Applied Physics Letters **73**, 1379. 5

Wu, F. Y., R. E. Grove, and S. Ezekiel, 1975, Physical Review Letters **35**(21), 1426. 64

Yokoyama, H., 1992, Science **256**, 66. 11

Yonn, H. W., A. Ron, M. D. Sturge, and L. N. Pfeiffer, 1996, Solid State Communications **100**, 743. 2

Yusa, G., H. Shtrikman, and I. Bar-Joseph, 2000, Physical Review B **62**(23), 15390. 15, 28

Zimmermann, R., 1988, Physica Status Solidi B **146**, 371. 47

Index

Jean Berney

Rue du Clos-de-Bulle 11, CH-1004 Lausanne • Tél. : 079 785 91 59 • Email : jean.berney@a3.epfl.ch • Célibataire • 27 ans • Suisse

Etudes

ECOLE POLYTECHNIQUE FEDERALE DE LAUSANNE (EPFL) — **Lausanne, VD**

Septembre 2006	**Candidat pour un titre de Docteur en Physique.** Travail expérimental dans le domaine de l'optique des semiconducteurs. ***Directeurs de thèse:*** Professeur B. Deveaud-Plédran et M. Portella-Oberli.
Février 2002	**Diplôme d'Ingénieur Physicien EPF.**

UNIVERSITY OF WATERLOO — **Canada**

1999 - 2000	Echange académique, 2 semestres.

Expériences professionnelles

UNIVERSITY OF MISSOURI-ROLLA — **USA**

Eté 2000	Etude de l'impact sur l'environnement des aérosols émis par le trafic aérien.

GUINCHARD OPTICAL GLASS OF SWITZERLAND — **Yverdon-les-Bains, VD**

Mai 2000	Optimisation de l'utilisation de l'eau au sein de l'entreprise (réalisation: diminution de 20% de la consommation). Planification du traitement des eaux.

Activités associatives

PRESIDENT, ASSOCIATION DU CORPS INTERMEDIAIRE DE L'EPFL (ACIDE)

2005 - présent	Représentation du corps intermédiaire auprès de la direction de l'EPFL. Engagement au sein d'un comité de 8 personnes. Gestion d'un budget de 65'000 CHF. Supervision de l'activité d'une administratrice.

RESPONSABLE RELATIONS EXTERIEURES, ASSOCIATION PARRAINAGE EPFL

2000 - 2001	Accueil des étudiants d'échange sur le site de l'EPFL. Organisation de visites d'entreprises. Budget: 7'000 CHF.

DELEGUE, SECTION DE PHYSIQUE (1998-1999)

Langues

Français	Langue maternelle.
Anglais	Très bonne maîtrise (18 mois au Canada, USA et Royaume-Uni).
Allemand	Bonne maîtrise (*au pair* en Allemagne, été 1997).

Compétences informatiques

OS	Linux (administration d'un cluster), Windows.
Programmation	***Calcul numérique:*** Matlab, Fortran & MPI. ***Automatisation:*** Labview. ***Applications Web:*** PHP & MySQL (développement d'un outil de gestion de bibliographies en ligne).
Logiciels	Microsoft Office, Adobe Creative Suite, AutoCad, Mathematica.

Centres d'intérêt

Volley	Capitaine de l'équipe de physique (tournoi inter-instituts EPFL, 2003-2006).
Ski de randonnée	Patrouille des Glaciers 2006, Zermatt-Verbier.
Cyclisme	Voyage : Suisse-Iran-Russie, 5137 km (avril-août 2002).

Annexe

Publications

[1] B. Deveaud, L. Kappei, J. Berney, F. Morier-Genoud, M. T. Portella-Oberli, J. Szczytko, and C. Piermarocchi. Excitonic effects in the luminescence of quantum wells. *Chemical Physics* **318** (2005), 104.

[2] B. Deveaud, J. Szczytko, L. Kappei, J. Berney, F. Morier-Genoud, and M. T. Portella-Oberli. Exciton formation rate in quantum wells from a direct comparison between free-carrier and exciton contributions to time resolved luminescence. *Physica Status Solidi (c)* **2** (2005), 2947.

[3] J. Szczytko, L. Kappei, J. Berney, F. Morier-Genoud, M. T. Portella-Oberli, and B. Deveaud. Origin of excitonic luminescence in quantum wells: direct comparison of the exciton population and coulomb correlated plasma models. *Physical Review B* **71** (2005), 195313.

[4] M. T. Portella-Oberli, J. Berney, V. Ciulin, M. Kutrowski, T. Wojtowicz, and B. Deveaud. How do electrons, excitons and trions share the reciprocal space in a quantum well? In *27th International Conference on the Physics of Semiconductors (ICPS-27)* (2005), Eds. J. Menendez and C. VanDeWalle, AIP Conference Proceedings, p. 957.

[5] J. Szczytko, L. Kappei, J. Berney, F. Morier-Genoud, M. T. Portella-Oberli, and B. Deveaud. On the origin of excitonic luminescence in quantum wells: direct measure of the exciton formation in quantum wells from time resolved interband luminescence. In *27th International Conference on the Physics of Semiconductors (ICPS-27)* (2005), Eds. J. Menendez and C. G. VanDeWalle, vol. 772 of AIP Conference Proceedings, p. 1149.

[6] M. T. Portella-Oberli, J. Berney, B. Deveaud, V. Ciulin, M. Kutrowski, and T. Wojtowicz. Many-body interaction evidenced through exciton-trion-electron correlated dynamics. *Acta Physica Polonica A* **106** (2004), pp. 423–434.

[7] M. T. Portella-Oberli, Ciulin, V., J. Berney, B. Deveaud, M. Kutrowski, and T. Wojtowicz. Interacting many-body systems in quantum wells: evidence for exciton-trion-electron correlations. *Physical Review B* **69**, 23 (2004), 235311.

[8] M. T. Portella-Oberli, V. Ciulin, J. Berney, M. Kutrowski, T. Wojtowicz, and B. Deveaud. Correlated dynamics of trions and excitons in modulation-doped CdTe quantum wells. *Physica Status Solidi (c)* **1** (2004), 484.

[9] J. Szczytko, L. Kappei, J. Berney, F. Morier-Genoud, M. T. Portella-Oberli, and B. Deveaud. Determination of the exciton formation in quantum wells from time-resolved interband luminescence. *Physical Review Letters* **93** (2004), 137401.

Conférences

[1] J. Berney, M. T. Portella-Oberli, M. Kutrowski, T. Wojtowicz, and B. Deveaud. Optical stark shift demonstrates biexciton stabilty in cdte modulation-doped quantum wells. In 8th International Workshop on Nonlinear Optics and Excitation Kinetics in Semiconductors (NOEKS 8) (Münster, Germany, 2006).

[2] J. Szczytko, J. Berney, F. Morier-Genoud, M. T. Portella-Oberli, and B. Deveaud. Exciton formation rate in quantum wells: correlation between the evolution of the plasma luminescence and the excitonic line broadening. In 8th International Workshop on Nonlinear Optics and Excitation Kinetics in Semiconductors (NOEKS 8) (Münster, Germany, 2006).

[3] J. Berney, J. Szczytko, L. Kappei, F. Morier-Genoud, M. T. Portella-Oberli, and B. Deveaud. Dynamics of trion formation in GaAs quantum wells. In 9th Conference on Optics and Excitons in Confined Systems (OECS9) (Southampton, England, 2005).

[4] J. Berney, M. T. Portella-Oberli, M. Kutrowski, T. Wojtowicz, and B. Deveaud. Evidence for stable biexciton in a modulationdoped quantum well. In 9th Conference on Optics and Excitons in Confined Systems (OECS9) (Southampton, England, 2005).

Conférences (suite)

[5] J. Berney, M. T. Portella-Oberli, M. Kutrowski, T. Wojtowicz, and B. Deveaud. How electrons, excitons, trions share phase-space. In Quantum Technology and Optical Processes in Semiconductor Nanostructures (EQUONT-3) (Clare College, Cambridge, 2004).

[6] J. Szczytko, L. Kappei, J. Berney, F. Morier-Genoud, M. T. Portella-Oberli, B. Deveaud, and C. Piermarocchi. Determination of the exciton formation in quantum wells from time-resolved interband luminescence. In Quantum Technology and Optical Processes in Semiconductor Nanostructures (EQUONT-3) (Clare College, Cambridge, 2004).

[7] B. Deveaud, J. Szczytko, L. Kappei, J. Berney, F. Morier-Genoud, and M. T. Portella-Oberli. Exciton formation in quantum wells from a direct comparison between free-carrier and exciton contributions to time resolved luminescence. In International Conference on Superlattices, Nano-structures and Nano-devices (ICSNN-04) (Cancun, Mexico, 2004).

[8] B. Deveaud, J. Szczytko, L. Kappei, J. Berney, and M. T. Portella-Oberli. Excitons, free carriers, Mott transition and related topics in quantum wells. In FOPS International Meeting (Colorado, United States, 2004).

[9] J. Szczytko, L. Kappei, J. Berney, F. Morier-Genoud, M. T. Portella-Oberli, and B. Deveaud. On the origin of excitonic luminescence in quantum wells: direct measure of the exciton formation from time resolved inteerband luminescence. In 27th International Conference on the Physics of Semiconductors (ICPS-27) (Flagstaff, Unided States, 2004).

[10] M. T. Portella-Oberli, V. Ciulin, J. Berney, M. Kutrowski, T. Wojtowicz, and B. Deveaud. Many-body interactions inducing exciton-trion-electron correlated dynamics. In Workshop on Optical Properties of 2D systems with interacting carriers (Warsaw, Poland, 2004).

[11] M. T. Portella-Oberli, J. Berney, B. Deveaud, V. Ciulin, M. Kutrowski, and T. Wojtowicz. How do electrons, excitons and trions share the reciprocal space in a quantum well? In 27th International Conference on the Physics of Semiconductors (ICPS-27) (Flagstaff, Unided States, 2004).

[12] M. T. Portella-Oberli, V. Ciulin, J. Berney, M. Kutrowski, T. Wojtowicz, and B. Deveaud. Correlated dynamics of trions and excitons in modulation-doped CdTe quantum wells. In 8th Conference on Optics of Excitons in Confined Systems (OECS-8) (Lecce, Italy, 2003).

[13] J. Szczytko, L. Kappei, J. Berney, F. Morier-Genoud, T. Guillet, M. T. Portella-Oberli, and B. Deveaud. Excitons or free carriers? That is the question. In 8th Conference on Optics of Excitons in Confined Systems (OECS-8) (Lecce, Italy, 2003).